

https://dspace.org/

Applications of mesostructured carbonaceous materials as supports for fischer-tropsch metal catalyst

Mbileni, Charity Nonkululeko

2007-02-21T12:32:55Z
http://hdl.handle.net/10539/2058

Downloaded from a DSpace repository. https://dspace.org/

APPLICATIONS OF MESOSTRUCTURED CARBONACEOUS MATERIALS AS SUPPORTS FOR FISCHER-TROPSCH METAL CATALYST

Charity Nonkululeko Mbileni

A thesis submitted to the Faculty of Science,

University of the Witwatersrand, Johannesburg,

in fulfilment of the requirements

for the degree of Doctor of Philosophy

Johannesburg, 2006

Declaration

I declare that this thesis is my own, unaided work. It is being submitted for the degree of Doctor of Philosophy in the University of the Witwatersrand, Johannesburg. It has not been submitted before for any degree or examination in any other university.

_____ day of _____ 2006

Abstract

Mesoporous MCM-48 was synthesized and used as a template to synthesize mesoporous carbon (MC) materials. Polystyrene, the carbon source, together with sulfuric acid and toluene were added to the template (160 ^{o}C for 6 h) and this procedure generated a low surface area carbon supported/MCM-48 material. A repeat addition and carbonization step was needed to form the precursor carbon/MCM-48 material that was pyrolysed at 900 ^{o}C to generate graphitic mesoporous carbon materials. After removal of the silica template, mesoporous carbons were characterized by XRD, HR-TEM, Raman spectroscopy and surface area analysis. The effect of the amount of polystyrene as well as the role of the pyrolysis temperature on the final product was investigated. This synthesis methodology can readily be controlled to produce partially ordered graphitic mesoporous carbon supports with predictable pore width and surface area.

In this study, the effect of three different supports (activated carbon (AC), mesoporous carbon (MC) and MCM-48) and of the potassium loading (2, 5 and 10 %) on the iron metal catalyst was investigated for the Fischer-Tropsch synthesis (FTS) activity. Characterization of the dried and calcined Fe catalysts by electron microscopy revealed that the iron was found on the surface of the

supports and in most cases the Fe nano-particles aggregated with neighboring particles to form Fe nano-clusters.

The three catalysts precursors supported on activated carbon with different amount of potassium: 15%Fe/2%K/AC, 15%Fe/5%K/AC and 15%Fe/10%K/AC, were evaluated for the FTS. It was observed that the three promoted and precipitated Fe/AC catalyst gave an initially high (~90 mol%) CO conversion that decreased with time on stream to ~30 mol% after ~200 h. On average, a CO_2 yield of ~40% was obtained for all the three catalysts, indicating similar water gas shift reaction behavior. Also, three catalysts precursors supported on mesoporous carbon were prepared, 15%Fe/2%K/MC, 15%Fe/5%K/MC and 15%Fe/10%K/MC and evaluated for the FTS. The activity of the 2 and 5% K loaded catalysts was found to be similar (~40 mol% CO conversion). Whereas, the 10% loaded K catalysts showed slightly lower CO conversion when compared to the other two catalysts.

The catalytic performance of 15%Fe/2%K/AC, 15%Fe/2%K/MC and 15%Fe/2%K/MCM-48 were compared. The type of the support had a marked effect on the product selectivities and product distributions of the catalysts. The carbon dioxide selectivity was shown to have been decreased more with 15%Fe/2%K/MCM-48.

The methane selectivity was low (below 6%) and stable, and the overall olefin fraction was found to be good for all the supported catalysts studied. The potassium promoter increased the hydrocarbon chain growth to C_{68} giving α-1 and α-2 both between 0.79 and 0.90 for all supported catalysts with an exception of MCM-48 supported Fe catalyst that selectively produced hydrocarbons up to C_{28}.

Dedications

This thesis is dedicated to my special mother, ***Matshedis****o and my wonderful sister* ***Olympia*** *for their invaluable support, their unconditional love and for their guidance throughout my life.*

I love you so much!!!

And… to my other family members, relatives and friends for believing in me and looking up to me as a role model.

Thank you so much!

Acknowledgements

This thesis is a result of a very large collective enterprise. I would like to express my appreciation to the following people for assisting me professionally and also, making this thesis possible.

The All Mighty GOD for his protection, love and seeing me through each day as it comes, and more importantly without whom I would not be in existence.

Prof. N. J. Coville, my supervisor for believing in me by accepting me as his student, for his guidance, immeasurable contribution to this work and investing knowledge in me.

Dr. F. F. Prinsloo, my mentor, for his interest and valuable input in this work.

Dr. B. H. Davis, for allowing me to spend time with his research group at the Center for Applied Energy Research (CAER) in the University of Kentucky, USA and whose knowledge in the field of Fischer-Tropsch is invaluable.

Mr. S. Bao, Dr. M.S. Luo, Mr. R. Spicer, Mr. D. Sparks for helping me with technical laboratory work and Mr. B. Kyoo for the analysis of my GC samples at CAER.

Dr. U. Graham, Dr. G. Jacobs and Mr. R. Gonzalez for their assistance with TEM, TPR, BET, SEM and XRF techniques at CAER.

Prof. M. J. Witcomb, Mr. A. Seema and Mrs. C. Lalkhan for assisting me with electrom microscopy work at Wits University.

Mr. M. Bahome for helping me get started with the Fischer-Tropsch reactor work.

Mr. J. A. Moma, Mrs. A. Pointeer, K. Banda, E. Valoyi, S. Ganon, B. Fairbrother and B. Chassoulas of the chemistry department for their assistance in various ways.

Mr. M. W. Ngobeni for proof-reading this thesis.

The Wits Catalysis and Organo-metallic group for showing me how to use characterization equipments and for creating a conducive environment for doing my research.

The University of the Witwatersrand for accepting me as a student, for giving me site to do my research and also for funding.

SASOL for giving me this project and funding;

CCETSA for financial assistance.

Publications and Presentations arising from this Work

Poster Presentations:

Synthesis of mesoporous carbon supports via template-mediated structural transformation, CATSA- Durban (November, 2003).

Template-directed synthesis of mesoporous carbonaceous materials, African Materials Science conference, University of the Witwatersrand, Johannesburg (December 2003).

Oral Presentation:

Synthesis of mesoporous carbon supports via liquid impregnation of polystyrene onto a MCM-48 silica template, CATSA conference – Potchefstroom (November 2004).

Publication:

Synthesis of mesoporous carbon supports via liquid impregnation of polystyrene onto a MCM-48 silica template, C. N. Mbileni, F. F. Prinsloo, M. J. Witcomb and N. J. Coville, *Carbon*, **44**, 1476 (2006).

Thesis outline

Attention has recently been drawn to the synthesis of porous carbons by using porous inorganic materials as templates. This technique represents an advance over the methods currently employed to prepare porous carbons (i.e. physical or chemical activation) because the structural characteristics (i.e. surface area, pore volume, pore size, particle size, morphology, etc) of the materials synthesized in this way can be finely tuned by selecting the appropriate template and synthesis conditions. Carbon materials represent a unique family of supports because of the diverse nature of the different forms of carbon that can be used and the complex functions they can perform. The increasing importance of carbon materials in catalytic process is analyzed in terms of the most important characteristics of these materials compared to oxidic supports. It remains, however, true that the main use of carbon materials in heterogeneous catalysis is as a catalyst support.

The extent of the Fischer-Tropsch synthesis depends on the reaction conditions and on the catalyst properties. In this thesis both properties will be dealt with. It must be noted that the catalyst properties are more difficult to control, since they depend *e.g.* on the active metal, the support, the dispersion of the active metal and the promotor employed. Iron is chosen as the active metal for its ability to dissociatively adsorb carbon monoxide faster than hydrogen, thus producing a

large amount of olefins. However, an iron catalyst is also liable to deactivate faster than other (Co, Ni, Ru, etc.) FTS catalysts. It is anticipated that the support must be able to stabilize the metal dispersion and moreover should not interact with an applied promotor. For this reason, carbonaceous supports (with particular interest in mesoporous carbons) have been screened for suitability in the FTS reaction. Finally, a potassium promotor is chosen since it is reported that potassium enhances the formation of unsaturated hydrocarbons and increases the hydrocarbon chain growth. In view of the above, Fe catalysts on different supports with different amounts of potassium loadings were prepared and their FTS synthesis performance evaluated. This thesis is divided into two parts, and a brief summary of each chapter is given below.

Part I: Template directed synthesis of structural and porous materials

Chapter 1: The literature review on the sol-gel chemistry; and the synthesis and applications of porous materials are described in this chapter. It is noteworthy that the template method used in the sol-gel chemistry has become a very simple yet a powerful process for the synthesis of structural materials. These materials constitute a challenging domain in materials chemistry, which is experiencing explosive growth.

Chapter 2: It has been shown that by in situ carbonization of organic compounds, carbon nanocomposites and carbons with a well developed pore structure and high surface areas can be obtained. In addition, highly ordered mesoporous carbon materials using mesoporous silica as templates, are now available with a rich variety of structures. In general, the preparation of these materials consists of: the infiltration of the porous structure of an inorganic material (template) by the carbon precursor (generally a polymer or a prepolymer), the polymerization of the infiltrated substance, the carbonization of the nanocomposites formed and finally, elimination of the template. The templated synthesis of the ordered mesoporous carbons is a remarkable achievement in the field of porous materials because the synthesis is easy, inexpensive and suitable for large scale production. The resulting high-surface-area materials and uniform pores promise to be suitable as adsorbents, catalyst supports, and materials for advanced electronics applications.

Chapter 3: A well defined synthesis route to mesoporous graphitic carbon using polystyrene as a carbon source is reported in this work. The template used was MCM-48. The use of a template is essential in the synthesis of the mesoporous carbon framework, as carbons synthesised under otherwise identical conditions without a template were found to have low surface areas, and no pore structure. The catalytic carbonisation procedure used has an advantage as

uniform infiltration of the carbon precursor can be easily accomplished inside the silica mesopores so that the resultant carbon materials retain the mesostructural order of the silica templates. The Raman, XRD and TEM techniques confirmed the partially graphitic nature of the resultant synthesised carbonaceous materials

Part II: Application of mesostructured carbonaceous materials as catalystssupports for the Fischer-Tropsch reaction

Chapter 4: The Fischer-Tropsch (FT) chemistry, the reactors and catalysts used in FT are described in order to fully understand parameters influencing the overall performance of the FT process. Furthermore, the main objective of this study which was to prepare novel mesoporous carbonaceous materials, and then use them as catalyst supports for the FT reaction is outlined.

Chapter 5: In this chapter, the procedures and techniques used to prepare and characterize the prepared precipitated Fe/K/carbon catalysts for FTS are described. The pretreatment method used in this study is compared to other methods used in the literature. The equipment used to perform experiments (gas-slurry FTS) as well as the experimental procedures and product analyses are also described.

Chapter 6: Characterization of precipitated and promoted Fe catalysts was performed using XRF, XRD, BET, TPR, SEM and TEM techniques. It was found that the elemental composition of the catalysts were comparable to the calculated values. The BET surface area of the mesoporous carbon support was remarkably reduced after impregnation with the Fe metal catalyst. The data on the reduction of iron oxide revealed that the supported and precipitated catalysts reduce in two steps, with the reduction of the Fe/mesoporous catalyst being enhanced relative to Fe/activated carbon and Fe/MCM-48. Different iron oxide phases were observed and identified from the XRD data provided. Characterization with electron microscopy revealed that iron was found on the surface of the supports and in most cases the Fe nano-particles aggregated with neighboring particles to form Fe nano-clusters.

Chapter 7: The effect of potassium promotion (2, 5, and 10 % K atomic ratio) on precipitated iron catalysts supported on activated carbon was investigated. It was observed that the three promoted and precipitated Fe/AC catalyst gave an initially high (~90 mol %) CO conversion that decreased with time on stream to (~30 mol %). The deactivation was consistent for all the catalysts and was speculated to have been due to a contribution of sulfur poisoning, phase changes and also to complete filling or blockage of catalyst pores. The methane selectivity was low (below 6 %) and stable, and the overall olefin fraction was found to be

good for all three catalysts. On average, a CO_2 yield of ~40 % was obtained for all the three catalysts, indicating similar water gas shift reaction behaviour. The potassium promoter increased the hydrocarbon chain growth to C_{55} giving α-1 and α-2 both between 0.79 and 0.88 for all three catalysts.

Chapter 8: The effect of potassium promotion (2, 5, and 10 % K atomic ratio) on precipitated iron catalysts supported on mesoporous carbon was investigated. The activity of the 2 and 5 % K loaded catalysts was found to be similar (~40 mol %) for the 2 and 5 % K loaded catalysts. The 10 % loaded K catalysts showed slightly lower CO conversion when compared to the other two catalysts. The methane selectivity for all three catalysts was low (between 1 and 5 mol %) compared to other reported Fe/C catalysts. Also, the CO_2 selectivity was found to be low with the 10 % K loaded catalyst exhibiting a significant decrease (~5 mol %) compared to 2 % K loaded catalyst (~20 mol %) and 5 % K loaded catalyst (~10 mol %). A shift in the selectivity to higher molecular weight hydrocarbons with Fe/mesosoporous carbons was observed.

Chapter 9: The catalytic performance of three precipitated and promoted Fe catalysts supported on activated carbon (15%Fe/2%K/AC), mesoporous carbon (15%Fe/2%K/MC) and mesoporous silica MCM-48 template (15%Fe/2%K/MCM-48) are compared. It appears that the type of the support had

a marked effect on the product selectivities and product distributions. The methane selectivity of the three catalysts was shown to be similar and low (between 4 and 6 mol %). The carbon dioxide selectivity was shown to have been decreased more with 15%Fe/2%K/MCM-48. The 15%Fe/2%/MCM-48 catalysts produced a slightly higher percentage of gaseous and liquid organic products when compared to the other two catalysts. Larger molecular products were dominant in the catalyst supported on mesoporous carbon and activated carbon.

Chapter 10: In conclusion, the studies that were carried out in this thesis showed that from the supports that were used, mesoporous carbons seem to have a remarkable potential for use as FT catalyst supports. In future, it would be interesting to conduct studies on more highly reduced Fe catalysts. The data will be evaluated to obtain insight in the obtained crystallite size distribution, the dispersion of the crystallites over the support material, and the degree of reduction of the catalyst precursor. It would also be of interest to investigate other process conditions like space velocity, temperature, pressure and extended time on stream to determine the life span of the catalyst.

Table of Contents

Declaration……. i

Abstract……. ii

Dedications……. v

Acknowledgements…… vi

Publications and Presentations arising from this Work…….. ix

Thesis Outline…….. x

Table of Contents…… xvii

List of Tables……... xxv

List of Figures…….. xxvi

List of Abbreviations and Symbols……. xxxiv

PART I: Template-directed synthesis of mesostructured slica and carbonaceous materials…… 1

Chapter One:

Template –Directed Synthesis of Structural Materials: A Review……. 2

1.1 Introduction…… 2

1.2 Porous materials…… 3

1.2.1 Zeolites…….. 5

1.2.2 Applications of Zeolites…… 11

1.2.3 The Mobil M41S materials…… 12

1.3 The Sol-Gel Process……... 16

1.4 Structured Metal Oxides and Organic-Inorganic Composites…… 22

1.5 Conclusion…….. 29

1.6 References…… 30

Chapter Two:

Carbonaceous Materials for Catalytic Applications…… 36

2.1 Introduction……. 36

2.1.1 Carbon as a catalyst……. 36

2.1.2 Carbon as a catalyst…… 36

2.1.3 Carbon as a catalyst support…… 37

2.2 Porous carbons……..……. 40

2.2.1 Carbon nanotubes…… 42

2.2.2 Activated carbon…….. 45

2.3 Templated Porous Carbons…….. 46

2.4 Ordered Mesoporous Carbons……. 48

2.5 Conclusion…… 66

2.6 References…… 67

Chapter Three:

Synthesis of mesoporous carbon supports via liquid impregnation of polystyrene onto a MCM-48 silica template…… 73

3.1 Introduction……. 73

3.2 Experimental section…… 77

3.2.1 Synthesis of MCM-48……. 77

3.2.2 Preparation of polystyrene…….. 77

3.2.3 Synthesis of mesoporous carbons…… 78

3.2.4 Characterization…… 79

3.3 Results and discussion…….. 80

3.3.1 Effect of the amount of polystyrene added to the pores of MCM-48 silica template……..... 80

3.3.2 Effect of carbonization on MCM-48 silica template…… 86

3.3.3 Investigation of the degree of the retention order of crystal morphology of MCM-48…….. 89

3.3.4 Adsorption properties of inverse carbon replicas of MCM-48…… 97

3.3.5 Investigation of the carbon/silica composite ratios in the resultant carbons…….. 101

3.4 Conclusion…… 108

3.5 References…… 110

PART II: Application of mesostructurals carbonaceous materials as supports for Fischer-Tropsch metal catalyst……..... 117

Chapter Four:

The Fischer-Tropsch Process and Technology: A Review…….. 118

4.1 Introduction…….. 118

4.2 The Fischer-Tropsch process…… 124

4.2.1 Syngas production and purification…….. 126

4.2.2 The Fischer-Tropsch synthesis……. 128

4.2.3 Product Upgrading and Separation……... 128

4.3 Fischer-Tropsch Chemistry…….. 129

4.4 FTS reactors…….. 133

4.5 FTS catalysts…… 135

4.6 Objectives of the study…… 139

4.7 Conclusion…… 140

4.8 References…… 141

Chapter Five:

Experimental Section…… 146

5.1 Introduction…….. 146

5.2 Preparation of supported iron catalyst…… 148

5.3 Reactor set up…….. 150

5.3 In situ activation of the catalysts…… 154

5.4 Fischer-Tropsch synthesis…… 157

5.5 Product sampling and analysis……. 158

5.6 Fischer-Tropsch data calculations…… 161

5.7 Characterization of the Fe supported catalysts…… 162

5.8 References…… 164

Chapter Six:

The characterization of the iron supported catalysts…… 167

6.1 Introduction…….. 167

6.2 Results and discussions…… 169

6.2.1 Elemental analysis of Fe-supported catalyst precursors….. 169

6.2.2 Textural properties of Fe-supported catalyst precursors…. 170

6.2.3 Reduction behavior of the Fe-supported catalyst precursors……. 173

6.2.4 Structural properties of Fe-supported catalyst precursors… 177

6.2.5 Electron microsopy studies…….. 180

6.3 Conclusion…… 187

6.4 References…… 188

Chapter Seven:

Fischer-Tropsch synthesis over an iron catalyst supported on activated carbon: effect of potassium loading…… 190

7.1 Introduction…… 190

7.2 Experimental…… 196

7.3 Results and discussion…… 197

7.3.1 The Fischer-Tropsch activity of the Fe/AC catalyst precursors…… 197

7.3.2 Deactivation of the Fe/AC catalysts…… 200

7.3.3 Selectivity of the Fe/AC catalysts…… 208

7.3.4 Productivity of the catalyst…….. 211

7.3.5 Product distribution…….. 214

7.4 Conclusion…… 216

7.5 References…… 218

Chapter Eight:

Fischer-Tropsch synthesis over an iron catalyst supported on mesoporous carbon: effect of potassium loading……. 223

8.1 Introduction……. 223

8.2 Experimental section…… 227

8.3 Results and discussions…… 228

8.3.1 The Fischer-Tropsch activity of the precipitated and Promoted Fe/MC catalysts…….. 228

8.3.2 Selectivity of the precipitated and promoted Fe/MC catalysts…….. 232

8.3.3 Productivity of the catalyst……. 236

8.4 Conclusion…….. 240

8.5 References…….. 242

Chapter Nine:

Comparative studies of Fe catalysts supported on activated carbon, mesoporous carbon and MCM-48 silica template…….. 247

9.1 Introduction…… 247

9.2 Experimental section…….. 247

9.3 Results and discussion…… 248

9.3.1 The Fischer-Tropsch activity of the precipitated and promoted Fe/MCM-48 catalysts……. 248

9.3.2 Selectivity of the precipitated and promoted Fe catalysts on different supports…… 250

9.3.3 Productivity of the precipitated and promoted Fe catalysts on different supports…… 252

9.4 Conclusion…….. 257

9.5 References…… 258

Chapter Ten:

Conclusions…….. 259

List of Tables

Page number

Table 2.1: Summary of the different literature methods employed to synthesize mesoporous carbons…… 61

Table 3.1: Pore characteristics of mesoporous carbons……. 82

Table 5.1: Reactor dimensions……152

Table 5.2: Instruments used for the analysis of FTS products……... 161

Table 6.1: Supported catalysts composition…….. 169

Table 6.2: Textural properties of supported catalysts…… 171

Table 7.1: Summary of reactions conditions used for the FTS of Fe/carbon catalysts…… 193

Table 7.2 Changes in deactivation rate as a function of time on stream..202

Table 7.3: FTS conversion, Productivity and Selectivity for potassium promoted Fe catalysts……. 212

Table 8.1: FTS conversion, Productivity and Selectivity for potassium promoted Fe catalysts…….. 237

Table 9.1: FTS conversion, Productivity and Selectivity for potassium promoted Fe catalysts…….. 253

List of Figures

Page number

Figure 1.1: The structure of Zeolite A. Silicon or aluminium atoms surrounded by four oxygen atoms link together to form an open network cavities connected by pores……... 6

Figure 1.2: Tetraalkylammonium ions (a), in which a positively charged nitrogen atom contains a four carbon chain, can act as templates around which silicate and aluminate ions link together to form the walls of a zeolite's cavities…… 8

Figure 1.3: Schematic diagram of the pore structure of ZSM-5…….. 9

Figure 1.4: Diagram of cloverite. The material was so named because the internal cavity of the molecule is reminiscent of a four leaf clover…… 10

Figure 1.5: Schematic diagram showing the formation mechanism of MCM-41……. 15

Figure 1.6: General steps proceeding in the sol-gel synthesis of ceramic materials…… 19

Figure 1.7: A schematic overview of the three liquid crystal templating models……. 25

Figure 2.1: An electronic devise known as a diode can be formed by joining two nanoscale carbon tubes with different

electronic properties…… 43

Figure 2.2: Template synthesis route to nanostructured materials using mesoporous silica templates…….. 49

Figure 2.3: TEM image of CMK-1 prepared from mesoporous MCM-48 template…….. 51

Figure 2.5: Transmission electron micrograph (TEM) of mesoporous SNU-1 carbon. …… 55

Figure 2.4: TEM image of CMK-5 obtained after the complete removal of SBA-15 template…… 53

Figure 2.6: TEM image of ordered and graphitic mesoporous carbon CMK-3G……. 57

Figure 3.1: TGA profile (in nitrogen) of a blank of polystyrene, acid + toluene…….. 81

Figure 3.2: TEM image of sample formed by single impregnation of MCM-48 with polystyrene/acid/toluene……. 83

Figure 3.3: Plot of amount of polystyrene impregnated onto MCM-48 (in the 1st step of the two carbonization process); (a) ▲ - against product pore volume and (b) ● - against product surface area…… 85

Figure 3.4: XRD patterns of MCM-48 after different treatments: (a) - MCM-48 calcined, (b) – two step carbonised MCM-48

(0.5 g polystyrene in the 1st step); (c) – two step carbonized MCM-48 (1.25 g polystyrene in the 1st step); (d) – two step carbonised MCM-48 (1.50 g polystyrene in the 1st step); (e) one step carbonised MCM-48 (1-2 g polystyrene)…….. 86

Figure 3.5: XRD patterns of (a) MCM-48 calcined, (b) MCM-48 carbonised and (c) pyrolysed mesoporous carbon sample, template removed……. 88

Figure 3.6: SEM images of (a) - MCM-48 silica template and (b) - mesoporous carbon…….. 90

Figure 3.7: SEM images of MCM-48 silica template (a) - calcined (b) – calcined and heated to 900 ^{o}C for 2 h. The material in the circle was used to calculate the size of the particles… 91

Figure 3.8: High resolution TEM images showing the (a) morphology and (b) structural organization of MCM-48 silica particles; and (c) morphology and (d) structural organization of sample carbonised with polystyrene/acid/toluene, pyrolysed at 900 ^{o}C for 2 h…….. 94

Figure. 3.9: A graphitised carbon deposited onto MCM-48 silica, two step carbonisation (1st step = 0.5 g and 2nd step = 0.75 g polystyrene). The figure shows limited interaction

between carbon and silica particles…… 95

Fig 3.10: A highly graphitised mesoporous carbon (taken at a higher magnification) showing the parallel order of graphene sheets that are linearly arranged…….. 96

Figure 3.11: Nitrogen adsorption-desorption isotherm of (a) MCM-48 silica template and (b) a mesoporous carbon, two step carbonization (1st step = 0.5 g and 2nd step = 0.75 g polystyrene)…… 99

Figure 3.12: Pore size distributions of (a) - MCM-48 silica template and (b) a mesoporous carbon from the desorption curve, two step carbonization (1st step = 0.5 g and 2nd step = 0.75 g polystyrene)…….. 101

Figure 3.13: TGA profiles of (a) - MCM-48, (b) – carbonized MCM-48 sample and (c) mesoporous carbon (template removed)…. 102

Figure 3.14: EDX profile of a typical mesoporous carbon……. 104

Figure 3.15: XRD pattern of mesoporous carbon (2 theta > 10°) showing the structural organization of carbon, (C = carbon), two step carbonization (1st step = 0.5 g and 2nd step = 0.75 g polystyrene)…… 106

Figure 3.16: Raman spectra of the mesoporous carbon, two step carbonization (1st step = 0.5 g and 2nd step = 0.75 g

polystyrene)…… 107

Figure 4.1: Trends in crude oil prices from 1970 to 2005…… 120

Figure 4.2: The overall Fischer-Tropsch process scheme……. 127

Figure 4.3: Anderson-Shulz-Flory distribution plot. Hydrocarbon selectivity as a function of the chain growth probability factor α, calculated using the above ASF equation……. 132

Figure 4.4: Possible reactors for Fischer-Tropsch synthesis. a. Slurry bubble column reactor; b. ARGE Multitubular fixed bed reactor; c. Circulating fluidized bed reactor; d Fluidized bed reactor…….. 134

Figure 5.1: Schematic diagram of the CSTR reactor set up……. 151

Figure 5.2: Typical on-line gas chromatograms for hydrocarbon products. (a) oil and (b) wax FID signals……. 160

Figure 6.1: TPR spectra of (a) 15%Fe/2%K/AC; (b) 15%Fe/2%K/MC and (c) 15%Fe/2%K/MCM-48……. 175

Figure 6.2: XRD patterns of (a) 15%Fe/2%K/MC, (b) 15%Fe/2%K/MCM-48 and (c) 15%Fe/2%K/AC. Peaks: 1 – mesoporous materials; 2 – α-Fe_2O_3; 3 – Carbon and 4 - α-Fe_3O_4 and γ-Fe_2O_3……. 178

Figure 6.3: Electron microscopy of activated carbon support;

a – SEM image and b – high resolution TEM image…… 181

Figure 6.4: The HR-TEM images of two 15%/2%/AC samples; a – Fe particles on the surface of the carbon fiber and Fe particles dispersed on the surface of the activated carbon..182

Figure 6.5: HR-TEM images of Fe nanoparticles; a – nucleation of Fe nanoparticles and b – crystallinity of the Fe nanoparticles……. 183

Figure 6.6: SEM images images of (a) mesoporous carbons and (b) 15%Fe/2%K/MC…….. 184

Figure 6.7: HR-TEM images of 15%Fe/2%K/MC samples…… 185

Figure 6.8: HR-TEM images of 15%Fe/2%K/MCM-48 taken from different angles…… 186

Figure 7.1: CO conversion as a function of time on stream for 15% Fe /AC promoted with 2, 5 and 10 % K…….. 198

Figure 7.2: Syngas conversion as a function of time on stream for 15%Fe/AC promoted with 2, 5 and 10 % K…… 199

Figure 7.3: Deactivation for 15% Fe on activated carbon with 2, 5 and 10% K promotion as a function of time on stream…….. 203

Figure 7.4: EDX spectrum of activated carbon support……. 207

Figure 7.5: Methane selectivity as a function of time on stream for 15% Fe on activated carbon after 2, 5 and 10 % K promotion…. 209

Figure 7.6: CO_2 selectivities as a function of time on stream for 15% Fe/AC catalysts after 2, 5 and 10 % K loadings…….. 210

Figure 7.7: ASF product distribution for the 15%Fe/AC catalyst impregnated with various amounts of potassium……. 215

Figure 8.1: CO conversion as function of time on stream for 15 %Fe/mesoporous carbon loaded with different amounts of potassium……. 229

Figure 8.2: Syngas conversion function of time on stream for 15%Fe/mesoporous carbon loaded with different amounts of potassium…….. 229

Figure 8.3: Methane selectivity function of time on stream for 15%Fe/mesoporous carbon loaded with different amounts of potassium…….. 233

Figure 8.4: CO_2 selectivity function of time on stream for 15 %Fe/mesoporous carbon loaded with different amounts of potassium……. 234

Figure 8.5: ASF- product distribution of 15%Fe/MC impregnated with various amounts of potassium……. 239

Figure 9.1: CO conversion as a function of time on stream of the 15%Fe/2%K catalyst on different supports…… 249

Figure 9.2: Syngas conversion as a function of time on stream of

15%Fe/2%K catalyst on different supports…… 250

Figure 9.3: Methane selectivity of 15%Fe/2%K on different supports as a function of time on stream……. 251

Figure 9.4: CO_2 selectivity as a function of time on stream of the 15%Fe/2%K catalyst on different supports…….. 252

Figure 9.5: ASF distribution of precipitated and promoted Fe catalysts on different supports……...256

List of Abbreviations and Symbols

α	-	Alpha
AC	-	Activated carbon
ASF	-	Anderson, Schultz and Flory
θ	-	Theta
BET	-	Brunuaer, Emmet and Teller
BJH	-	Barret, Joyner and Halenda
^{o}C	-	Degrees celcius
CO	-	Carbon monoxide
CO_2	-	Carbon dioxide
EDX	-	Energy dispersive X-ray
$Fe(NO_3)_3.9H_2O$	-	Iron nitrate (III) nonahydrate
Fig.	-	Figure
FID	-	Flame ionization detector
FT	-	Fischer-Tropsch
FTS	-	Fischer-Tropsch synthesis
GC	-	Gas chromatography
GHSV	-	Gas hour space velocity
H	-	Hour
H_2	-	Hydrogen

HF	-	Hydrofluoric acid
H_2O	-	Water
ml	-	Milliliters
MC	-	Mesoporous carbon
MCM-48	-	Mobil's composition of matter – 48
nm	-	Nanometer
Pa	-	Pascal
PSD	-	Pore size distribution
NaOH	-	Sodium hydroxide
NH4OH	-	Ammonium hydroxide
SAS	-	Sasol advanced synthol
SiO_2	-	Silica
SEM	-	Scanning electron microscopy
SV	-	Space velocity
TCD	-	Thermal conductivity detector
TEM	-	Transmission electron microscopy
TEOS	-	Tetraethoxyorthosilane
TGA	-	Thermogravimetric analysis
TPR	-	Temperaure programmed reduction
WGS	-	Water gas shift
XRD	-	X-ray diffraction spectroscopy

XRF	-	X-ray fluorescence spectroscopy
%	-	Percentage

PART I: TEMPLATE-DIRECTED SYNTHESIS OF MESOSTRUCTURED SILICA AND CARBONACEOUS MATERIALS

Chapter One

Template–Directed Synthesis of Structural Materials: A Review

1.1 Introduction

Over the last decade, there has been an ever increasing interest and research effort in the synthesis, characterization, functionalisation, molecular modeling and design of porous materials. The main challenges in this research area include the fundamental understanding of structure-property relations and the tailor-design of nanostructures with specific properties and for particular applications. Research efforts in this field have been driven by rapidly emerging applications of these materials such as in biosensors, drug delivery, gas separation, energy storage and fuel cell technology, nanocatalysis and photonics [1]. These applications offer exciting new opportunities for scientists to develop new strategies and techniques for the synthesis of these materials.

This chapter provides a review of recent developments in nanoporous materials. It covers the following topics: introduction to porous materials and the synthesis

and applications thereof, the background of the sol-gel chemistry process and the synthesis of metal oxides and organic-inorganic composites.

1.2 Porous materials

In the past decade, significant advances in the synthesis of porous materials have given rise to the preparation of a myriad of various supports [1]. These porous materials have been tailor-made for their intended purposes.

The presence of "holes" in a material can give that material a number of unique properties that the equivalent dense materials would not possess. A classical example to illustrate this phenomenon is a "bone". A bone has an open porous structure which is rigid and strong enough to provide support for our bodies, yet it is light and does not overburden us with its weight. Making holes in a material reduces the density of that material at a much faster rate than it reduces its strength [1]. Thus, porous materials can be viewed as a kind of composite between solid and air in which the air spaces play an active role in determining the properties of the material.

In recent times, the pores in materials have taken on a new significance. These micro-environments provide a medium in which scientific experiments can be

conducted in the nano-scale range. So, in a sense, the channels are like "molecular test tubes" and can be used for carrying out reactions with only a few atoms at a time. Thus, constructing and manipulating porous materials has become one of the hallmarks of the ever increasingly popular science of nanotechnology as well as catalysis [1,2].

Furthermore, the design and synthesis of porous materials is a current challenge in solid-state chemistry. For many applications, the precise control of pore dimensions is the limiting factor. A porous material of good quality should provide the following properties [2]:

1. A narrow pore size distribution.
2. A readily tunable pore size over a wide range of sizes.

In addition, high chemical, thermal, hydrothermal and mechanical stabilities as well as appropriate particle size, high surface area and pore volume are required. Depending on the predominant pore size, the solid materials are classified by IUPAC rules [3]:

1. microporous: pore size < 2 nm,
2. mesoporous: 2 nm < pore size < 50 nm,
3. macroporous: pore size > 50 nm.

At the present time, applications for macroporous compounds are relatively limited due to their low surface area and large non-uniform pores. In contrast, micro- and mesoporous materials, generally called nanoporous materials, are very suitable for size-specific applications in catalysis and separation [4].

1.2.1 Zeolites

The most well known and possibly best studied of all forms of materials is the zeolite family. The name zeolite is derived from the Greek word for "boiling stone" and its name hails from the fact that when heated, these minerals bubble and steam due to the vaporisation of water trapped inside the labyrinth of channels and cavities that comprise these materials [1].

Experimental studies have shown that the pores (channels) of zeolites are only a few angstroms wide and hence they are classified as microporous materials. As already mentioned above, such materials typically have pore diameters less than 2 nm. These pores, unlike the larger pores in pumice and sandstone, are not merely flaws in the minerals but are intrinsic elements in their crystal structures. These channels take on a very ordered, periodic structure and this is of great consequence for many of the important applications of zeolites.

Natural zeolites are comprised of the elements: aluminium, silicon, and oxygen interlinked into an extended network with the general chemical formula: $[M_{x/n}(AlO_2)]_x \cdot [SiO_2]_y \cdot mH_2O$ [5]. The basic structural units are tetrahedral SiO_4 and AlO_4 units. These units are linked via the oxygen atoms at their corners into rings, which define the necks and the faces of cavities into which the pores feed (Fig. 1.1).

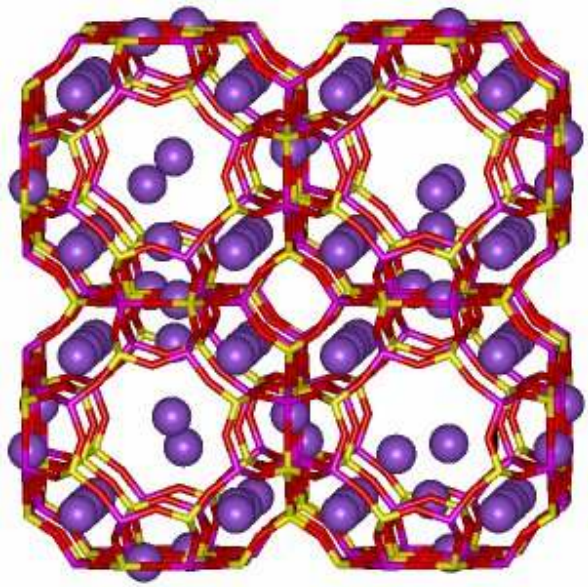

Figure 1.1: The structure of Zeolite A. Silicon or aluminium atoms surrounded by four oxygen atoms link together to form an open network cavities connected by pores [1].

The pore diameter of a typical zeolite is 0.4 – 0.7 nm and the cavities or "supercages" that these pores open into can be as large as 1 – 1.3 nm across [6]. In a sense, zeolites can be considered to be "all surface". For example, a crystal weighing just 1 gram can have a surface area as large as 900 m^2 [1] – the size of two basketball courts!

The aluminosilicate framework bears a negative charge that is cancelled out by a positively charged metal ion, such as sodium, which sits within the cavities of the material. These counter ions are held loosely within the cavities and can be easily exchanged, thus making zeolites good ion-exchange materials.

Many non-natural zeolites have also been synthesized by chemical means, providing a gallery of pore sizes and shapes. Scientists at Imperial College in London made the first synthetic zeolites in the 1930's [1]. They dissolved silica and aluminium hydroxide under high pressures and temperatures, thus mimicking the natural conditions under which zeolites form. In later years, less extreme methods of synthesizing zeolites were found. However, it wasn't until the 1960's when a team of researchers at Mobil Oil Corporation discovered that they could control the pore size of zeolites that the field of zeolites blossomed. The researchers added an organic ion to the reaction mixture and found that the

structure that formed could be accurately controlled by the choice of the ion. The organic ion that they used was the tetraalkylammonium ion (Fig. 1.2).

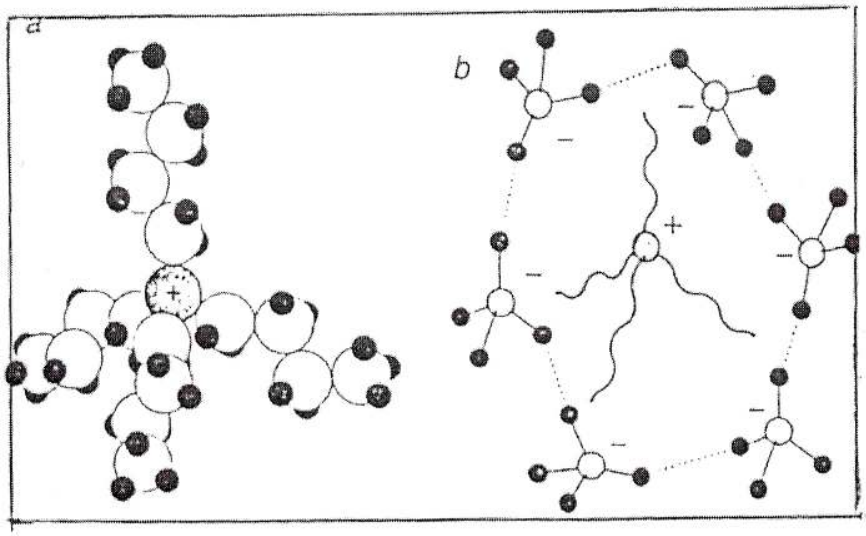

Figure 1.2: Tetraalkylammonium ions (a), in which a positively charged nitrogen atom contains a four carbon chain, can act as templates around which silicate and aluminate ions link together to form the walls of a zeolite's cavities [1].

They suggested that these ions become incorporated into the crystal lattice in place of the metal ions. Since they are much larger than sodium or calcium ions, they yield zeolites with larger aluminosilicate frameworks. This has led scientists into proposing that the organic ion acts as a template for the formation of the zeolite pores [7]. The negatively charged silicate and aluminate ions come

together around the positive alkylammonium ions and link together to form "shells" whose size is determined by the templating agent.

The Mobil approach yielded a synthetic zeolite that has become one of the most important zeolitic catalysts synthesised to date. This zeolite was christened ZSM-5 and was templated from the tetralkylammonium ions with three carbons in each alkyl chain. It contains a series of parallel pores interlinked by short channels (Fig. 1.3).

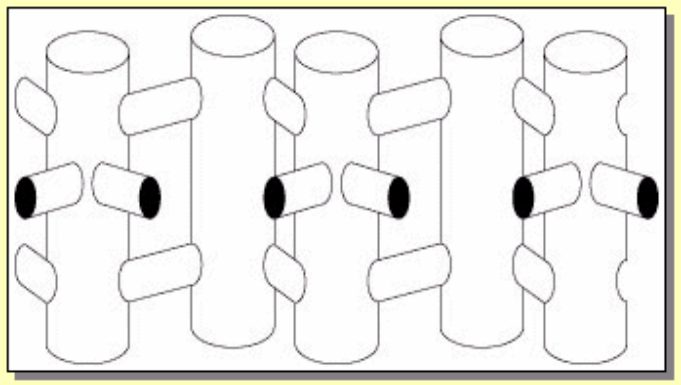

Figure 1.3: Schematic diagram of the pore structure of ZSM-5 [1].

Other variations in the synthetic strategies of scientists include exchanging the SiO_4 units with PO_4 units as well as substituting oxygen atoms with sulphur and selenium atoms. Both techniques have proven to be successful. However, the

thermal stability of aluminophosphates is poor and thus they are not suitable for catalytic applications. An example of such a compound that was synthesized is "cloverite" (Fig. 1.4).

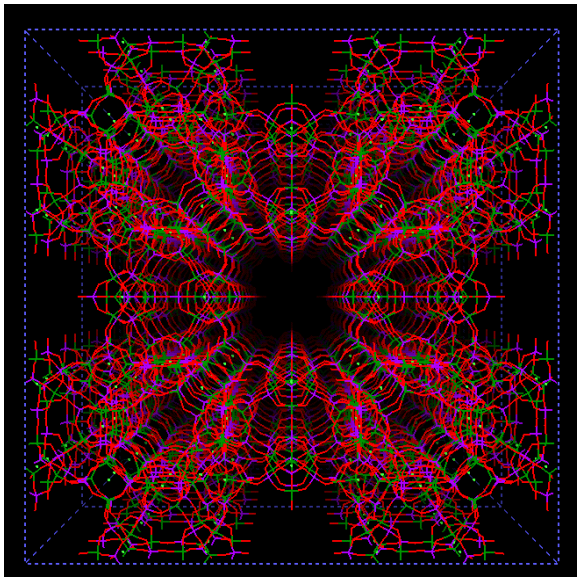

Figure 1.4: Diagram of cloverite. The material was so named because the internal cavity of the molecule is reminiscent of a four leaf clover [1].

In retrospect, it is now obvious that a zeolite-like synthesis with larger templating agents should also lead to larger pore sizes. With this strategy it should be possible to transfer the specific advantages of zeolites, i.e. their crystallinity and

sharply defined pore sizes, from the micro- to the mesoporous regime. But for a long time, all the attempts to enlarge the pore size distinctly beyond the 1.3 nm limit failed.

1.2.2 Applications of Zeolites

As previously mentioned, the aluminosilicate framework of the zeolite houses a positively charged metal ion (typically sodium) in its cavity. These metal ions sit loosely in the cavities and can be easily exchanged with other similarly sized metal ions. This makes zeolites ideally suited for ion exchange processes such as the removal of calcium from water to soften it or the extraction of toxic metals from industrial wastes [1,4].

Due to their acidic nature, zeolites also make good catalysts for the petrochemical industry. When a proton from water becomes attached to the aluminosilicate framework, the zeolite becomes a very powerful acid (much stronger than concentrated sulphuric acid). This acid is capable of protonating even the most inert hydrocarbons. Once protonated, these molecules can then undergo skeletal rearrangements or isomerisations to form new compounds. Typically, either small fragments are lost or branches are shifted within the hydrocarbon molecule.

Another critical reason why zeolites make good industrial catalysts is that the particular reactions that they catalyze are determined by the size and shape of their pores [4]. Thus, they are highly selective rather than indiscriminate. Consequently, hydrocarbons that are too big to fit into pores of the catalyst will not be transformed. This means that they can "selectively extract" only certain compounds from the complex mixture of hydrocarbons in crude oil, leaving the others untouched. Product specifity also occurs. This implies that only products with the "right" dimensions can form in the cavities of the catalysts.

Due to their high selectivity and ability to absorb only specific molecules into their cavities, zeolites have also been dubbed as "molecular sieves" [1].

1.2.3 The Mobil M41S materials

In the 1990's, a team of researchers at Mobil made a novel discovery [1,8,9]. They were exploring the use of surfactants for the templated synthesis of zeolitic materials, using tetraalkylammonium ions (similar to those used in the synthesis of ZSM-5) but with longer alkyl chains – typically 12 – 20 carbons in each chain. They anticipated that the longer alkyl chains would generate stronger interactions between the organic molecules thus enabling them to construct new framework structures. In reality they actually synthesized structures that they could never

have imagined were possible! These new materials were named M41S materials and are characterized by pore diameters that can be adjusted in the wide range between 1.5 and 10 nm. The pore size distribution is nearly as sharp as that of conventional zeolite-type materials.

After calcination at 500 ^{o}C to burn off the template molecules, a material with extremely high surface area was obtained. They called this material MCM-41 [10 – 19] and it was the first mesoporous material to be prepared. This structure had an ordered array of hexagonally-packed cylindrical pore channels, a surface area greater than 1000 m^2/g and uniform pore sizes that can be tailored from 20 to 100 Å in diameter. In addition to the hexagonal form, cubic (MCM-48) [20–30] and layered (MCM-50) phases were also obtained [31], all of which were classified as members of the M41S family.

(a) Formation mechanism of MCM-41

The surfactant molecules used in the synthesis of MCM-41 are not large enough to imprint pores the size of those found in the structure and this led scientists to believe that the surfactant molecules were aggregating to form micelles and that it was the micelles that were acting as the templating agent for the observed material [1].

Although the details of the mechanism are unclear, it is assumed that the mechanism outlined below is the general manner in which the MCM-41 structure is formed.

At sufficiently high surfactant concentrations, cylindrical micelles are formed from the templating agent. This concentration corresponds to the critical micelle concentration for the particular surfactant used [1]. At slightly higher concentrations, hexagonal close packed arrays appear i.e. micelles stack together like logs. This phase is referred to as a liquid crystalline mesophase [8,9]. There is some uncertainty as to whether the mesophase forms prior to the addition of the silica species to the solution or whether the addition of the silica to the reaction medium assists in the formation of the mesophase. The silica precipitates into the gaps between the cylinders, thereby becoming imprinted with a hexagonal honeycomb pattern.

The surfactant molecules are removed by heating, leaving behind large cylindrical pores (Fig. 1.5).

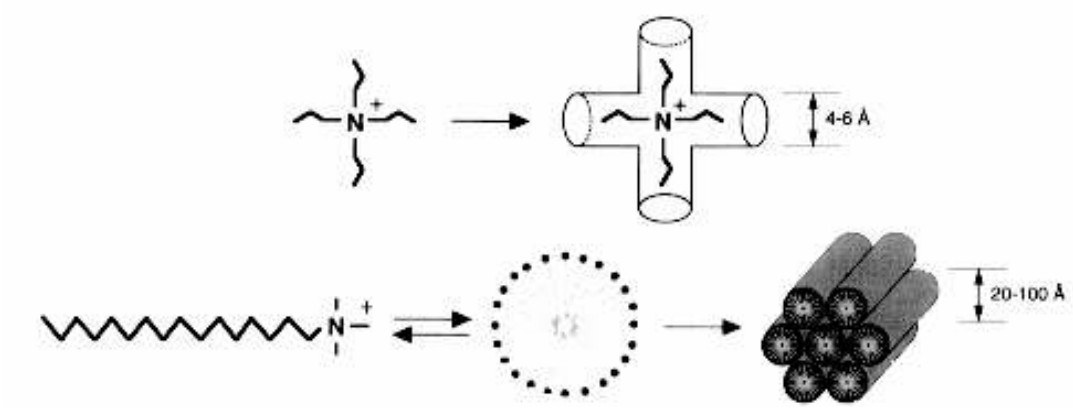

Figure 1.5: Schematic diagram showing the formation mechanism of MCM-41 [9].

(b) Formation mechanism of MCM-48 and MCM-50

The liquid crystal template mechanism for the formation of MCM-48 and MCM-50 is the same as the one reported for MCM-41 above. The mechanism is strongly supported both by the fact that, the alkyl chain length of the template influences the pore size and that the cubic and layered crystallization products corresponding to cubic (MCM-48) and lamellar (MCM-50) liquid crystal phases were found.

Further studies provided evidence, that no pre-existing liquid crystal phase is required for the formation of M41S silicates. Instead, a dynamic model, the co-

operative templating mechanism, has been proposed [32–36]. The basic idea is that the inorganic species promote the formation of the liquid crystal phase below the critical micelle concentration. Prior to the addition of the inorganic precursor, the surfactant molecules are in a dynamic equilibrium of different forms of micelles and single molecules. Upon the addition of the inorganic species, an inorganic-organic mesophase is formed. The polymerizing inorganic precursor leads to a continuous change of the charge density at the surfactant-inorganic interface, thus the system responds by steadily re-arranging the mesophase morphology. As a consequence, each surfactant can act as a template for the formation of several different mesostructures, depending on the reaction conditions [33].

1.3 The Sol-Gel Process

The conventional synthesis of certain ceramic materials involves the direct reaction of a mixture of powders. For these solid-state reactions, high temperature and small particle sizes are needed to provide high mobility of the reactants and maximum contact surface between the particles. Several difficulties are associated with this approach: thermodynamic factors often prevent, the metastable phases from forming, control over the size and morphology of solid particles is almost impossible, the stochiometry is difficult to reproduce,

impurities influence the process, poor chemical homogeneity and the formation of undesirable phases often occurs.

In the field of ceramics, chemistry has two major roles. It has to provide methods for the synthesis of novel ceramics, and techniques for the fabrication of these materials into useful shapes. Thus, new synthesis methods have been developed to synthesize ceramic materials [37,38].

Among these chemical methods e.g. co-precipitation (formation of intermediate precipitates with the correct stochiometry), reactions in molten salts (molten salts as solvent), hydrothermal techniques, polymer pyrolysis (synthesis of a polymeric compound, which is then fabricated into a shape and pyrolysed to the ceramic), topochemical and ion-exchange reactions, especially sol-gel processes have been extensively studied [39–47]. Starting from molecular precursors, an oxide network is obtained via inorganic polymerization reactions. Since these reactions occur in solution, sol-gel processing broadly describes the synthesis of inorganic oxides by wet chemistry methods. Compared to the conventional powder route, sol-gel processes allow a better control from the molecular precursor to the final product, offering possibilities in the tailoring of materials which result in high purity, high homogeneity, low temperature preparations, size and morphological

control of the particles, and the opportunity for the preparation of new crystalline and non-crystalline solids.

In general, the sol-gel procedure (Fig. 1.6) consists of the following steps [48]:

1. Preparation of the homogeneous solution either by dissolution of a metal organic precursors in an organic solvent that is miscible with water, or by dissolution of inorganic salts in water.
2. Conversion of the homogeneous solution to a sol by treatment with a suitable reagent (pure water or water with either HCl, NaOH or NH_4OH).
3. Aging: The sol changes into a gel by self-polymerization.
4. Shaping of the gel to the finally desired form (thin films, fibers, spheres, etc).
5. Conversion (sintering) of the shaped gel to the desired ceramic material generally at temperatures around 500 ^{o}C.

The most important step in this route is the formation of an inorganic polymer by a hydrolysis reaction, i.e. the transformation of the molecular precursor into a highly cross-linked solid. Hydrolysis leads to a sol, a dispersion of colloidal particles (solid particles with diameters of 1 – 100 nm) [41] and condensation forms a gel, an interconnected porous network filled with a liquid phase. This transformation is called the sol-gel transition [44]. During removal of the pore

liquid under hypercritical conditions, the network does not collapse and aerogels [49] are produced. When the pore liquid is removed by evaporation under normal conditions, shrinkage of the pores occurs and a xerogel is formed (Fig. 1.7).

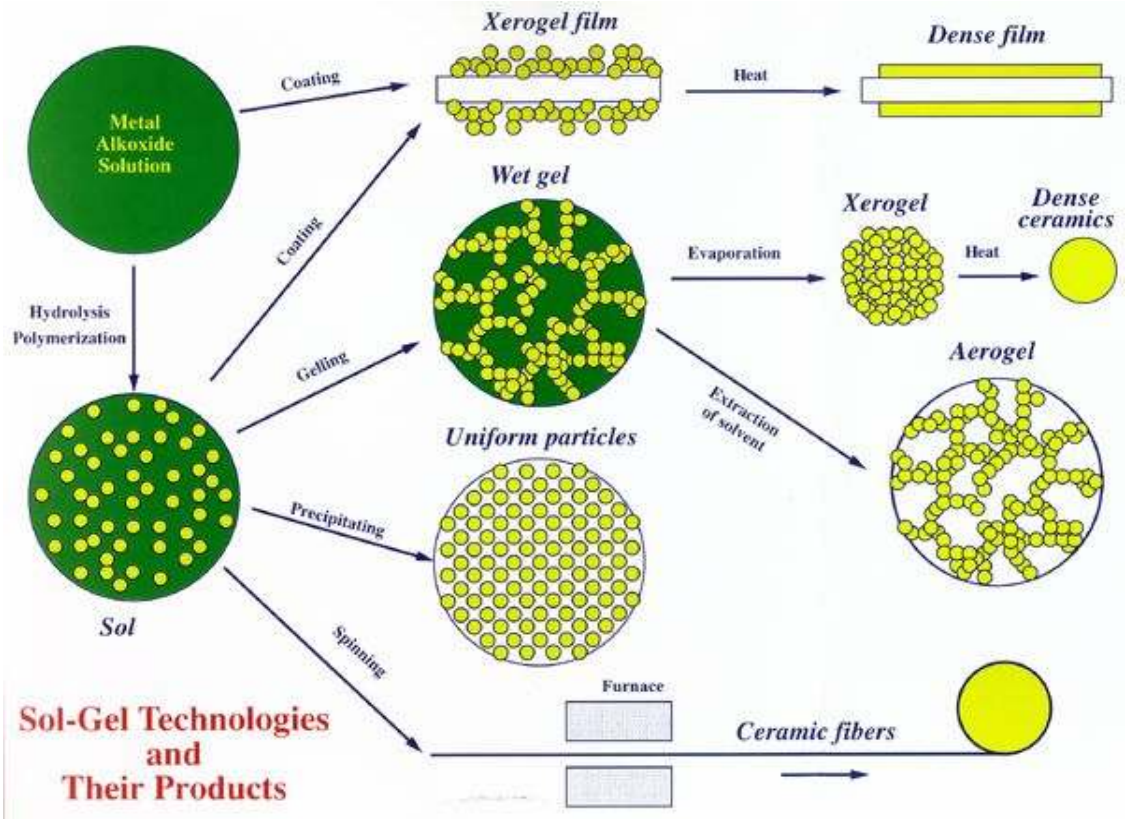

Figure 1.6: General steps proceeding in the sol-gel synthesis of ceramic materials [5].

One of the highly attractive features of the sol-gel process is the possibility to obtain the final ceramic materials in different forms like fibers, coatings, spheres, irregular aerogels and others by the control of the process conditions (cf. Fig. 1.6).

The sol-gel processes can be classified into two different routes depending on the nature of the precursors. The precursor can be:

a) an aqueous solution of an inorganic salt or

b) a metal organic compound [39].

The inorganic route involves the formation of condensed species from aqueous solutions of inorganic salts by adjusting the pH, by increasing the temperature or by changing the oxidation state. But this method has several disadvantages. The aqueous chemistry of transition metal ions can be rather complicated because of the formation of a large number of oligomeric species, which depend on the oxidation state and the pH or the reactant concentration. The role of the counter anions, which are able to coordinate the metal ion giving rise to a new molecular precursor with different chemical reactivity towards hydrolysis and condensation, is almost impossible to predict. These ions can influence the morphology, the structure and even the chemical composition of the resulting solid phase. Also, the removal of these anions from the final metal oxide product is often a problem. In addition, the formation of a gel rather than a precipitate from an inorganic

precursors is a very complicated process [39]. The process depends on the pH, concentration, addition mode, order of mixing the reactants, temperature, chemical composition of the aqueous solution and even the geometry of the reaction vessel can play a role.

In order to avoid all these problems, in many cases metal alkoxides are used for the preparation of metal oxides [50,51]. Metal alkoxides are strongly preferred as precursors, because they are soluble in organic solvents providing high homogeneity and they can easily be converted to the corresponding oxide. They are known for nearly all the elements [48,52-55]. The disadvantages are that only a few materials are commercially available and they can be, in general, very expensive.

The sol-gel process involving metal alkoxides is normally based on hydrolysis and condensation reactions. These nucleophilic reactions can be described as the substitution of alkoxy ligands by hydroxylated species XOH as follows [39]:

$$M(OR)z + yXOH \xrightarrow{-yROH} [M(OR)z\text{-}y(OX)y] \xrightarrow{\Delta T} MOx ,$$

where X stands for hydrogen (hydrolysis), a metal atom (condensation), or even an organic or inorganic ligand (complexation). Finally, heat treatment of the wet

gel results in the formation of the corresponding metal oxide. In this step, the amorphous network is first dried and then solidified.

Chemical aspects play an important role in studying and controlling the sol-gel process. The chemical reactivity of metal alkoxides towards hydrolysis and condensation depends mainly on the electronegativity of the metal atom, its ability to increase the coordination number, the steric hindrance of the alkoxy group, and on the molecular structure of the metal alkoxides (monomeric or oligomeric) [39]. The amount of added water in the hydrolysis step and how the water is added, determines whether the alkoxides are completely hydrolysed or not, and which oligomeric intermediate species are formed. Additional parameters are the polarity, the dipole moment, and the acidity of the solvent [43]. Thus, the large number of different reaction parameters as well as the simultaneous occurrence of hydrolysis and condensation reactions still prevents reliable methods to control completely the sol-gel transformation.

1.4 Structured Metal Oxides and Organic-Inorganic Composites

The principle of template synthesis has been known since the 1960's. But in the last few years the interest in this technique increased rapidly because of surprising discoveries in the field of supramolecular chemistry. The progress in the

synthesis of supramolecular assemblies is strongly connected with the introduction of template ions or molecules. The template acts as a structure-directing agent favouring the connection of the decisive bonds. As guests, the metal ion or molecule co-ordinates a ligand or host molecule, which is thereby brought into a suitable conformation for the formation of a specific product [56].

For the synthesis of a mesoporous media, long range ordered molecular arrays were used as templates instead of single molecules. The concept is based on the self-assembly of surfactants into micelles or into lyotropic liquid crystal phases with highly symmetric architectures [57]. Upon addition of a precursor molecule, condensation and polymerization at the surfactant-precursor interface gives rise to the corresponding organic-inorganic composite, i.e. the structure phase of the template assembly is imprinted on the inorganic framework. One important point in the preparation of such mesostructures is the adaptation of the template head-group to that of the inorganic precursor. Several different interactions at the interface between the organic and inorganic phase are possible [58]: i) ionic interactions, ii) hydrogen bonding and, iii) covalent bonds.

Cationic surfactants were used for the structuring of negatively charged inorganic species, and vice versa. Interestingly, also organic-inorganic combinations with identically charged partners are possible, but then a counter-charged ion has to

mediate the mesostructure. Mesostructures can also be formed without participation of charged building units. Using neutral template molecules, the interaction at the organic-inorganic interphase can either occur through hydrogen bonds or covalent connections.

As mentioned on page 10, in 1992 researchers at the Mobil Research and Development Corporation reported the exciting discovery of the novel family of molecular sieves called M41S [7,8]. Many research groups all over the world have since exploited this technique of supramolecular templating to produce not only mesoporous silicate and aluminosilicate materials but also mesostructured metal oxides [2,4,58-60]. The extension of this liquid-crystal templating mechanism into the field of transition metal oxide synthesis represented a major step forward towards tailoring catalytic, electronic and magnetic properties of redox-active materials.

Since one of the most important aspects in the synthesis of mesoporous materials is the interaction at the interphase between the organic and inorganic phase, three basic models were proposed (Figure 1.7). The *charged matched templating approach* is based on the compensation of the ionic charges between the surfactant head groups and the inorganic species. Hydrogen-bonding and van der Waals interactions are present between non-charged organic surfactants and

inorganic precursor, leading to the *neutral templating approach*. The *ligand-assited templating approach* assumes ligation of the surfactant head group directly to the metal alkoxide prior to hydrolysis and condensation [60].

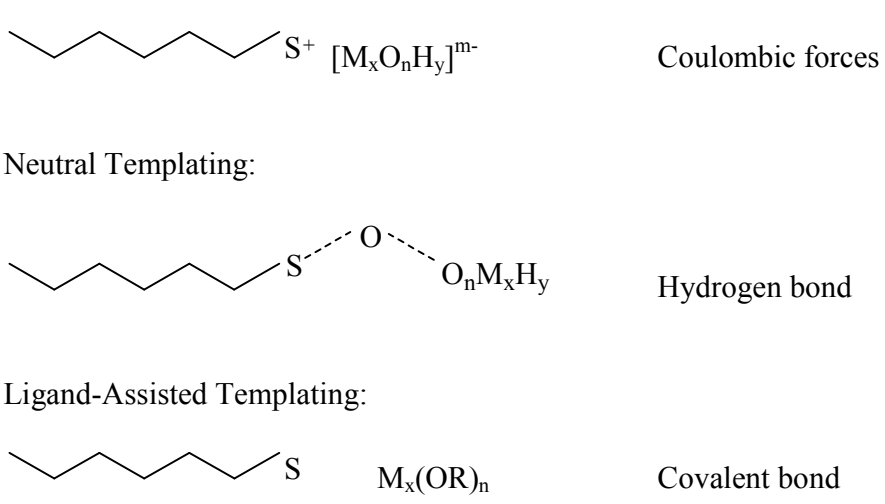

Figure 1.7: A schematic overview of the three liquid crystal templating models [39].

The first reports on the preparation of non-silica based mesostrucrures were published in 1994 by Stucky and co-workers [31,32]. Both, cationic and anionic surfactants were used in the presence of water soluble inorganic species. Control of the charge, geometry and association of the molecular inorganic species in solution by adjusting the pH, co-solvent, counter ions, and temperature opened up

the possibility to direct the formation of a particular phase [32]. But the materials obtained, except antimony, tungsten, and lead oxides, rather formed lamellar than hexagonal phases, and they were all thermally unstable and collapsed upon surfactant removal.

Many attempts have been made to apply this charge density matching approach for the synthesis of mesostructured metal oxides. Unfortunately, the use of methods based on electrostatic interactions generally met limited success, because most of the obtained phases were lamellar and thermally unstable. Both, lamellar phases as well as the three dimensional structures did not withstand any surfactant removal technique. One possible reason for the lack of stability is the low degree of condensation of the inorganic walls.

So the next step forward involved a neutral templating route for the preparation of mesoporous molecular sieves, based on hydrogen-bonding interactions and self-assembly between neutral surfactants and neutral inorganic precursors. Pinnavaia and co-workers used primary amine templates [61] or polyethylene oxide surfactants [62] and alkoxides as precursors for the synthesis of mesoporous silicates and mesoporous alumina [63]. In contrast to electrostatic templating pathways, the use of neutral templates allows for the facile recovery of the template by simple solvent extraction or evaporation methods.

A further extension in the field of template directed synthesis of transition metal oxides followed in 1995, when Ying and co-workers introduced the ligand assisted templating approach, based on the dative co-ordinate bond interactions between the template molecules and the inorganic precursor units [4,60,64-66].

In general, the procedure involves selective hydrolysis and condensation of metal alkoxides, chemically linked to a long-chain amine surfactant molecule prior to the hydrolysis step. It is important that the surfactant-precursor bond is strong enough to resist hydrolysis, but at the same time allowing easy chemical removal without damage to the mesostructure after aging. The formation mechanism is still not fully understood, since it does not require preformed micelles. It is unclear, how and at what stage of the synthesis self-assembly occurs [65].

These new families of mesoporous transition metal oxide molecular sieves, termed M-TMS1 (M = Nb, Ta, Ti, Zr) have remarkable thermal stabilities, and consist of a high surface area and hexagonally packed array of inorganic tubules. By varying the synthesis parameters like surfactant-to-metal ratio or surfactant chain length, layered and cubic faces were also achieved [60]. In addition, short-chain amines [67] or a template with a second hydrophilic functional group can be applied to generate microporous transition metal oxides with pore sizes of less than 2 nm [68].

The big limitation of the ligand-assisted templating approach is the fact that, up to now only the synthesis of mesoporous metal oxides was possible by starting from transition metal alkoxides and amine template molecules. Covalent bonding to atoms like oxygen and sulphur is still to be developed.

The synthesis of these mesoporous non-silica materials were carried out generally in aqueous solutions, using metal alkoxides or inorganic salts as precursors and low molecular weight surfactants for the assembly of the mesostructures. Recently, a new generalised method for the synthesis of large-pore mesoporous metal oxides with semi-crystalline frameworks was published by Stucky and co-workers [69, 70]. Compared to the pore sizes of the M41S materials (1.5 – 10 nm) and M-TMS1 (2 – 4 nm), the novel material exhibits large pores up to 14 nm. Amphilic poly-(alkylene oxide) block copolymers were used as structure directing agents and inorganic salts, rather than alkoxides, as precursors. The special feature of this procedure is the use of the inorganic precursors in predominantly non-aqueous media. Metal chlorides were reacted with an alcohol solvent to form metal-oxygen-chlorine networks [70]. The calcined samples showed no detectable chlorine, and the inorganic walls only consist of metal and oxygen. It is proposed that, the mechanism combines block copolymer self-assembly with complexation of the inorganic species [69].

Since the template-directed synthesis is a rapidly growing field, many different structured metal oxides and inorganic-organic composites have been reported since 1992.

1.5 Conclusions

The template method has become a very simple yet a powerful process for the synthesis of structural materials. These materials constitute a challenging domain in materials chemistry, which is experiencing explosive growth. The potential of these new structures has been recognized in the domain of optical devices, catalysis, separation techniques, controlled delivery, adsorption, and sensors.

Optimization of the properties of these materials requires a sound knowledge of the structure-property relationships, as well as a deeper understanding of the formation mechanisms. In the past five years, the increasing number of successful synthesis methods for mesostructured and mesoporous silica, metal oxides, etc. is the proof of the deeper knowledge and better design techniques that have become available.

1.6 References

[1] P. Ball, *Made to Measure*, Princeton Paperbacks, New York (1998).

[2] A. Sarayi and P. Liu, *Micropor. Mater.*, **12**, 149 (1997).

[3] K. S. W. Sing, D. H. Everett, R. A. W. Haul, L. Moscou, R. A. Pierotti, J. Rouquerol and T. Siemieniewska, *Pure & Appl. Chem*, **57**, 603 (1985).

[4] M. J. Niederberger, *Synthesis and characterisation of novel micro- and nanostructured vanadium, molybdenum, and iron oxides*, PhD thesis, Switzerland (2000).

[5] L. V. Interrante and M. J. Hampden-Smith, *Chemistry of Advanced Materials*, An Overview, WILEY-VCH (1998).

[6] P. Behrens and G. D. Stucky, *Angew. Chem. Int. Ed. Engl.*, **32**, 696 (1993).

[7] P. Behrens, *Adv. Mater.*, **5**, 127 (1993).

[8] C. T. Kresge, M. E. Leonowicz, W. J. Roth, J. C. Vartuli and J. S. Beck, *Nature*, **359**, 710 (1992).

[9] J. S. Beck, J. C. Vartuli, W. J. Roth, M. E. Leonowicz, C. T. Kresge, K. D. Schmitt, C. T-W. Chu, D. H. Olson, E. W. Sheppard, S. B. McCullen, J. B. Higgins and J. L. Schlenker, *J. Am. Chem. Soc.*, **114**, 10834 (1992).

[10] S. Biz and M. L. Occelli, Catal. *Rev.-Sci. Eng.*, **40**, 329 (1998).

[11] G. K. Chuah, X. Hu, P. Zhan and S. Jaenicke, *J. Mol. Catal. A: Chemical*, **181**, 25 (2002).

[12] R. Ryoo, J. M. Kim, C. H. Ko and C. H. Shin, *J. Phys. Chem*., **100**, 17718 (1996).

[13] V. B. Fenelonov, V. N. Romannikov and A. Y. Derevyankin, *Micropor. Mesopor. Mater.,* **28**, 57 (1999).

[14] L. Zhu, F-S. Xiao, Z. Zhang, Y. Sun, Y. Han and S. Qiu, *Catal. Today*, **68**, 209 (2001).

[15] A. Galarneau, D. Desplantier-Giscard, F. Di Renzo and F. Fajula, *Catal. Today*, **68**, 191 (2001).

[16] J. Rathousky, M. Zukalova, A. Zukal and J. Had, *Collect. Czech. Chem. Commun*., **63**,1893 (1998).

[17] G. Øye, J. Sjöblom and M. Stöcker, *Micropor. Mesopor. Mater.*, **27**, 171 (1999).

[18] M. Jaroniec, M. Kruk, H. J. Shin, R. Ryoo, S. Sakamoto and O. Terasaki, *Micropor. Mesopor. Mater.*, **48**, 127 (2001).

[19] W. Zhou and J. Klinowski, *Chem. Phys. Lett.*, **292**, 207 (1998).

[20] M. Kruk, M. Jaroniec, R. Ryoo and S. H. Joo, *Chem. Mater*., **12**, 1414 (2000).

[21] J. Xu, Z. Luan, M. Hartmann and K. Larry, *Chem. Mater*., 2928 (1999).

[22] J. M. Kim,Y. Sakamoto, Y.K. Hwang, Y-U. Kwon, O. Terasaki, S-E. Park and G.D. Stucky, *J. Phys. Chem*. *B*, **106**, 2552 (2002).

[23] R. Ryoo, S. H. Joo and J. M. Kim, *J. Phys. Chem. B*, **103**, 7435 (1999).

[24] W. Zhao and Q. Li, *Chem. Mater*., **15**, 4160 (2003).

[25] M. J. Kim, S. K. Kim and R. Ryoo, *Chem. Commun*., **259**, (1998).

[26] K. Schumacher, P.I. Ravikovitch, A. Du Chense, A. V. Neimark and K. A. Unger, *Langmuir*, **16**, 4648 (2000).

[27] D. Kumar, K. Schumacher, C. von Hohensche, M. Grun and K. A. Unger, *Coll. Surf. A: Physicochem. Eng. Aspects*, **187**, 109 (2001).

[28] A. Sarayi, *Chem. Mater*., **8**, 1840 (1996).

[29] C-G. Wu and T. Bein, *Science*, **264**, 1757 (1994).

[30] Z. Li and M. J. Jaroniec, *J. Phys. Chem. B*, **108**, 824 (2004).

[31] J. C. Vartuli, K. D. Schmitt, C. T. Kresge, W. J. Roth, M. E. Leonowicz, S. B. McCullen, S. D. Hellring, J. S. Beck, J. L. Schlenker, D. H. Olson and E. W. Sheppard, *Chem. Mater*., **6**, 2317 (1994).

[32] X. S. Zhao, G. Q. Lu and G. J. Millar, *Ind. Eng. Chem. Res*., 35 (1996).

[33] Q. Huo, D. I. Margolese, U. Ciesla, P. Feng, T. E. Gier, P. Sieger, R. Leon, P. M. Petroff, F. Schuth and G. D. Stucky, *Nature*, **368**, 317 (1994).

[34] Q. Huo, D. I. Margolese, U. Ciesla, D. G. Demuth, P. Feng, T. E. Gier, P. Sieger, A. Firouzi, B. F. Chmelka, F. Schuth and G. D. Stucky, *Chem. Mater*., **6**, 1176 (1994).

[35] A. Monnier, F. Schuth, Q. Huo, D. Kumar, D. Margolese, R. S. Maxwell, G. D. Stucky, M. Krishnamurty, P. Petroff, A. Firouzi, M. Janicke, B. F. Chmelka, *Science*, **261**, 1299 (1993).

[36] A. Firouzi, F. Atef, A. G. Oertli. G. D. Stucky and B. F. Chmelka, *J. Am. Chem. Soc*., **119**, 3596 (1997).

[37] D. Segal, *J. Mater. Chem*., **7**, 1297 (1997).

[38] J. Gopalakrishnan, *Chemistry of Advanced Materials, A 'Chemistry for the 21st Century' monograph*, Blackwell Scientific Publications, Oxford (1993).

[39] J. Livage, M. Henry and C. Sanchez, *Prog. Solid St. Chem*., **18**, 259 (1988).

[40] C. J. Brinker and G. W. Scherer, *Sol-Gel Science: The Physics and Chemistry of Sol-Gel Processing*, Academic Press, San Diego (1990).

[41] L. L. Hench and J. K. West, *Chem Rev*., **90**, 33 (1990).

[42] H. Reuter, *Adv. Mater*., **3**, 258 (1991).

[43] H. Reuter, *Adv. Mater*., **3**, 568 (1991).

[44] R. Corriu and D. Leclercq, *Angew. Chem. Int. Ed. Engl*. **35**, 1420 (1996).

[45] C. P. Ballard and A. J. Fanelli, *Chemistry of Advanced Materials, A 'Chemistry for the 21st Century' monograph*, Blackwell Scientific Publications, Oxford (1993).

[46] J. Livage, *Adv. Zeol. Sci. Appl.*, **85**, 1 (1994).

[47] S. Sakka, *J. Sol-Gel Sci. Tech.*, **3**, 69 (1994).

[48] R. C. Mehrota and A. Singh, *Prog. Inorg. Chem.*, **46**, 239 (1997).

[49] N. Husing and U. Schubert, *Angew. Chem. Int. Ed. Engl*., **37**, 22 (1998).

[50] L. G. Hubert-Pfalzgraf, *New J. Chem.*, **11**, 663 (1987).

[51] D. C. Bradley, *Chem. Rev*., **89**, 1317 (1989).

[52] D. C. Bradley, R. C. Mehrota and D. C. Gaur, *Metal Alkoxides*, Academic Press, London (1978).

[53] R. C. Mehrota, *Advances in Inorganic Chem. Radiochem.*, **26**, 269 (1983).

[54] R. C. Mehrota, A. Singh and S. Sogani, *Chem. Rev*., **94**, 1643 (1994).

[55] W. A. Herrmann, N. W. Huber and O. Runte, *Angew. Chem. Int. Engl*., **34**, 2187 (1995).

[56] R. Hoss and F. Vogtle, *Angew. Chem. Int. Engl*., **33**, 375 (1994).

[57] M. Antonietti and C. Goltner, *Angew. Chem. Int. Engl*., **36**, 911 (1997).

[58] P. Behrens, *Angew. Chem. Int. Engl*., **35**, 515 (1996).

[59] J. Y. Ying, C. P. Mehnert and M. S. Wong, *Angew. Chem. Int. Engl*., **38**, 57 (1999).

[60] D. M. Antonelli, A. Nakahira and J. Y. Ying, *Inorg. Chem*., **35**, 3126 (1996).

[61] P. T. Tanev and T. J. Pinnavaia, *Science*, **267**, 865 (1995).

[62] S. A. Bagshaw, E. Prouzet and T. J. Pinnavaia, *Science*, **269**, 1242 (1995).

[63] S. A. Bagshaw and T. J. Pinnavaia, *Angew. Chem. Int. Engl.*, **35**, 1102 (1996).

[64] D. M. Antonelli and J. Y. Ying, *Angew. Chem. Int. Engl.*, **35**, 426 (1996).

[65] D. M. Antonelli and J. Y. Ying, *Chem. Mater.*, **8**, 874 (1996).

[66] M. S. Wong and J. Y. Ying, *Chem. Mater.*, **10**, 2067 (1998).

[67] T. Sun and J. Y. Ying, *Nature*, **389**, 704 (1997).

[68] T. Sun and J. Y. Ying, *Angew. Chem. Int. Engl.*, **37**, 664 (1998).

[69] P. Yang, D. Zhao, D. I. Margolese, B. F. Chmelka and G. D. Stucky, *Nature*, **396**, 152 (1998).

[70] P. Yang, D. Zhao, D. I. Margolese, B. F. Chmelka and G. D. Stucky, *Chem. Mater.*, **11**, 2813 (1999).

Chapter Two

Carbonaceous Materials for Catalytic Applications

2.2 Introduction

Carbon is the sixth most abundant element in the universe. In addition, it is a very special element because it plays a dominant role in the chemistry of life. It was discovered in prehistory and was known to the ancients, who manufactured it by burning organic material, making charcoal. In homogeneous catalysis, carbon features as a prominent ligand in metal systems. Carbon is also used as a catalyst support material as it allows the anchoring of catalyst particles on a substrate which does not exhibit solid acid-base properties [1-4].

2.1.1 Carbon as a catalyst

Carbon may be used as a catalyst without an active component supported on it [2]. All applications are based on the simultaneous action of two functions. The first function is the selective chemisorption of an educt at the carbon through either ion-exchange or directly through the dispersive forces involving the

graphite valence electronic system. The other is the production of atomic oxygen occurring on the graphene faces of every carbon material. Both processes play a crucial role in catalysis, and in particular, surface patches with an intact graphene electronic structure act as a sink or source of electrons in catalytic reaction steps.

The fact that carbon is already catalytically active at ambient conditions and in aqueous media has led to considerable efforts in applying carbon as a catalyst in the condensed phases.

2.1.2 Carbon as a catalyst support

Carbon materials represent a unique family of supports because of the diverse nature of the different forms of carbon and complex functions they can perform [5-6]. From the sp^2 hybridized chemical bonding in the orderly structure of the graphitized carbons and the disordered turbostratic carbons like activated carbon, to the sp^3 hybridized configuration in diamond, the different allotropic forms of elemental carbon possess distinct bulk and surface properties which can be altered to modify their characteristics [7].

The reactivity of carbon without functional groups is low with respect to most elements. Exceptions occur when strong oxidising agents such as fluorine and the

alkali metals interact with carbon. Carbon supports are also relatively thermally stable, but in oxidising environments they are much less stable than the macroscopic burn-off temperature. Carbon is only reduced by hydrogen at high temperatures [1].

Carbon is thus a good material for catalyst supports because it is chemically inert, stable in an oxidising and reducing environment (at temperatures below 400 ^{o}C), exhibits mechanical resistance and has a high surface area [8]. Another appealing property of carbon is that there are many possibilities of modifying the surface with functional groups [9].

In the past three decades, the use of different forms of carbons as heterogenous catalyst supports has grown. Graphite and diamond have received some attention, with activated carbon perhaps being the most studied catalyst support of the other carbons because of the versatility of its properties such as porosity, surface area, and chemical nature, in addition to its mechanical resistance, stability and inertness [7]. Consequently, a voluminous literature on critical analyses of these aspects has been published [10-15].

Recently, there has been a growing interest in the synthesis of mesoporous carbonaceous materials for use in catalysis and nanotechnology applications [16-

19]. A strong incentive for their use is the replacement of activated carbons, whose properties have been shown to be difficult to control [10,11,13]. Furthermore, fewer problems with diffusion of reactants and products to and from the catalytically active sites are expected than with the microporous materials. The use of mesoporous silica templates for the preparation of such carbonaceous materials has attracted attention due to the special features portrayed by these silica materials. These silica templates have been shown to have a high surface area (1000-1500 m^2/g), high thermal and mechanical stability, tailored porosity and possibility of functionalization [20-30]. A considerable amount of research on the synthesis of mesoporous carbonaceous materials prepared from mesoporous silica frameworks has been performed by Ryoo and his co-workers [31-51]. These carbons are of great interest for certain emergent applications such as the adsorption/catalysis of large molecules or for energy storage in double layer capacitors, and more importantly as catalytic supports.

Even though porous carbonaceous materials are actually used in some industrial catalytic processes, their full potential has not been exploited yet because fundamental issues relating to their use have not become clear until the last decade. This chapter provides an introduction via a detailed literature review of the porous (templated and non-templated), ordered and mesoporous carbons. The chapter further describes the different methods used to synthesise these

carbonaceous materials by various authors. The advantages and disadvantages of the prepared carbons are also described.

2.2 Porous carbons

Porous carbons are commonly used as adsorbents and catalyst supports [32,37,39,40,42]. While many porous carbons are known to exhibit periodic structures resulting from the uniform stacking of graphene sheets and periodic arrangement of atoms within these sheets, carbons with periodic porous structures have only been synthesised recently.

Most porous carbons are primarily microporous. They are usually obtained by carbonization of precursors of natural or synthetic origin, followed by activation [39]. The microporous nature of the majority of porous carbons is well suited for many applications, including: molecular sieving and catalytic reactions of small molecules. However, there are numerous applications in which materials with mesoporous carbonaceous surfaces would be attractive. In these cases, the presence of wider pores, preferably in the mesopore range would be advantageous.

As a result of the need for emergent applications of mesoporous carbonaceous materials, there has been a great deal of interest in the synthesis of such materials. There are several methods to achieve this goal, including: carbonization of polymer aerogels [52,53], catalytic activation in the presence of certain metals [54], combination of physical and chemical activation [55], carbonization of polymer blends with one thermally unstable component [56], use of multiwalled carbon nanotubes [57] and the infiltration of an appropriate template by carbon precursors, followed by carbonization and template dissolution [33, 41, 45-49]. Until recently, none of these synthesis approaches was shown to be suitable for the synthesis of mesoporous carbons with mono-dispersed pores of well-defined size and shape.

Macroporous structures with periodic inverse opal structures were also reported recently [58], but the employed approach based on the templating with porous silica opal crystals cannot be readily generalised to the synthesis of carbons with periodic mesoporous or microporous systems. Other carbons that have been of interest as catalysts supports are described below.

2.2.1 Carbon nanotubes

Carbon nanotubes are cylindrical carbon molecules with properties that make them potentially useful in extremely small scale electronic and mechanical applications. They exhibit unusual strength and unique electrical properties, and are efficient conductors of heat [57].

A simple nanotube has a structure similar to a fullerene, but where a fullerene molecule has a spherical symmetry, a nanotube is cylindrical, with one end typically being capped with half a fullerene molecule. Their name derives from their size; nanotubes are only a few nanometers in width, and their length can be millions of times greater than their width. There are two main types of nanotubes: single-walled nanotubes (SWNTs) and multi-walled nanotubes (MWNTs) [57,59,60]. SWNTs comprise of a cylindrical graphene sheet of diameter ~1 nm capped by hemispherical ends. MWNTs comprise of several to tens of concentric cylinders of graphitic shells with a layer spacing of 0.3-0.4 nm, and their diameters range between 2 and 100 nm [60].

Carbon nanotubes (Fig. 2.1) are composed entirely of carbon-carbon bonds with the carbon having sp^2 bonds, similar to graphite. Stronger than the sp^3 bonds found in diamond, this bonding structure provides nanotubes with their unique

strength. The strength and flexibility of carbon nanotubes makes them of potential use in controlling other nanoscale structures, which suggests they will have an important role in nanotechnology engineering [57].

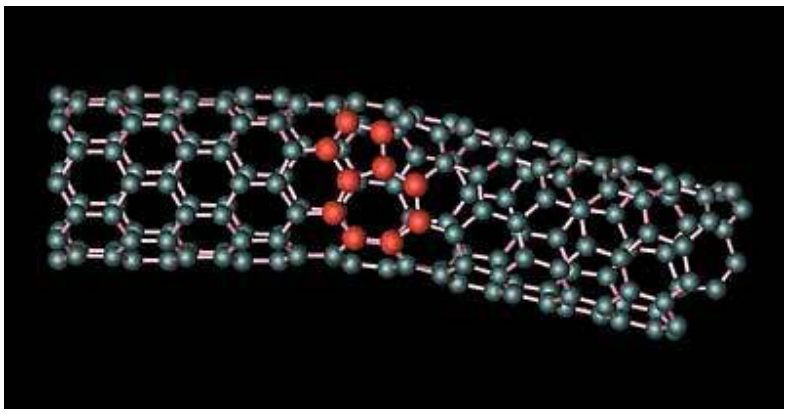

Figure 2.1: An electronic devise known as a diode can be formed by joining two nanoscale carbon tubes with different electronic properties [59].

While it has long been known that carbon fibers can be produced by means of a carbon arc, it was not until 1991 that Sumio Iijima [57], a researcher with the NEC laboratory in Tsukuba, Japan, observed that these fibers were hollow. This feature of nanotubes is of great interest to the physics community because it permits experiments in one-dimensional quantum physics.

Techniques have been developed to produce nanotubes in sizeable quantities, but their cost still prohibits their large scale use. Fullerenes and carbon nanotubes are not only products of high-tech laboratories; they are also formed in candle flames [59]. However, these naturally occurring varieties are highly irregular in size and quantity, and the high degree of uniformity necessary to meet the needs of research and industry is impossible in such an uncontrolled environment. There are several methods employed to make nanotubes, such as arc discharge, laser ablation, and chemical vapor deposition (CVD). In general, the CVD method has shown the most promise in being able to produce large quantities of nanotubes (compared to other methods) at lower cost. This is usually done by reacting a carbon-containing gas (such as acetylene, ethylene, ethanol, etc.) with a metal catalyst particle (usually cobalt, nickel or iron) at temperatures above 600 ^{o}C [59,60].

SWNT's exhibit periodic structures. Moreover, SWNT's can be opened, thus rendering their interiors accessible to adsorbate molecules [32]. However, the periodically arranged SWNT's are held together by weak van der Walls interactions, so these materials cannot be considered as systems with permanent ordered porosity. Moreover, MWNTs were found to exhibit broad pore size distribution in the micropore and mesopore ranges, and relatively small surface

areas, the latter being not only attributable to adsorption inside the tubes but also to a large extent to adsorption on the external surface of the tubes.

2.2.2 Activated carbon

Activated carbon (also called activated charcoal) is the more general term which is used to describe carbon materials mostly derived from charcoal. It denotes a material which has an exceptionally high surface area, typically determined by nitrogen adsorption, and this material contains a large amount of microporosity. These micropores provide superb conditions for adsorption to occur, since an adsorbing material can interact with many surfaces simultaneously. Sufficient activation for useful applications may come solely from the high surface area, though often chemical treatment is used to enhance the adsorbing properties of the material [7,53,54,61,62].

Activated carbon can generally be produced by two different processes [54]:

1. Chemical activation: Acids are usually mixed with the source material in order to cauterise the fine pores.
2. Steam activation: The carbonized material is mixed with vapours and /or gases at high temperature to activate it. The source material can be generated from several carbonic materials, e.g. nutshells, wood, coal.

Activated carbon may have a surface are in excess of 500 m^2/g with 1000 m^2/g being readily achievable. Other than the low mechanical and thermal stability of activated carbons, their broad pore size distribution and microporosity pose a disadvantage for the proper diffusion of the active metal to make mesoporous carbon materials for catalytic applications.

2.3 Templated Porous Carbons

Two decades ago, Knox *et al*. prepared the first ever templated porous carbon [63]. The authors reported that amorphous silica gel could be impregnated with polymer precursors that were then polymerized to form a continuous network surrounding the silica particles. Carbonization of the polymer coating and the subsequent dissolution of the silica template rendered a templated amorphous carbon. Later on, Bandosz and co-workers used the lithium form of taeniolite, intercalated with hydroxyaluminium and hydroxyl-aluminium-zirconium cations, to serve as the molecular template for the synthesis of microporous carbon-mineral nano-composites and derived carbons [64].

Zeolitic templates with periodic microporous structures were also employed in the carbon synthesis. An attempt was made by Kyotani and co-workers to prepare porous carbons by impregnating the channels of Y zeolite with propylene [65].

Pyrolytic carbon deposition was carried out by exposing the zeolite to propylene at high temperature and then the carbon was liberated by subjecting the zeolite/carbon to acid treatment.

On the other hand, phenol-formaldehyde polymers were synthesized and cured within the channel networks of zeolites Y, β and L, and dissolution of the aluminosilicate framework in HF yielded organic replicas. In contrast, complete collapse of the organic replica, to give a nonporous material occurred upon removal of zeolite L [66]. In this case, the authors claimed that the collapse of the structure was due to the one dimensional channel structure of the zeolite. Kruk *et al*. also used zeolitic templates and observed that the ordering characteristic of the template necessary to obtain the porous carbon structure was lost upon its dissolution [32]. Apparently, carbon frameworks formed in narrow pores of zeolites were not rigid enough to retain periodicity, although their integrity and structure were often retained to such an extent that the templated carbon particles exhibited the morphology of the zeolite template particles. Moreover, the zeolite-templated carbons had large specific surface areas and micropore volumes, without the activation usually required to develop an accessible microporous structure [32].

2.4 Ordered Mesoporous Carbons

The discovery of ordered mesoporous materials opened new opportunities in the synthesis of periodic carbon structures using the templating approach. Numerous techniques for preparing mesoporous carbons are well documented in the literature. However, only a few of these permit for an accurate control of the mesoporosity.

In general, the preparation of these materials [55] consists of:

a) the infiltration of the porous structure of an inorganic material (template) by the carbon precursor (generally a polymer or a prepolymer),
b) the polymerization of the infiltrated substance,
c) the carbonization of the nanocomposites formed
d) and finally, elimination of the template.

This procedure is very useful for synthesizing mesoporous carbons with controlled porous characteristics (Fig. 2.2).

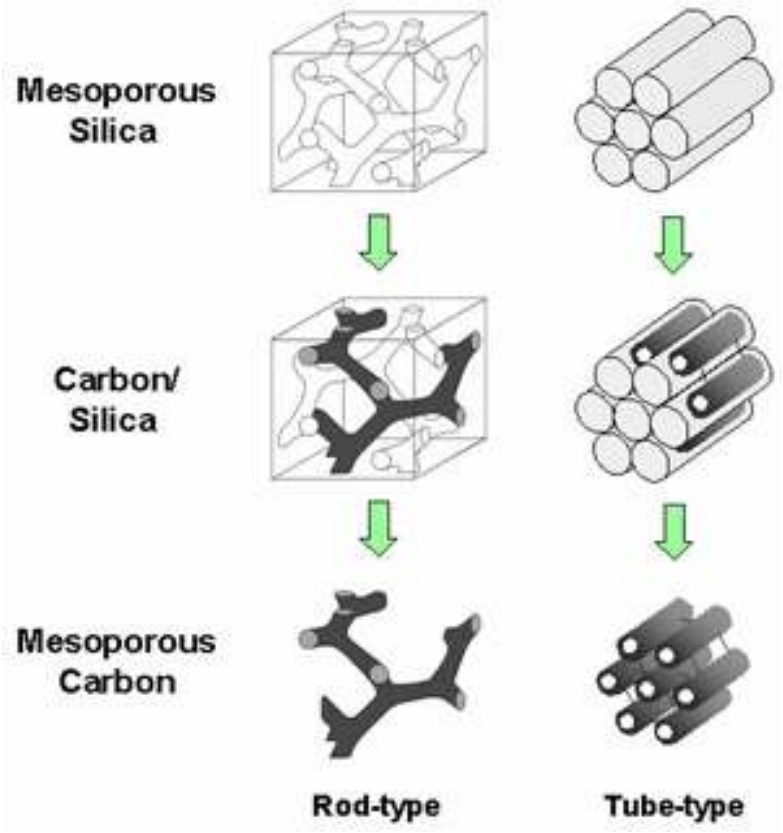

Figure 2.2: Template synthesis route to nanostructured materials using mesoporous silica templates [33]

In a typical synthesis, various carbon sources such as sucrose solution, furfuryl alcohol, phenol-resin monomers and acetylene gas are polymerized on heating inside mesoporous silicas or aluminosilicates [31,32-34,37]. The polymers are then converted to carbon by the pyrolysis, similar to the preparation of ordinary porous carbon materials. However, in the case of the templated synthesis, the

pyrolysis should be restricted to the inside of the template pores. An effective method for the restriction of carbonization is to place a suitable catalyst inside the pores, such as sulfuric acid, for the decomposition of carbohydrates. Alternatively, the silica frameworks can be acidified by the incorporation of alumina.

These acid catalysts catalyze the polymerization exclusively inside the region where the catalysts are located, so that subsequent carbonization results in the formation of nanostructured carbons inside the pores. The template can easily be removed at room temperature using a 10 % HF solution in ethanol-water or a hot ethanol-water solution of 1 M NaOH. It is also noteworthy that 3-D pore connectivity is essential for the formation of carbon networks that can retain the structure after the template is removed. Thus, depending on the type of structured silica that is used as a template, carbons with different structures and pore sizes are prepared [67].

As already mentioned above, the pursuit for an ordered microporous carbon [65,66,68] was successfully finalized through a two step carbon infiltration of a zeolite template [69,70]. In an extension to this work, but using mesoporous templates, Ryoo *et al*. [31-38], synthesized the first ordered mesoporous carbons (denoted as CMK-1 and CMK-2) from sucrose, furfuryl alcohol or a phenol resin

by reaction of the carbon based material with sulfuric acid inside the mesopores of MCM-48. As a result of the template pores being completely filled with the carbon precursor during the carbonisation process, rod-type carbons were then prepared (Fig. 2.3).



Figure 2.3: TEM image of CMK-1 prepared from mesoporous MCM-48 template [18]

Other nanoporous carbons (CMK-3) have also been synthesized by Jun *et al*. [34] and Darmstadt *et al*. [35] using an SBA-15 silica template. The structure of the carbon is composed of a hexagonal arrangement of 1-D carbon rods. CMK-4 carbon was prepared with partially disordered MCM-48 silica, which was

obtained by hydrothermal treatment of high-quality MCM-48. In this case, carbon nano-rods were also obtained. On the other hand, tube-type carbons are obtained if carbon precursors are carbonized and coated on the pore walls. The film coating of carbon precursors was reported to be difficult due to capillary condensation (pore-filling phenomenon). Consequently, the authors also mentioned that the tube type carbons were much more difficult to synthesize than the rod-type. Even if the film was coated, the carbon precursors could undergo pore filling during subsequent polymerization and carbonization processes, depending on the pore diameters and the nature of the carbon precursors. In fact, the authors reported that, all four CMK members except CMK-5 (which was also prepared by Ryoo and co-workers) were obtained as rod-type materials.

This interesting CMK-5 material represented in Fig. 2.4 was constructed with hexagonal arrays of carbon nanotubes or nanopipes [40,41]. The carbon is synthesized with SBA-15 silica as in the case of CMK-3, but the pore walls of the SBA-15 template are only coated with carbon films instead of being completely filled. The carbon nanopipes retain the hexagonally ordered arrangement permanently, due to interconnection similar to the CMK-3 structure. The wall thickness of the carbon nanopipes can be controlled to a certain degree by the amount of carbon source. It was also interesting to note that the specific BET

surface area of the CMK-5 varies from 1500 to 2200 m^2/g depending on the wall thickness.



Figure 2.4: TEM image of CMK-5 obtained after the complete removal of SBA-15 template [41]

In recent work, Lee *et. al*. [42] also presented preliminary results on the electrochemical double layer capacitor performance (EDLC) of the mesoporous carbon. In their approach, a mesoporous MCM-48 aluminosilicate with MCM-48 structure has been utilized as a template. Aluminium was implanted onto MCM-48 to generate strong acid catalytic sites for the polymerization of phenol and formaldehyde. Phenol and formaldehyde were incorporated into the pores of

aluminium-implanted MCM-48 (AlMCM-48) by heating for 12 h at 90 °C under reduced pressure.

Inverse replication of the mesoporous silica KIT- 6 was performed by Kleitz *et al*. [51]. The authors reported the syntheses of CMK-8 (rod type) and CMK-9 (tube type) carbons following rigorously the procedures described above for CMK-3 and CMK-5, respectively.

The polymerization of phenol and formaldehyde to obtain the phenol resin inside aluminium MCM-48 was carried out by heating the mixture under a nitrogen atmosphere at 125 °C for 5 h. The resulting AlMCM-48–phenol resin composite was heated under an N_2 flow at a heating rate of 5 °C /min to 700 °C and held there for 7 h to carbonize phenol resin inside the MCM-48 channels. The dissolution of MCM-48 frameworks using 48 % aqueous hydrofluoric acid (HF) generated mesoporous carbon, designated SNU-1 (SNU = Seoul National University) [42]. This mesoporous SNU-1 carbon showed a regular array of 2 nm diameter holes separated by 2 nm thick carbon walls (Figure 2.5). The specific surface area of SNU-1 was found to be 1257 m^2/g from BET analysis.

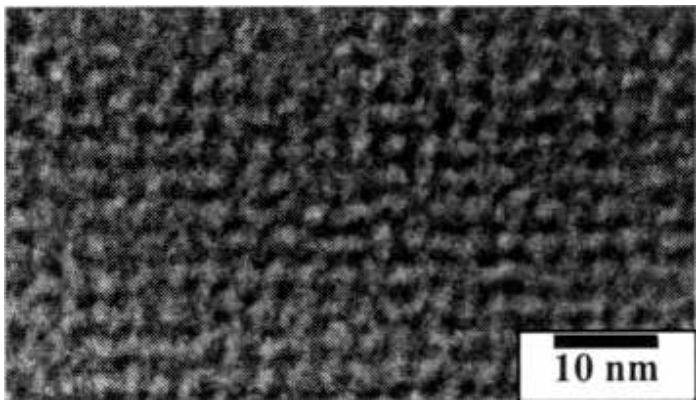

Figure 2.5: Transmission electron micrograph (TEM) of mesoporous SNU-1 carbon [23].

A carbon with a controlled mesostructure was prepared by Fuertes and Nevskaia [67] using a disordered mesoporous silica template, while Han and Hyeon developed a new synthetic method to generate porous carbon materials with pores of > 50 nm using commercial silica sol as a template. They reported the fabrication of a mesoporous carbon with narrow pore size distribution and high pore volume through surfactant stabilized silica particles as templates. They simply added a carbon precursor, resorcinol and formaldehyde (RF) into Ludox HS-40 silica sol solution. The resulting RF–silica composite was carbonized and etched with HF solution to give carbon materials with pores ranging in size from 10 to 60 nm. The average particle size of the HS-40 silica sol was reported to be 12 nm, with the aggregates of silica particles acting as templates. In order to

obtain a more uniform pore size distribution, isolated silica particles stabilized by surfactant were applied as templates.

By contrast, MCM-41 has been found to be unsuitable for the preparation of a mesoporous carbon [32]. Compared to the SBA-15 template, the MCM-41 silica has 1-D channels that are not interconnected. However, the large 1-D mesoporous channels (typically, 9 nm in diameter) of the SBA-15 silica are interconnected through smaller pores, which are less than 3.5 nm in diameter, and randomly located perpendicular to the 1-D channels. Due to this, the structure of the SBA-15 silica can be converted to the negative carbon replica exhibiting the same kind of structural symmetry. On the other hand, the replication of the MCM-41 silica with carbon results in the formation of carbon fibers that do not retain the 1-D hexagonal arrangement.

Recently, Kim *et al*. [71] reported the successful synthesis of ordered and graphitic mesoporous carbons CMK-3G (Fig. 2.6) prepared through the *in-situ* conversion of aromatic compounds (e.g. acenaphthylene, indene, indan and substituted naphthalenes) to a mesophase pitch using mesoporous silicas MCM-48, SBA-1 and SBA-15 as templates. Aluminum is incorporated into silica templates during the synthesis of the templates. First, the mesoporous template and the carbon source are placed into an autoclave. The aluminum sites on the

silica wall act as catalysts to form in situ mesophase pitch in the silica template pores at a low pyrolysis temperature (400 ^{o}C). Subsequently, the temperature of the autoclave is increased to 750 ^{o}C for carbonisation of the mesophase pitch in the template. After the autoclave was cooled down, the product was further heated to 900 ^{o}C under vacuum in a fused-quartz reactor for the complete carbonisation of the carbon source. The carbon product was then recovered by the removal of the silica template using an aqueous solution of HF or NaOH.

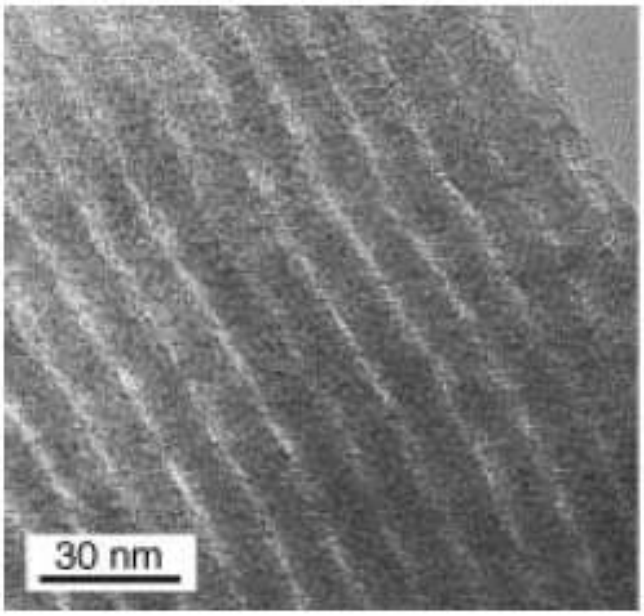

Figure 2.6: TEM image of ordered and graphitic mesoporous carbon CMK-3G [71]

Moreover, it was mentioned that these nanoporous carbons with highly graphitic frameworks exhibited remarkably improved mechanical strength and thermal stability, in comparison with mesoporous carbon prepared with sucrose and furfuryl alcohol.

The performance of these carbons has been evaluated in 5V devices using aqueous and organic electrolyte for double layer capacitors. It was found that the mesopores greatly improve the capacitance and frequency response of these carbons compared to commercial activated carbons [72]. It has also been reported that mesoporous carbons often provide a better rate of dechlorination [73]. Strano and co-workers have recently published a patent on the use of a supported mesoporous carbon ultra-filtration membrane. It is reported that the porous metal supports provides excellent strength and structural properties, and allows for increased operating pressures allowing for greater membrane flow rates [74]. Joo *et al*. prepared mesoporous carbons containing Pd materials that showed high catalytic activity in liquid phase hydrogenation [75].

In summary, mesoporous carbons with different structures can be synthesised using a variety of templates and carbon precursors. Templates such as MCM-48 and SBA-15 have been preferred in the synthesis of such carbons due to their 3-D cubic and 2-D hexagonal pore system, respectively. The template synthesis of

these carbons is particularly interesting because it provides the precise control of the porous structure of the final material. Basically, it consists of the impregnation of the porous structure of a template with the carbon precursor. Various carbon precursors such as sucrose, furfuryl alcohol, ethylene gas and *in-situ* polymerised phenol resins have been used for the synthesis of the ordered mesoporous carbons, although the resulting carbons had little or no graphitic character even when processed at 900 ^{o}C. These organic substances after carbonisation formed rigid carbon frameworks in the 3-D mesoporous network of the silica template. The structural order of the carbon frameworks was retained after silica template dissolution with NaOH and HF.

It is noteworthy that the addition of an acid catalyst such as H_2SO_4 is required for the successful synthesis of these carbons when the synthesis is performed in non-acidic silica. However, this is not necessary if the synthesis is performed in an acidic aluminosilicate matrix. Hydroxyl groups adjacent to aluminum in the aluminosilicate framework can catalyse the polymerization reaction as Brønsted acid sites.

Techniques such as XRD, TEM, BET, TGA and Raman spectroscopy have been used to study and characterise the resultant carbon materials. It is noteworthy that two types of carbons with the same mesostructural symmetry but different

framework configurations were obtained, i.e. rod- and tube-like carbons. Alternatively, more graphitic carbons can be obtained *via* synthesis routes that used the *in-situ* conversion of aromatic compounds into mesophase pitch inside silica template or *via* direct use of mesophase pitch as a carbon source.

Due to their high surface area, relatively uniform pore sizes, ordered pore structure, interconnected pore network, graphitic pore walls, tailorable surface properties, chemical inertness, good thermal and mechanical stabilities, these porous carbons have found promising applications as catalyst supports, electrode materials, adsorbents, energy storage for fuel cell super-capacitors, optical materials and templating matrixes for the fabrication of other nanostructures.

Table 2.1 gives a summary of various micro- and mesoporous carbons that have been reported in the literature and discussed in this review. The data includes information on the carbon sources used, the method used in their preparation and in addition, the techniques used to analyse the materials.

Table 2.1: Summary of the different literature methods employed to synthesize mesoporous carbons

Template	Carbon source	Conditions	Etching reagent	Product	Characterization technique used	Reference
Amorphous silica gel	Polymer precursors	Heated to 2000 ^{o}C	-	Rigid Mesoporous carbon PGC	XRD, SEM and ED	[63]
Layered materials (e.g. lithium form of taeniolite)	Furfuryl alcohol	Heated under N_2 flow at 100 ^{o}C for 24 h and then at 160 ^{o}C for 6 h. Samples were heated at 700 ^{o}C for 3 h under N_2	HCl and HF solutions	Microporous carbons	XRD, SEM, IGC and sorption techniques	[64]
Zeolites Y, β and L	Phenol-formaldehyde	Heated to 125 ^{o}C for 5h at 1 ^{o}C/min. Temperature was then ramped at 5 ^{o}C to 500 or 900 ^{o}C and the	HF solution	Microporous polymer replicas	BET, TEM and SEM	[66]

		resin/zeolite still under flowing Ar was pyrolyzed for 14 h				
Zeolite Y	Polyacrylonitrile and polyfurfuryl alcohol	Samples were heated under N_2 flow at 80 ^oC for 24 h and then at 150 ^oC for 8 h. Resulting carbon/zeolite samples were heat treated to 700 ^oC for 3 h.	46 % HF solution at 25 ^oC and sunsequently refluxed in 36 % HCl solution	Carbon	SEM, TEM, XRD and BET	[65]
MCM-48	Sucrose, furfuryl alcohol or phenol resin	Dried at 100 ^oC, subsequently raised to 160 ^oC. Sample carbonized at 900 ^oC under vacuum	Aqueous ethanol solution of NaOH	CMK-1	XRD, BET and TEM	[31,33,43, 44]
SBA-1	Sucrose	Same as for CMK-1	NaOH	CMK-2	XRD and TEM	[34,35]

			solution			
SBA-15	Sucrose	Same as for CMK-1	NaOH solution	1-D carbon rod CMK-3		[36,37]
FDU-5 (Partially disordered MCM-48)	Acetylene gas	Heated to 800 ^{o}C in a quartz fused reactor, after acetylene gas flow, temperature was increased to 900 ^{o}C under vacuum	HF or NaOH	Carbon rods CMK-4	XRD, SEM, EDX and HRTEM	[50]
SBA-15	Furfuryl alcohol and acenaphthene	Silica and carbon source were put into vacuum sealed pyrex, heated to 250 ^{o}C over 3 h. Kept at 250 ^{o}C for 6 h. Resultant product was pyrolysed at 900 ^{o}C for 11 h under	HF solution	Carbon nanopipes CMK-5	XRD, BET and TEM	[41]

		vacuum				
MCM-48 aluminosilicate	Phenol and formaldehyde	Heated in a nitrogen atmosphere at 125 °C for 5 h. Then heated under an N_2 flow at a heating rate of 5 °C /min to 700 °C and held there for 7 h	48 % HF solution	Mesoporous SNU-1	BET	[48]
Ludox HS-40 silica sol	Resorcinol and formaldehyde	Sample heated under N_2 from 25 to 850 ^oC with a heating rate of 5 ^oC/min and held at 850 ^oC for 3 h	HF solution	Silica-sol Mediated carbon (SMC-1)	XRD, TEM and BET	[43]
Mesoporous silica KIT-6	Sucrose	Same as for CMK-3	NaOH solution	Rod type CMK-8	XRD, TEM and BET	[51]
Mesoporous silica KIT-6	Sucrose	Same as for CMK-5	HF solution	Bicontinous arrays of	XRD, TEM and BET	[51]

				nanotube type CMK-9		
SBA-1, MCM-48, SBA-15	aromatic compounds (e.g. acenaphthylene, indene, indan and substituted naphthalenes)	aluminum acts as a catalysts to form *in-situ* mesophase pitch in the silica template pores at 400 ^{o}C. The temperature is then increased to 750 ^{o}C. The product was further heated to 900 ^{o}C under vacuum in a fused-quartz reactor	HF or NaOH solution	CMK-3G	XRD, TGA, TEM	[71]

2.5 Conclusion

The overview presented in this chapter on the synthesis and preparation of carbon materials demonstrates their flexibility in tailoring their chemical and physical properties of carbons to specific needs, thus illustrating their remarkable wide range of potential applications. However, the future growth of the use of carbon materials in catalysis will depend on the better understanding and subsequent control of the chemistry of the carbon surface, which can then be exploited in the design of truly unique catalysts.

Thus, in summary it has been shown that by in situ carbonization of organic compounds, carbon nanocomposites and carbons with a well developed pore structure and high surface areas can be obtained. In addition, highly ordered mesoporous carbon materials are now available with a rich variety of structures, by templated synthesis, using mesoporous silica as templates. The templated synthesis of the ordered mesoporous carbons is a remarkable achievement in the field of porous materials because the synthesis is easy, inexpensive and suitable for large-scale production. The resulting high-surface-area materials and uniform pores promise to be suitable as adsorbents, catalyst supports, and materials for advanced electronics applications.

2.6 References

[1] L. R. Radovic and F. Rodriguez-Reinoso, *Chem. Phys. Carbon*, **25**, 243 (1997).

[2] F. Rodriguez-Reinoso, *Carbon*, **36**, 159 (1998).

[3] C. Moreno-Castilla, O. P. Mahajan, P. L. Walker Jr., H.-J. Jung and M. A. Vannice, *Carbon*, **18**, 271 (1980).

[4] http://www.mpg.de/pdf/europeanWhiteBook/wb_materials_055_057.pdf

[5] R. C. Bansal, J. B. Donnet and H. F. Stoeckli, *Active Carbon*, ed. Marcel Dekker, New York (1988).

[6] H. F. Stoeckli, *Carbon*, **28**, 1 (1990).

[7] A. Dandekar, R. T. K. Baker and M. A. Vannice, *J. Catal.*, **183**, 131 (1999).

[8] A. B. Stiles, *Catalyst Supports and Supported Catalysts*, Butterworths, Boston, (1987).

[9] H. Tamai, K. Shiraki, T. Shiono and H. Yasuda, *J. Coll. Int. Sci.*, **295**, 299 (2006).

[10] W. Xing, S. Z. Qiao, R. G. Ding, F. Li, G. Q. Lu, Z. F. Yan and H. M. Cheng, *Carbon*, **44**, 216 (2006).

[11] M. Sevilla and A. B. Fuertes, *Carbon*, **44**, 468 (2006).

[12] D. J. Kim, H. I. Lee, J. E., Yie, S.-J. Kim and J. M. Kim, *Carbon*, **43**, 1868 (2005).

[13] K. Bőhme, W-D. Einicke and O. Klepel, *Carbon*, **43**, 1918 (2005).

[14] Q. Hu, J. Pang, N. Jiang, J. E. Hampsey and Y. Lu, *Micopor. Mesesopor. Mater.*, **81**, 149 (2005).

[15] A. B. Fuertas, G. Lota, T. A. Centeno and E. Frackowiak, *Electochim. Acta*, **50** 2799 (2005).

[16] M. Kruk and M. Jaroniec, *Chem. Mater*., **12**, 1414 (2000).

[17] M. Wildenmeyer and R. Anwander, *Chem. Mater*., **14**,1827 (2000).

[18] T. Tatsumi, K. A. Koyano, Y. Tanaka and S. Nakata, *J. Por. Mater.*, **6**, 13 (1999).

[19] J. M. Kim, Y. Sakamoto, Y. K. Hwang, Y.-U. Kwon, O. Terasaki, S.-E. Park and G.D. Stucky, *J. Phys. Chem*. *B*, **106**, 2552 (2002).

[20] R. Ryoo, S. H. Joo and J. M. Kim, *J. Phys. Chem. B*, **103**, 7435 (1999).

[21] W. Zhao and Q. Li, *Chem. Mater*., **15**, 4160 (2003).

[22] M. J. Kim, S. K. Kim and R. Ryoo, *Chem. Commun*., **259**, (1998).

[23] K. Schumacher, P. I. Ravikovitch, A. Du Chense, A. V. Neimark and K. A. Unger, *Langmuir*, **16**, 4648 (2000).

[24] D. Kumar, K. Schumacher, C. von Hohensche, M. Grun and K. A. Unger, *Coll. Surf. A: Physicochem. Eng. Aspects*, **187**, 109 (2001).

[25] A. Sarayi, *Chem. Mater*., **8**, 1840 (1996).

[26] M. Hartmann, S. Racouchot and C. Bischof, *Micropor. Mesopor. Mater.*, **27**, 309 (1999).

[27] A. Galarneau, D. Desplantier-Giscard, F. Di Renzo and F. Fajula, *Catal. Today*, **68**, 191 (2001).

[28] Y. Wang, M. Noguchi, Y. Takahashi and Y. Ohtsuka, *Catal. Today*, **68**, 3 (2001).

[29] R. Ryoo, I-S. Park, S. Jun, C. W. Lee, M. Kruk and M. Jaroniec, *J. Am. Chem. Soc*., **123**, 1650 (2001).

[30] S. A. Bagshaw, E. Prouzet and T. J. Pinnavaia, *Science*, **269**, 1242 (1995).

[31] R. Ryoo, S. H. Joo and S. Jun, *J. Phys. Chem. B*, **103**, 7743 (1999).

[32] M. Kruk, M. Jaroniec, R. Ryoo and S. H. Joo, J. *Phys. Chem. B*, **104**, 7960 (2000).

[33] http://www.rryoo.kaist.ac.kr

[34] S. Jun, S. H. Joo and R. Ryoo, *J. Am. Chem. Soc*., **122**, 19712 (2000).

[35] H. Darmstadt, C. Roy, S. Kaliaguine, S. H. Joo and R. Ryoo, *Micropor. Mesopor. Mater.*, **60**, 139 (2003).

[36] S. H. Joo, S. Jun and R. Ryoo, *Micropor. Mesopor. Mater*, **44**, 153 (2001).

[37] J. S. Lee, S. H. Joo and R. Ryoo, *J. Am. Chem. Soc*., **124**, 1156 (2002).

[38] M. Kuno, T. Naka, E. Negishi, H. Matsui, O. Terasaki, R. Ryoo and N. Toyota, *Syn. Metals*, **135**, 721 (2003).

[39] R. Ryoo, S. H. Joo, M. Kruk and M. Jaroniec, *Adv. Mater.*, **13**, 677 (2001).

[40] S. H. Joo, S. J. Choi, I. Oh, J. Kwak, Z. Liu and O. Terasaki, *Nature*, **412**, 169 (2001).

[41] L. A. Solovyov, T-W. Kim, F. Kleitz, O. Terasaki and R. Ryoo, *Chem. Mater.*, **16**, 2274 (2004).

[42] J. Lee, K. Sohn and T. Hyeon, *J. Am. Chem. Soc.*, **123**, 5146 (2001).

[43] S. Han and T. Hyeon, *Carbon*, **37**, 1645 (1999).

[44] S. Han and T. Hyeon, *Chem. Commun.*, **6**, 1955 (1999).

[45] O. Terasaki, Z. Liu, T. Ohsuna, T. Kamiyama, D. Shindo, K. Hiraga, S. H. Joo, T.-W. Kim and R. Ryoo, *Stud. Surf. Sci. Catal.* **146**, 275 (2003).

[46] J. M. Kim, M. Kang, S. H. Yi, J. E. Yie, S. H. Joo and R. Ryoo, *Stud. Surf. Sci. Catal.* **146**, 53 (2003).

[47] S. H. Joo, R. Ryoo, M. Kruk and M. Jaroniec, *Stud. Surf. Sci. Catal.* **146**, 49 (2003).

[48] S. Jun, M. Choi, S. Ryu, H.-Y. Lee and R. Ryoo, *Stud. Surf. Sci. Catal.* **146**, 37 (2003).

[49] J.-S. Lee, S. H. Joo and R. Ryoo, *Stud. Surf. Sci. Catal.* **146**, 33 (2003).

[50] M. Kaneda, T. Tsubakiyama, A. Carlsson, Y. Sakamoto, T. Ohsuna, S. H. Joon and R. Ryoo, *J. Phys. Chem.*, **106**, 1256 (2002).

[51] F. Kleitz, S. H. Choi and R. Ryoo, *Chem Comm*., **9**, 2136 (2003).

[52] R. W. Pekala, *J. Non-Cryst. Solids*, **145**, 90 (1992).

[53] T. G. Lamond and H. Marsh, *Carbon*, **1**, 293 (1963).

[54] H. Marsh and B. Rand, *Carbon*, **9**, 63 (1971).

[55] Z. Hu, M. P. Srinivasan and Y. Ni, *Adv. Mater*., **12**, 62 (2000).

[56] T. Kyotani, *Carbon*, **38**, 269 (2000).

[57] S. Iijima, *Nature*, **354**, 56 (1991).

[58] P. M. Ajayan, T. Ichihashi and S. Iijima, *Chem. Phys. Lett*., **202**, 384 (1993).

[59] http://www.ncnr.nist.gov/staff/taner/nanotube/interlink.pdf

[60] A. Merkoci, M. Pumera, X. Llopis, B. Pěrez, M. Del Valle, S. Alegret, *Trends in Anal. Chem.*, **24**, 826 (2005).

[61] W.-P. Ma,Y-J. Ding, L.-W. Lin. *Ind. Eng. Chem. Res*., **43**, 2391 (2004).

[62] W.-P. Ma,Y.-J. Ding, J. Yang, X. Liu and L.-W. Lin, *React. Kinet. Catal. Lett*., **84**, 11 (2005).

[63] J. H. Knox, B. Kaur and G. R. Millward, *J. Chromatogr*., **353**, 3 (1986).

[64] T. J. Bandosz, J. Jagiello, K. Putyera, J. A. Schwarz, *Chem. Mater*., **8**, 2023 (1996).

[65] T. Kyotani, T. Nagai, S. Inoue and A. Tomita, *Chem. Mater*., **9**, 609 (1997).

[66] S. A. Johnson, E. S. Bringham, P. J. Olivier, T. E. Mallouk, *Chem. Mater*., **9**, 2448 (1997).

[67] A. B. Fuertas and D. M. Nevskaia, *J. Mater. Chem.,* **13**, 1843 (2003).

[68] J. Rodriguez-Mirasol, T. Cordero, L. R. Radovic, J. J. Rodriguez, *Chem. Mater*., **10**, 550 (1998).

[69] Z. Ma, T. Kyotani and A. Tomita, *Chem. Comm*., 2365 (2000).

[70] Z. Ma, T. Kyotani and A. Tomita, *Carbon*, **40**, 2367 (2002).

[71] T.-W. Kim, I.-S. Park and R. Ryoo, *Angew. Chem. Int. Ed*., **42**, 4375 (2003).

[72] S. D. Dietz and V. Nguyen, *Mesoporous Carbon Electrodes for Double Layer Capacitors*, Proceedings of the NSF design, service and manufacturing grantees and research conference, Tampa, Florida (2002) [available at www.tda.com].

[73] http://www.kxindustries.com

[74] M. Strano, H. C. Henry and H. Agarwal, Patent **844567** (2004) [available at www.freepatentsonline.com].

[75] S. H. Joo and R. Ryoo, Photon Factory Activity report B, 20 (2003) [available at http://pfwww.kek.jp/acr2002pdf].

Chapter Three

*Synthesis of Mesoporous Carbon Supports via Liquid Impregnation of Polystyrene onto a MCM-48 Silica Template

3.1 Introduction

A large number of new materials that are of great interest and have potential in emergent materials applications have been prepared by means of a template synthesis approach. An example are the mesostructured silica materials (MSMs) that have been synthesised by using surfactant micelles as templating agents [1,2]. These MSMs have recently attracted much attention in catalysis and nanoscience [3,4]. The most popular members of this family are MCM-41 and MCM-48. MCM-41 has a hexagonal packing of 1-D channels while the MCM-48 has a 3-D mesopore network [5–13]. Because of the 3-D pore arrangement in MCM-48 it is more desirable in catalytic reactions than MCM-41 due to reduced diffusional constraints. The rigid structure of the MSMs and their well structured pore network also make them suitable for use as templates in the synthesis of other materials which have a controlled structure and unique properties, e.g. noble

* C. N. Mbileni, F. F. Prinsloo, M. J. Witcomb and N. J. Coville, *Carbon*, **44**, 1476 (2006).

metal nanowires and networks, conductive polymer nanofilaments and mesoporous carbons [1,2,14-19].

Many technological applications of carbon (the adsorption of large molecules, their use as catalyst supports, in fuel cells or energy storage devices and in double layer capacitors [19-23]) require that the porous carbons have a narrow pore size distribution (PSD) in the mesopore range (2-50 nm). These mesoporous carbons have advantages over the classical active carbons which have a broad pore size distribution (PSD) and a high fraction of micropores [1].

Due to our interest in the synthesis of supported catalysts [24-30] we wished to evaluate the possibility of synthesising and using mesoporous carbons as catalyst supports. Carbon is ideally suited as a catalyst support due to its chemical inertness, excellent mechanical resistance and porosity [31-33].

The literature on the synthesis of mesoporous carbons, synthesised from MSMs, is well documented and provided the framework for our synthetic strategies to make carbonaceous catalyst supports [1–3,9,19-22,34-66]. In most studies sucrose, furfuryl alcohol or phenol resin have been used as carbon sources for the preparation of such carbons. These carbon sources contain a considerable amount of oxygen and other elements that are usually released in the gaseous form during

carbonisation [42,43]. The use of sources that could lead to graphitic mesoporous carbon has been less studied [17,48-51]. Indeed, Li and Jaroniec reported the use of synthetic mesophase pitch (a mixture of naphthalene-derived compounds exhibiting liquid-crystal arrangement) as the carbon precursor to prepare colloidal imprinted spherical mesoporous carbons which featured a higher carbon content [16,23,63-65]. These studies resulted in others using mesophase pitch and related carbon precursors for the synthesis of ordered mesoporous carbons [43,62]. A report has only appeared recently on the use of styrene as a carbon source and this instance a CVD approach was used to produce mesoporous carbons [52].

Two decades ago, Knox *et al*. [34] reported that amorphous silica gel could be impregnated with polymer precursors that were then polymerised to form a continuous network surrounding the silica particles. Carbonisation of the polymer coating and the subsequent dissolution of the silica template rendered a templated amorphous carbon. In an extension to this work, but using mesoporous templates, Ryoo *et al*. [35-38], synthesised an ordered mesoporous carbon (denoted as CMK-1) from sucrose, furfuryl alcohol or a phenol resin by reaction of the carbon based material with H_2SO_4 inside the mesopores of MCM-48. Other nanoporous carbons have also been synthesised by Jun *et al*. using an SBA-15 silica template [39].

In more recent work a high surface area mesoporous carbon (denoted as SNU-2) was prepared by Lee *et al*. using a disordered HMS silica material [40,41] while a carbon with a controlled mesostructure was prepared by Fuertes and Nevskaia [44] using a disordered mesoporous silica template. Mesocellular foam carbon spheres prepared from a mesocellular silica template were also reported by Oda *et al*. [45]. Furthermore, these mesoporous carbons consisting of interconnected rods, tubes or spheres can be achieved by simply using different carbon sources (sucrose, furfuryl alcohol, phenol resin, ethylene gas, etc.) and/or different quantities of carbon.

In this chapter we have evaluated the use of polystyrene, and other related aromatic compounds, as a carbon source for the synthesis of mesoporous carbons (MCs). These benzene containing materials, should form fused rings that take on a sheet like form after deposition and reaction on the template surface [17,48-52]. In this way graphitic like mesoporous carbons should be synthesised. The new carbonaceous materials were synthesized by carbonisation and pyrolysis of polystyrene deposited on MCM-48.

3.2 Experimental section

3.2.1 Synthesis of MCM-48

MCM-48 templates were prepared by a room temperature method [12]. In a typical synthesis, 2.6 g of cetyltrimethylammonium bromide (CTAB, Fluka, Germany) was dissolved in 120 g distilled water and 50 ml ethanol. Aqueous ammonia (12 ml) (Riedel de-Haen, Germany) was then added to the surfactant solution. The solution was stirred for 10 min and then 3.4 g tetraethoxy-orthosilane (TEOS, Sigma Aldrich) was added to the solution at one time. After being stirred for 12 h at room temperature, the resultant solid was recovered by filtration, washed with distilled water, dried in air and calcined at 560 ^{o}C for 6 h. The yield was more than 80 %. The material was characterised by classical Raman spectroscopy, XRD, BET, SEM and TEM techniques.

3.2.2. Preparation of polystyrene [67,68]

Commercial styrene (35 ml; BDH) was purified by distillation under vacuum at water pump pressure. Benzoyl peroxide (0.5 g; BDH) was then added to the freshly purified styrene (28 ml) in a screw capped bottle and the resultant mixture was flushed with nitrogen. The closed vessel was wrapped in wire mesh and

placed in a convection oven at 85 ^{o}C for 24 h. After the reaction vessel had cooled to ambient temperature, it was broken and the polystyrene removed. The sample was purified by grinding with a mortar and pestle, the fine powder dissolved in toluene, and the solution poured drop-wise with vigorous stirring into methanol. The precipitated polystyrene polymer was washed thoroughly with methanol, and then dried in a vacuum oven at 100 ^{o}C for 24 h. This whole process gave a yield of 82 % of the desired polymer material.

3.2.3. Synthesis of mesoporous carbons

Carbonisation experiments were performed by a two step impregnation of the mesopores of MCM-48 with a solution of polystyrene using an incipient wetness method. In a typical experiment, polystyrene (0.5 g) and sulfuric acid (0.14 g; Saarchem) were dissolved in toluene (4 g), and this solution was then added to MCM-48 (1 g). The resultant mixture was dried in an oven at 100 ^{o}C for 0.5 h, and the oven temperature was subsequently raised to 160 ^{o}C for 6 h. A solution consisting of polystyrene (0.75 g) and sulfuric acid (0.08 g) in toluene (4 g) was then added to the MCM-48 silica/organic residue. The mixture was again heated in an oven at 100 ^{o}C for 0.5 h and the temperature of the oven subsequently raised to 160 ^{o}C. The oven was kept at this temperature until the sample turned dark brown (ca. 6 h). The resultant sample was pyrolysed in a fused quartz reactor

(connected to a vacuum pump) that was placed in an oven at 900 ^{o}C for 2 h. (We refer to the high temperature process as pyrolisation to differentiate it from the low temperature carbonisation process; in principle both are carbonisation processes).

The carbon–silica composites that were obtained were washed with a solution of 10% HF (Merck) in order to dissolve the silica template. After the removal of the template the samples were filtered, washed with distilled water and then dried at 100 ^{o}C. Both the carbon–silica and template removed carbon materials were characterised by Raman spectroscopy, XRD, BET, TGA SEM and TEM techniques.

3.2.5 Characterization

The BET specific surface area and pore size distribution measurements were determined from nitrogen adsorption isotherms measured at liquid nitrogen temperatures with a Micromeritics ASAP 2010 instrument. XRD patterns were obtained using a Phillips PW diffractometer (Cu K*a* source). TEM images were obtained with a Jeol CM 200 high resolution transmission electron microscope. TGA thermograms, recorded under nitrogen were collected using a Perkin Elmer Pyris 1 analyser. Raman spectra were recorded on a Jobin-Yvon T64000 Raman

spectrometer operating at λ = 514.5 nm line from an argon ion laser. A low laser power was used as a high power laser burnt the samples. SEM images were obtained with a Hitachi S-2700 scanning electron microscope with LaB_6 gun. The EDX system (PGT IMIX with thin window detector) was connected to the SEM instrument.

3.3 Results and discussion

3.3.1 Effect of the amount of polystyrene added to the pores of MCM-48 silica template

In an initial study, polystyrene, sulfuric acid and toluene in the absence of a template was carbonised at 160 ^{o}C for 6 h twice and then pyrolysed at 900 ^{o}C for 2 h. A porous carbon with a reasonable surface area (257 m^2/g) and large pore diameter (average - 8.4 nm) was obtained (Table 3.1). The TGA analysis (in a N_2 atmosphere) (Fig. 3.1) of the material revealed a clean decomposition of the polymerised material at about 400 ^{o}C with < 2% formation of residual material.

The first attempts to prepare MCs (mesoporous carbons) were carried out by adding 2 g polystyrene, acid and toluene to MCM-48. This material was then carbonised at 160 ^{o}C for 6 h and pyrolysed at 900 ^{o}C for 2 h. A non-porous

carbon with surface area of < 50 m^2/g (Table 3.1) was produced using this procedure. This result suggested that the pore volume (1 cm^3/g) of MCM-48 was not large enough to contain the quantity of polystyrene/toluene/acid needed to only infiltrate the MCM-48 and then form a rigid carbon structure. It also appeared that the polystyrene polymerised even before the heat treatment in an oven.

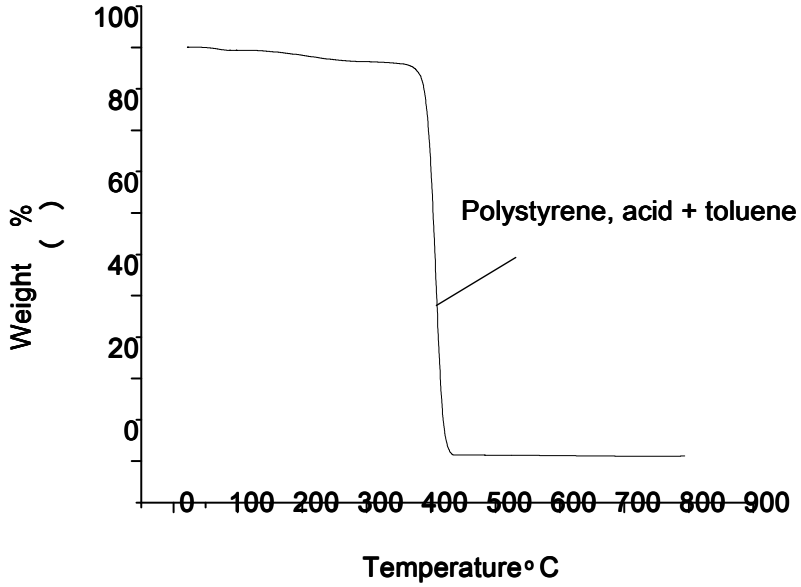

Figure 3.1: TGA profile (in nitrogen) of a blank of polystyrene + acid + toluene.

Table 3.1: Pore characteristics of mesoporous carbons

Parameter		Surface-area (m^2/g)	Pore-volume (cm^3/g)	Pore-diameter (nm)
MCM-48[a]		1293	0.9	2.9
Polystyrene blank		257	1.0	8.4
PS[b]	PS[c]			
1.5 – 2.50[d]	0.00	<50	0.06	5.3
0.50	0.75	748	0.5	2.3
1.00	0.75	456	0.4	3.6
1.25	0.75	408	0.2	2.7
1.50	0.75	226	0.09	2.2

[a] Calcined at 560 ^{o}C for 6 h

[b] Amount of polystyrene impregnated in the 1st step of the carbonisation process

[c] Amount of polystyrene impregnated in the 2nd step of the carbonisation process

[d] Similar results obtained when 1.5 - 2.5 g polystyrene were used

The excess polystyrene caused coagulation of the MCM-48 particles and consequently the formation of a non-porous amorphous carbon as shown by the TEM image in Fig. 3.2. Joo *et al*. [36], obtained similar results when they used sucrose as the carbon source.

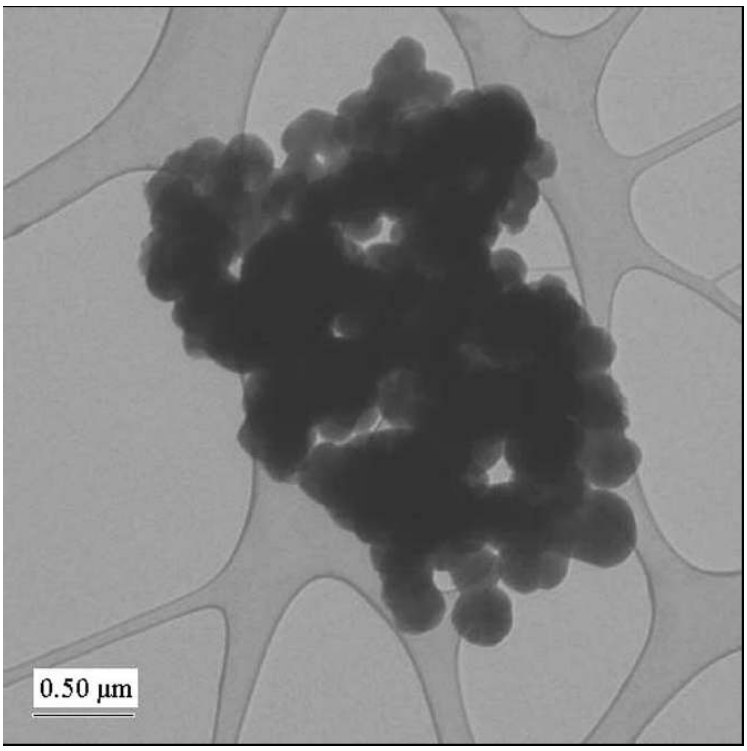

Figure 3.2: TEM image of sample formed by single impregnation of MCM-48 with polystyrene/acid/toluene.

Experiments were then performed using a double impregnation methodology. In this process a mixture of polystyrene/acid/toluene was added to the MCM-48 and after reaction at 160 ^{o}C the sample was again subjected to another addition/reaction cycle with the same reagents. Similar double addition/reaction cycles have been used in studies with other carbon sources [35-41, 44-46]. The amount of the polystyrene added to the silica material in the first reaction/addition cycle was found to control the carbon layer formed in the final synthesised product.

Thus, the amount of the polystyrene infiltrated into the silica pores was varied from 0.5 to 1.5 g in the first impregnation step while in the second step the amount of polystyrene used (0.75 g) was kept constant (Table 3.1). The effect of loading on the carbon surface area and pore volume is shown in Fig. 3.3. As can be seen a good correlation between the surface area and the pore volume and the amount of polystyrene added to the MCM-48 exists. The samples with higher polystyrene loadings show lower pore volumes, a similar phenomenon was observed by others with different carbon sources [44].

The corresponding XRD profiles of the differently loaded samples are shown in Fig. 3.4. The most intense peak at 2θ ca. 2 ^{o} (corresponding to formation of a mesoporous material) was found when 0.50 g polystyrene was used in the first

impregnation step. These results show that the intensity of the peaks is inversely proportional to the degree of reagent infiltration.

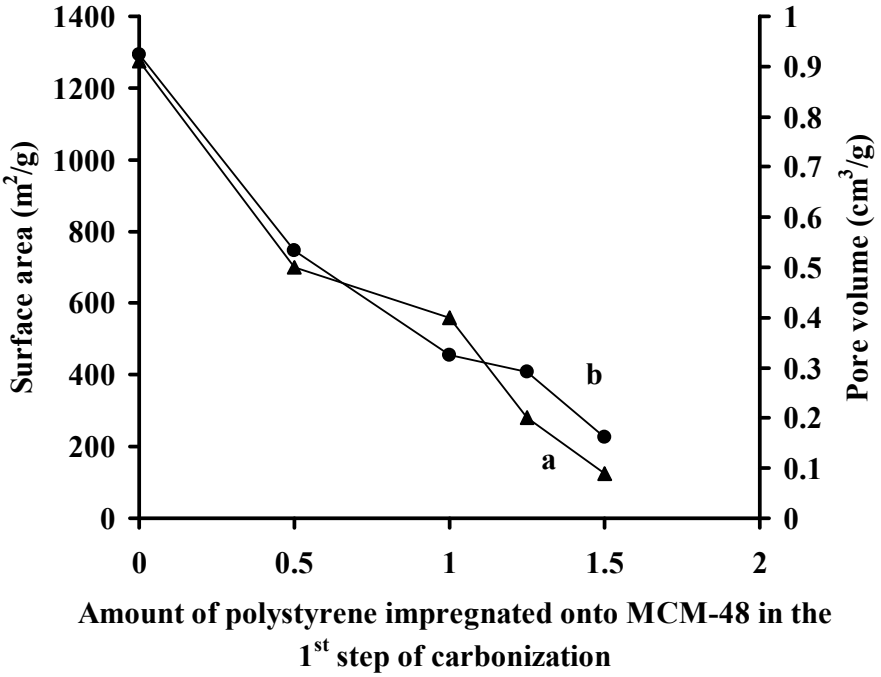

Figure 3.3: Plot of amount of polystyrene impregnated onto MCM-48 (in the 1st step of the two carbonization process); (a) ▲ - against product pore volume and (b) ● - against product surface area.

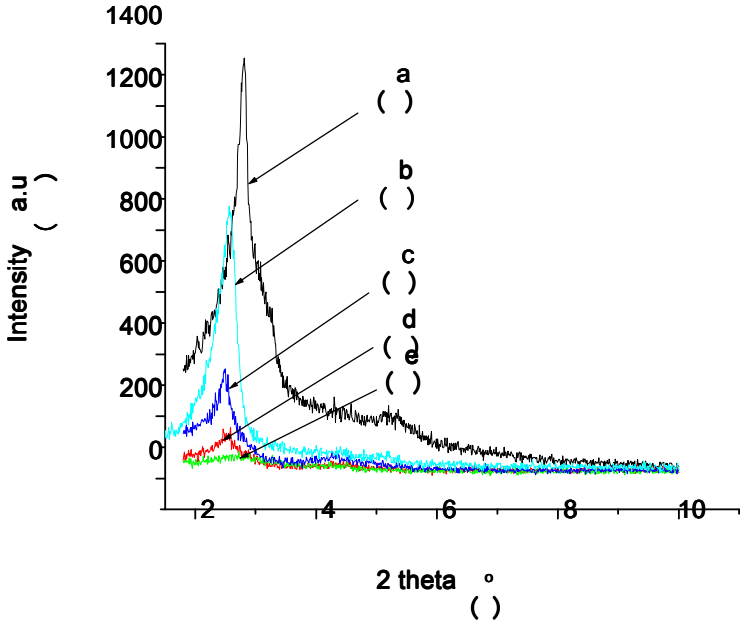

Figure 3.4: XRD patterns of MCM-48 after different treatments: (a) - MCM-48 calcined, (b) – two step carbonised MCM-48 (0.5 g polystyrene in the 1st step); (c) – two step carbonised MCM-48 (1.25 g polystyrene in the 1st step); (d) – two step carbonised MCM-48 (1.50 g polystyrene in the 1st step); (e) one step carbonised MCM-48 (1-2 g polystyrene).

3.3.2 Effect of carbonisation on the MCM-48 silica template

As reported previously [35-39], the silica framework of infiltrated MCM-48 shrinks during the preparation of the carbon/silica composite. Consequently the

available pore volume is observed to be lower than what might have been expected from the original silica template. Kruk *et al*. [38] have examined the extent of these resulting changes in an MCM-48 structure. Carbon from a carbon composite was removed via calcination and the MCM-48 recovered had a unit cell similar to that of the carbon/silica composite but significantly smaller than that of the initial MCM-48 before carbon infiltration. These results are consistent with our findings and suggest that the BET values measured result from a decrease in the pore volumes of the carbonized samples due to both the shrinkage and the pore filling of MCM-48 silica template. This is indicated by the XRD analysis of the MCM-48 before and after carbonization and pyrolysis (Fig. 3.5).

Distinct diffraction peaks observed in the XRD of MCM-48 crystals can be indexed by a cubic system, and reflection conditions are consistent with the space group system of an enantiomeric interpenetrating 3D network (*Ia3d*) of mesoporous channels [53]. In contrast, the diffraction peak intensity of the carbon/silica composite is reduced substantially from that of the parent MCM-48 material but the number of reflections of all the peaks is still maintained. As a result, the existence of long-range order is noticeable although the peaks shifted to lower angles (Fig. 3.5). Ryoo and co-workers [35] explained the intensity change in the XRD pattern indicating that both enantiomeric channel systems separated by the silica walls corresponding to periodic G-surface were statistically equally

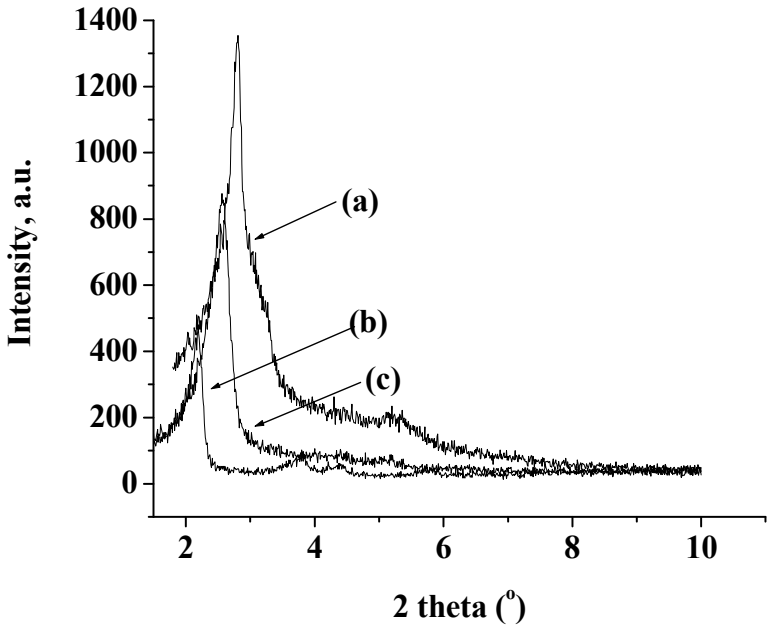

Figure 3.5: XRD patterns of (a) MCM-48 calcined, (b) MCM-48 carbonised and (c) pyrolysed mesoporous carbon sample, template removed

filled with carbon, maintaining the cubic *Ia*3*d* space group with inversion centers on the original G-surface.

After dissolution of the silica template, an improvement in the peak intensity was observed although the reflection of the other smaller peaks between 4 and 6 ^{o} 2 θ have disappeared. This observation can be attributed to the high temperature

treatment the samples have undergone during the pyrolysis step and also the removal of the template. As expected, the unit cell for the mesoporous carbon was reduced to 6.7 nm compared to 8.4 nm for MCM-48 silica.

3.3.3 Investigation of the degree of the retention order of the crystal morphology of MCM-48

Scanning electron microscopy images provided information regarding the morphology of MCM-48 silica template and resultant mesporous carbon. As can be seen in Fig. 3.6, the porous carbon particles retained the crystal morphologies of the silica template. In addition the figure indicates that most particles are nearly uniform and spherical for both the silica template and the mesoporous carbon, with particle sizes ranging from 25 to 60 nm and 15 to 45 nm, respectively.

Although a systematic transformation of structure occurred during the removal of silica framework as revealed by its change in the powder XRD patterns obtained during the framework removal as in Figure 3.5, the electron microscopy technique revealed that the template synthesis followed a replication process for the structure of the mesoporous silica. Nevertheless, the corresponding spherical particles are reduced due to the shrinkage of the silica template.

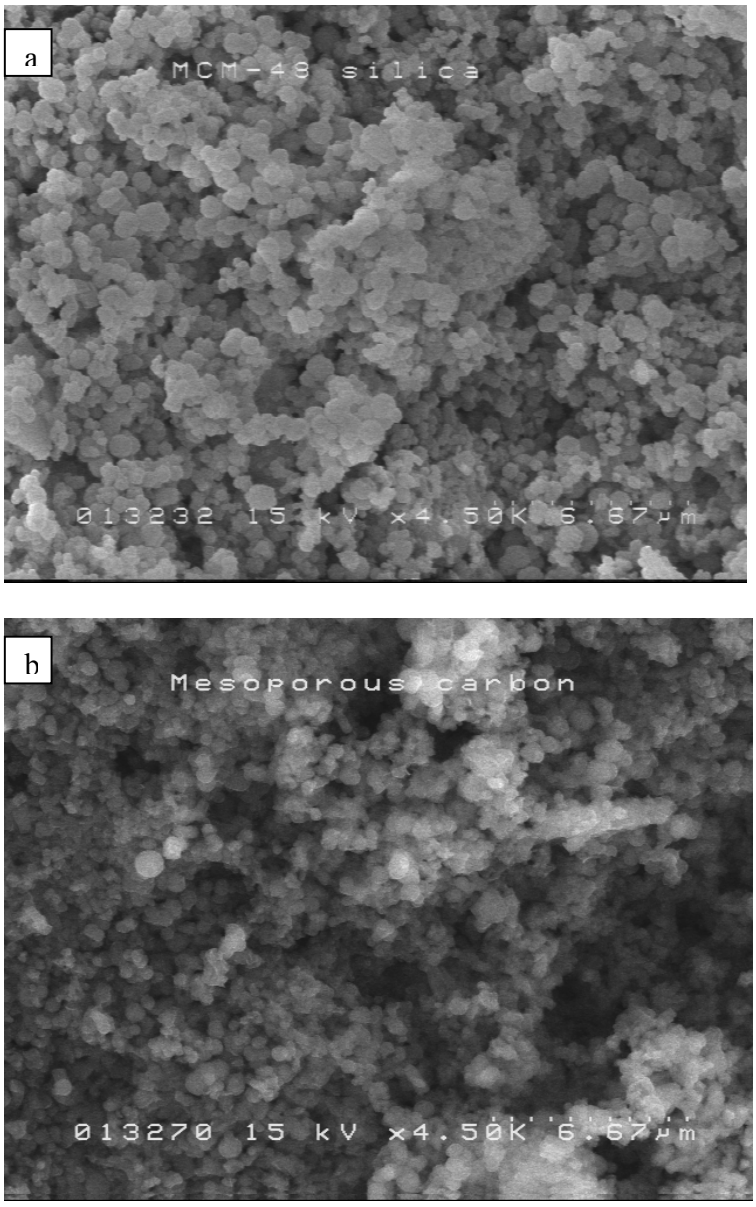

Figure 3.6: SEM images of (a) - MCM-48 silica template and (b) - mesoporous carbon.

To further confirm the latter statement, calcined MCM-48 was heated to 900 ^{o}C for 2 h in a furnace in order to establish the degree of the shrinkage. Indeed, the SEM images of the particles (Fig. 3.7) revealed that the size of the spherical particles had been reduced to 20 – 45 nm compared to 25 – 60 nm reported above for the calcined MCM-48. This explains why the mesoporous carbons are smaller than their parent template after dissolution of the silica template.

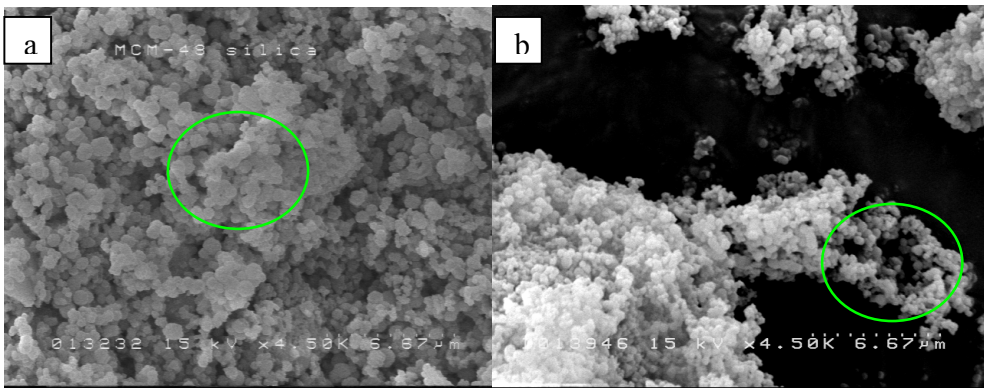

Figure 3.7: SEM images of MCM-48 silica template (a) - calcined (b) – calcined and heated to 900 ^{o}C for 2 h. The material in the circle was used to calculate the size of the particles.

The high resolution TEM image of a silica–carbon material is shown in Fig. 3.8 and also reveals that the resultant carbon particles (Fig. 3.8c) follow the same

structural organisation as that of the MCM-48 silica particles used for their preparation (Fig. 3.8a) and hence are a faithful replica of the silica template. It has been previously reported that porous polymers and metals [73, 74] prepared from the same kind of silica templates also contained ordered (and disordered) regions. In principle, this suggests that the degree of replication order is determined in this case by the crystallinity of the template used for the preparation of such carbons.

A HR-TEM micrograph of the MCM-48 is shown in Fig. 3.8b. This photograph is contrasted with that of the polystyrene coated carbonised MCM-48 sample shown in Fig. 3.8d. Furthermore, Fig. 3.8d reveals the coating of the silica by polystyrene and indicates the graphitic nature of the carbon. The coating appeared to be about 10–15 nm thick and while not completely graphitised indicates small domains of graphitic carbon (lattice spacing of ~3.3 nm, Fig. 3.8d). Thus, the carbon prepared in this work displays an ordered porosity and a partially graphitic structure. Interestingly, highly graphitised carbons were also observed in the sample (see Fig. 3.9 and Fig. 3.10). Su and co-workers [75] reported that the structural ordering of the resultant carbons produced from polymerisation and pyrolysis of the carbon precursors during high temperature carbonisation often lead to the emission of a large amount of small molecules such as water, which can deteriorate the pore strucute of the templates.

Figure 3.8 reveals that the carbon particles show limited interaction between the silica and the carbon, and furthermore the carbon particles are orthogonal to the surface of template. From this observation it was anticipated that the fraction of the graphitic carbon produced using this synthesis route would be lower compared to the armphous carbon produced. In fact, it has been lately established [76] that the CVD method, which is a well-established technique for preparing carbon molecular sieves [77], carbon nanofibers [78], and carbon nanotubes [79], has a number of advantages over the liquid-phase impregnation method, such as a high degree of pore filling [80], easy control over the amount of pyrolytic carbon deposited in the template pores [76], enabling the formation of graphitic pore walls [52], and avoiding the formation of additional microporosity [81].

In order to create graphitic pore walls, Xia and co-workers [52, 82] employed a CVD method with styrene and acetonitrile as the carbon precursors to synthesise ordered mesoporous carbons. However, the morphology of the replicated carbon particles was observed to be different from that of the silica template when CVD temperature was higher than 900 ^{o}C.

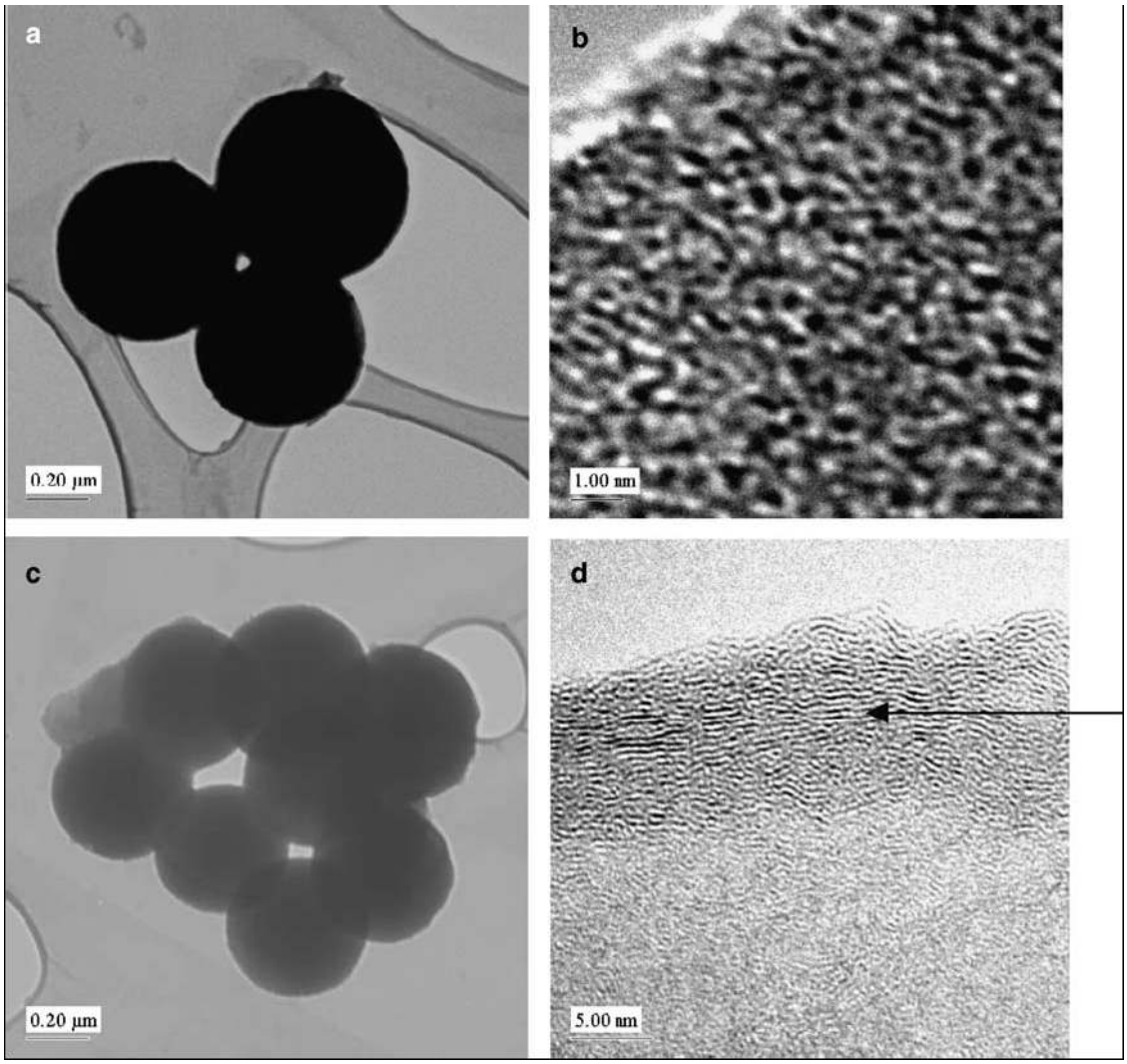

Figure 3.8: High resolution TEM images showing the (a) morphology and (b) structural organization of MCM-48 silica particles; and (c) morphology and (d) structural organization of sample carbonised with polystyrene/acid/toluene, pyrolysed at 900 ^{o}C for 2 h. Arrow shows the graphitic nature of the material.

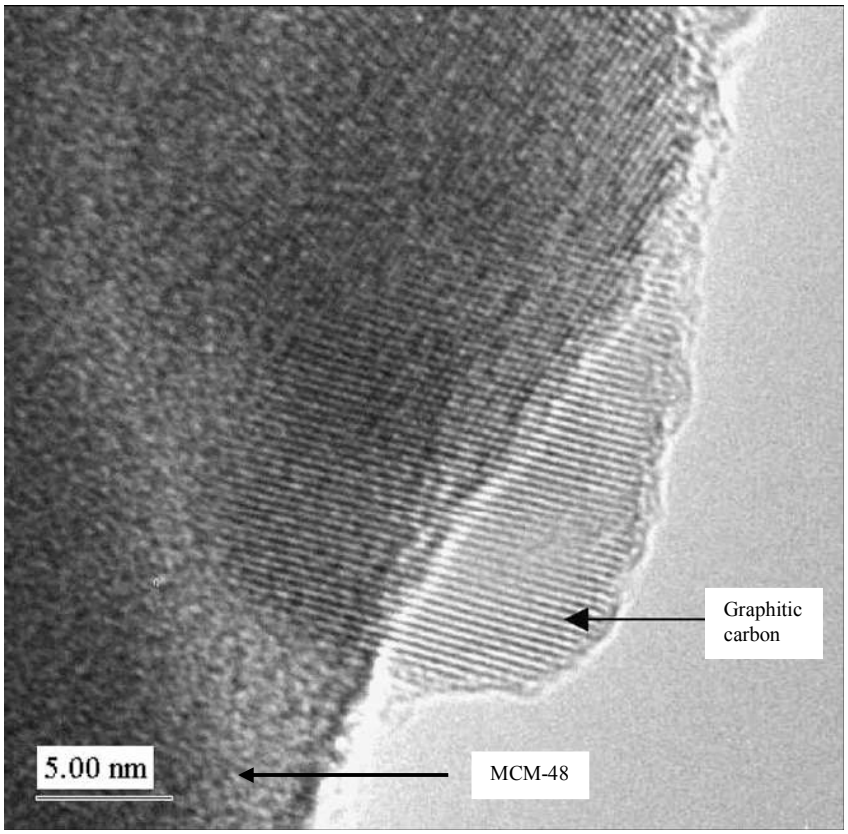

Figure. 3.9: A graphitised carbon deposited onto MCM-48 silica, two step carbonisation (1st step = 0.5 g and 2nd step = 0.75 g polystyrene). The figure shows limited interaction between carbon and silica particles.

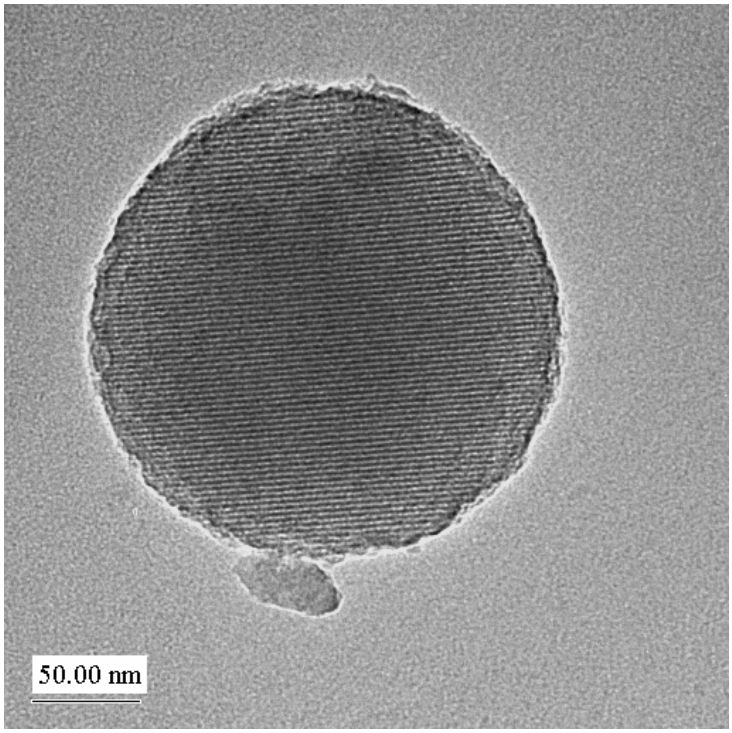

Fig 3.10: A highly graphitised mesoporous carbon (taken at a higher magnification) showing the parallel order of graphene sheets that are linearly arranged.

It is also interesting to note that the TEM image of the mesoporous carbon displayed in Fig. 3.9 shows the parallel ordering of graphene sheets that are linearly arranged. Using polystyrene as the carbon, it was expected that this benzene containing material, would form fused rings that take on a sheet like form after deposition and reaction on the template surface. This phenomenon was also observed by Kim and co-workers [51] in the preparation of an ordered mesoporous carbon using a synthetic mesophase pitch (mixture of naphthalene-derived compounds exhibiting liquid-crystal arrangement of discotic polyaromatic molecules) as the carbon precursor. It was also noted that using this kind of pitch is advantageous as it yields carbons with negligible amount of micropores due to a small percentage (below 20%) of non-carbon elements in the mesophase pitch, which are micropore-creating agents.

3.3.4 Adsorption properties of inverse carbon replicas of MCM-48

Gierszal *et al*. [42, 43] have investigated adsorption properties of different carbon replicas and have found that their properties depend on the type of the carbon precursor used. They further reported that carbons prepared from mesophase pitch with high SP, revealed a low total volume and a small surface area. This was attributed to the fact that the carbonised high SP pitch contains a considerable amount of large polyaromatic compounds, which after carbonisation afford

carbons with extremely low microporosity. In contrast, carbons prepared from pitches with lower SP possessed not only higher total pore volume but secondary porosity, which indicated some deterioration of their ordered structures. This was manifested by a steady increase in the adsorption isotherm curve, which appeared after the step reflecting capillary condensation in primary mesopores. On the other hand, carbons synthesized from the carbon precursor giving much lower coke yield such as sucrose, furfuryl alcohol, and petroleum pitch exhibited low external surface area and large total pore volume [42, 43].

The nitrogen adsorption-desorption isotherms of MCM-48 and the corresponding carbon prepared using 1.25 g in the whole double impregnation are presented in Fig. 3.11. The two isotherms are of type IV and exhibited hysteris loops, indicating mesoporous characteristics with a capillary condensation phenomenon. As seen in Fig. 3.11, there is a sharp condensation step in the adsorption and desorption curves of the parent silica template in the range of relative pressures of 0.4 - 0.7 corresponding to the existence of mesopores with a narrow pore size distribution. The nitrogen sorption isortherm for a mesoporous carbon shows a peculiar adsorption-desorption behaviour indicating the existence of two different

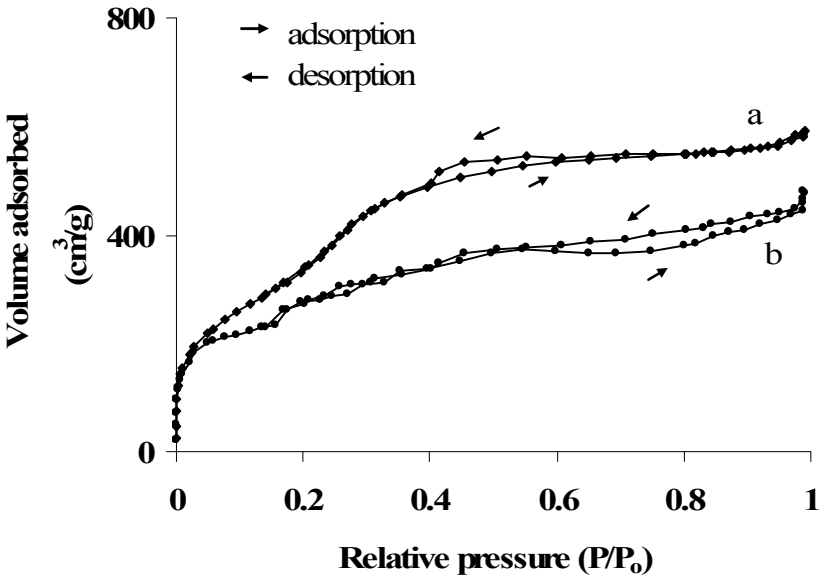

Figure 3.11: Nitrogen adsorption-desorption isotherm of (a) MCM-48 silica template and (b) a mesoporous carbon, two step carbonization (1st step = 0.5 g and 2nd step = 0.75 g polystyrene).

pore systems. Thus, a small fraction of micropores is observed at relative pressures <0.4 and above 0.4 there is a notable hysterisis loop attributable to the mesopore system of the mesoporous carbon.

Considering the adsorption behaviour of the two isotherms, it can be seen (Fig. 3.11) that their shapes looks similar at relative pressure between 0.5-0.9 indicating that the impregnating / coating process did not significantly change the accessible

surface. Although the BET surface area of the mesoporous material changed upon coating, its total pore volume also decreased remarkably (Table 3.1). This decrease depended on the coating level [23] and most probably the type of carbon source used, as other previously prepared carbons prepared using different carbon sources did not exhibit this behaviour [44,50].

The corresponding pore size distribution of the silica template and the carbon material calculated from the adsorption branches of the nitrogen isotherm by the BJH method [72] shows that the pore size distribution is narrow (see Fig. 3.12) with an average pore diameter of 2.9 and 2.3 nm, respectively.

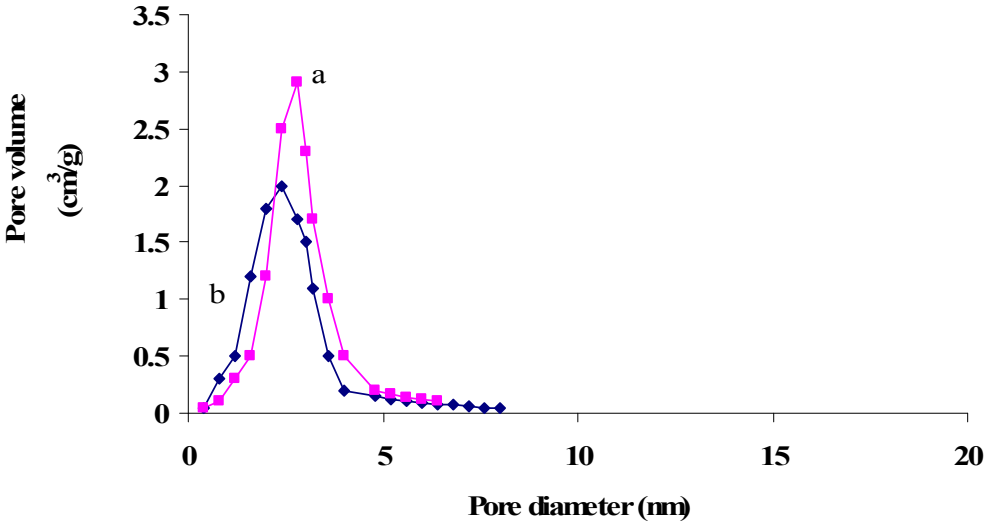

Figure 3.12: Pore size distributions of (a) - MCM-48 silica template and (b) a mesoporous carbon from the desorption curve, two step carbonization (1st step = 0.5 g and 2nd step = 0.75 g polystyrene).

3.3.5 Investigation of the carbon/silica composite ratios in the resultant carbons

Thermogravimetric weight changes were recorded under a nitrogen atmosphere and were used to determine the carbon and the silica contents in the composite materials. The corresponding results are presented in Fig. 3.13. The weight loss at temperatures below 100 ^{o}C amounted to 2 – 7 % and can be related primarily to the thermo-desorption of physisorbed water for all samples. A further weight loss

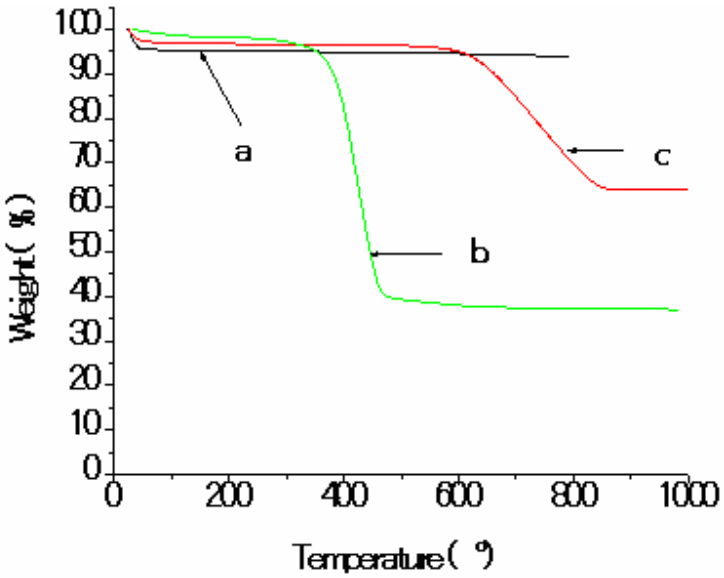

Figure 3.13: TGA profiles of (a) - MCM-48, (b) – carbonized MCM-48 sample and (c) mesoporous carbon (MC) (template removed).

was not observed with MCM-48 silica template indicating that more than 90 % silica was formed in the material. A major weight loss of ~ 60 % was centred at 400 ^{o}C for the carbon/silica composite, which can be attributed to the decomposition of carbon material and the remaining 40 % would be assigned to the silica content in the material.

The analysis of a typical mesoporous pyrolysed sample (silica template removed) gave no mass loss at T < 600 ^{o}C. Above 600 ^{o}C, 30 % of the carbon was combusted indicating that the partially graphitised more stable form of carbon

constituted about 70 % of the carbon formed after a pyrolysis step at 900 ^{o}C, which plays the crucial role of forming the polymerised mesoporous carbon material. These results provide additional confirmation of the graphitized nature of the mesoporous carbon frameworks, which is responsible for the much improved thermal stability.

Energy dispersive X-ray (EDX) analysis was performed and provided elemental concentration in the typical mesoporous carbon material (Fig. 3.13c) of interest. The EDX results represented in Fig. 3.14 complimented the TGA data above and clearly showed that more than 70 % of the material was carbon (distinct peak at low energy which is due to the Kα fluoerescence x-rays of carbon at 0.277 keV). A small peak at Kα = 1.74 keV is observed and is due to the silicon. This indicates that a small concentration of the silica template material is still present in the resultant carbon material, and was not completely dissolved during template removal with HF solution. Therefore, from the EDX data we can conlude that the carbon/silica ratio was 4:1.

In addition, Fig. 3.15 shows the XRD pattern of the observed carbonaceous material (shown in Fig. 3.8) which exhibit peaks at 2h = 27, 45 and 54 which can respectively be ascribed to (002), (101) and (004) planes associated with the

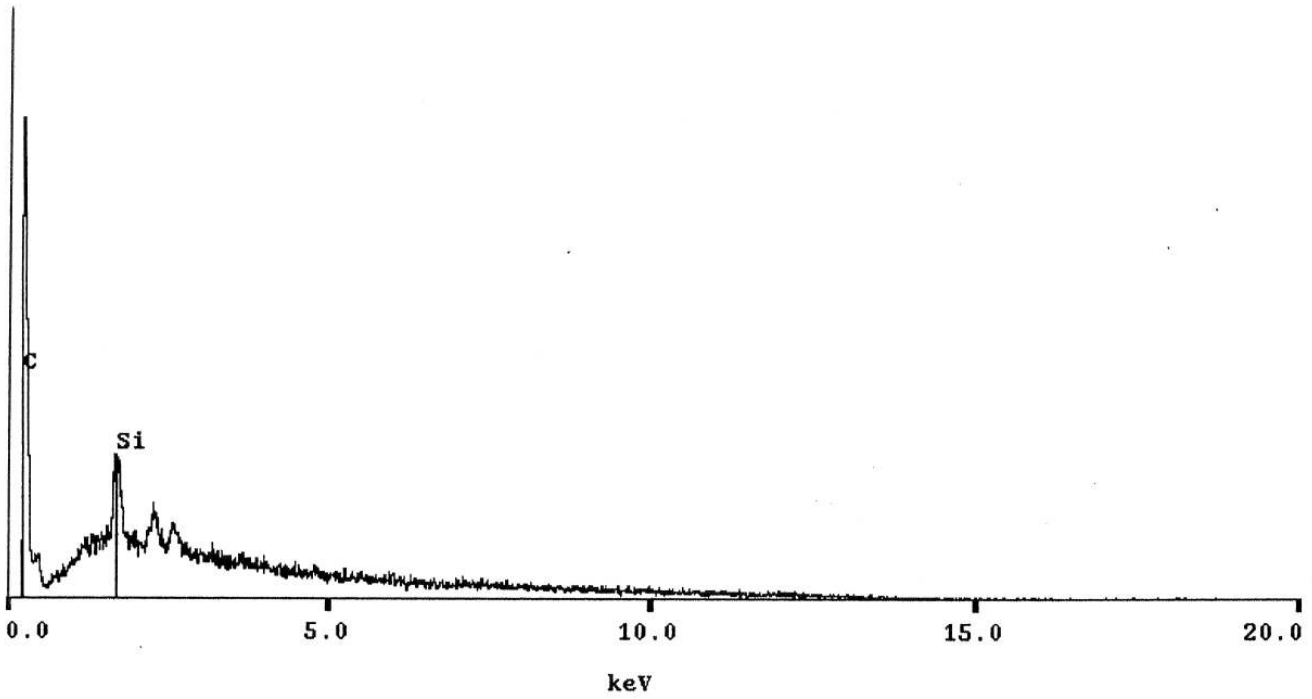

Figure 3.14: EDX profile of a typical mesoporous carbon.

Partially graphitic pore walls [52]. The information from the XRD indicated that the carbon framework was to a certain extent atomically ordered hence the appearance of Bragg lines in the region 2θ at approximately 26° [52].

Although the carbonisation reaction starts at low temperatures due to the sulfuric acid catalyst, the pyrolysis has to be performed at temperatures >700 ^{o}C. Below this temperature only weak diffraction intensity due to the incomplete cross linking of the carbon framework is observed [39]. As already mentioned earlier, the pyrolysis step plays the crucial role of forming the polymerized mesoporous carbon material.

The Raman spectrum for the resultant pyrolysed sample is shown in Fig. 3.16. The spectrum obtained for the MCM-48 template (not shown) revealed characteristics of a mesoporous silicate template [70]. The pyrolysed samples (Fig. 3.16) however gave good Raman spectra and two pronounced absorption bands associated with the stretching modes of carbon–carbon double bonds (C=C) of typical graphite, were clearly observed. These bands indicated the presence of both graphitic single crystals (G band; 1600 cm^{-1}) and non-graphitic (D band; 1350 cm^{-1}) carbon [69]. The D band is associated with vibrations of carbon atoms with dangling bonds in plane terminations of the disordered graphite and related to the defects and disorders in structures in carbon materials.

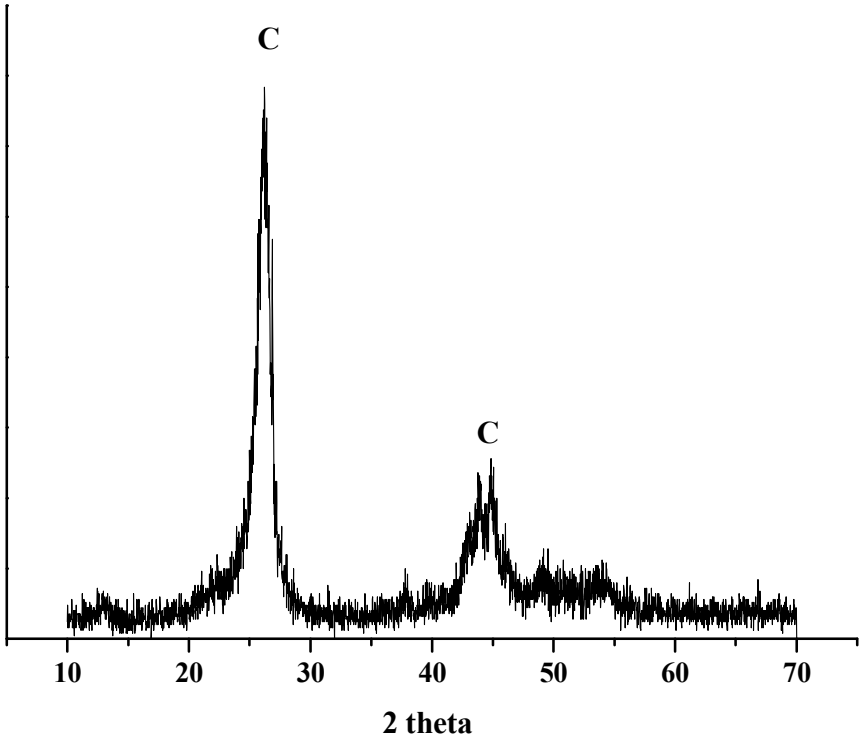

Figure 3.15: XRD pattern of mesoporous carbon (2 theta > 10°) showing the structural organization of carbon, (C = carbon), two step carbonization (1st step = 0.5 g and 2nd step = 0.75 g polystyrene).

The relative intensities of these two bands depend on the type of graphitic materials and reflect the graphitization degree. Su and co-workers [75] reported similar observations and further explained that the broad peak with a low intensity

at 1350 cm^{-1} and the narrow peak with a high intensity at 1600 cm^{-1} indicated that the carbons were possibly composed of small graphite sheets with a low graphitization degree [75]. Importantly, the Raman spectrum indicates the presence of the graphitic nature of the new mesoporous carbon material [50].

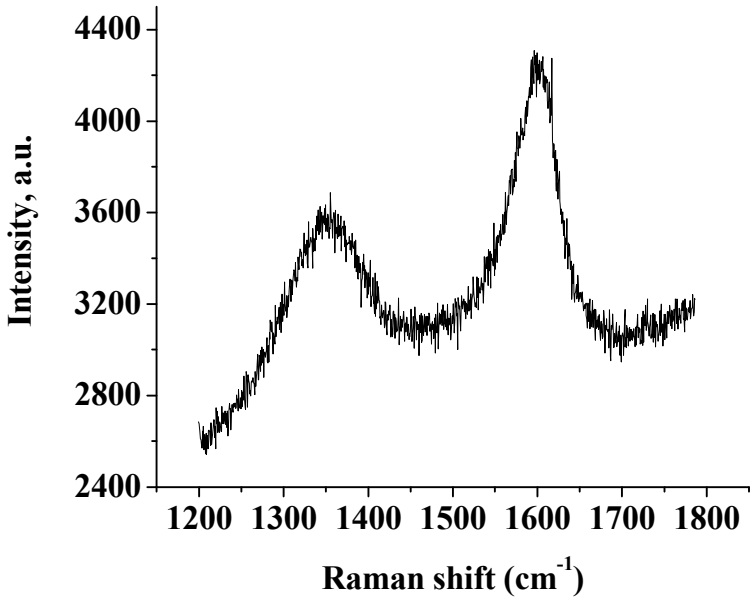

Figure 3.16: Raman spectra of the mesoporous carbon, two step carbonization (1st step = 0.5 g and 2nd step = 0.75 g polystyrene).

The only other Raman data reported for an equivalent graphitised mesoporous carbon revealed a poorly graphitised material as detected by the D/G band ratio [45].

3.4 Conclusion

A well defined synthesis route to mesoporous graphitic carbon is reported in this work. The use of a template is essential in the synthesis of the mesoporous carbon framework, as carbons synthesized under otherwise identical conditions without a template were found to have low surface areas, and no pore structure. The catalytic carbonization procedure used has an advantage as uniform infiltration of the carbon precursor can be easily accomplished inside the silica mesopores so that the resultant carbon materials retain the mesostructural order of the silica templates.

In principle, from the experimental observation in this study, both mesoporous MCM-48 and mesoporous carbon show similar crystal morphology, which indicates the following two important points:

(i) mesoporous MCM-48 plays a role as a template or "skeleton", as carbons are formed inside the pore system of the crystal without serious damage to the mesoporous material due to precipitation on the external surface and

(ii) The mesoporous carbons can keep the same structural order/organization after dissolution of the silica template.

Furthermore, it has been shown that by varying the concentration of polystyrene solution, mesoporous carbons with different pore sizes and surface areas can be obtained, with the pores formed within the parent MCM-48 channels dependent on the amount of polystyrene used. The Raman, XRD and TEM techniques confirmed the partially graphitic nature of the resultant synthesised carbonaceous materials.

3.5 References

[1] A. B. Fuertes, *J. Mater. Chem*., **13**, 3085 (2003).

[2] M. Kim, K. Sohn, H. Bin Na and T. Hyeon, *Nano Lett*., **2**, 1383 (2002).

[3] J. Y. Kim, S. B. Yoon and J.-S. Yu, *Chem. Mater*., **15**, 1932 (2003).

[4] M. Kruk, M. Jaroniec, R. Ryoo and S. H. Joo, *Chem. Mater*., **12**, 1414 (2000).

[5] J. S. Beck, J. C. Vartuli, W. J. Roth, M. E. Leonowicz, C. T. Kresge and K. D. Schmitt, *J. Am. Chem. Soc*., **114**, 10834 (1992).

[6] J. Xu, Z. Luan, M. Hartmann and K. Larry, *Chem. Mater*., 2928 (1999).

[7] J. M. Kim, Y. Sakamoto, Y. K. Hwang, Y.-U. Kwon, O. Terasaki, S-E. Park,. *J. Phys. Chem. B*, **106**, 2552 (2002).

[8] J. Rathousky, M. Zukalova, A. Zukal and J. Had, *Collect. Czech. Chem. Commun*., **63**, 1893 (1998).

[9] R. Ryoo, S. H. Joo and J. M. Kim, *J. Phys. Chem. B*, **103**, 7435 (1999).

[10] W. Zhao and Q. Li, *Chem. Mater*., **15**, 4160 (2003).

[11] M. J. Kim, S. K. Kim and R. Ryoo, *Chem. Commun*., 259 (1998).

[12] K. Schumacher, P. I. Ravikovitch, A. Du Chense, A. V. Neimark and K. A. Unger, *Langmuir*, **16**, 4648 (2000).

[13] D. Kumar, K. Schumacher, C. von Hohensche, M. Grun and K. K. Unger, *Coll. Surf. A: Physicochem. Eng. Aspects*, **187–188**,109 (2001).

[14] A. Sarayi, *Chem. Mater*., **8**, 1840 (1996).

[15] C.-G. Wu and T. Bein, *Science*, **264**, 1757 (1994).

[16] Z. Li and M. J. Jaroniec, *J. Phys. Chem. B*, **108**, 824 (2004).

[17] J. Lee, J. Kim, Y. Lee, S. Yoon, S. M. Oh and T. Hyeon, *Chem. Mater*., **16**, 3323 (2004).

[18] B. Tian, S. Che, Z. Lin, X. Liu, T. Tsatumi, O. Terasaki, *Chem. Commun*., 2726 (2003).

[19] F. Kleitz. T.-W. Kim and Ryoo, *Langmuir*, **22**, 440 (2006).

[20] S. Han and T. Hyeon, *Carbon*, **37**,1645 (1999).

[21] S. Han and T. Hyeon, *Chem. Commun*.,1955 (1999).

[22] S. Han, M. Kim and T. Hyeon, *Carbon*, **41**, 1525 (2003).

[23] Z. Li and M. Jaroniec, *J. Am. Chem. Soc*., **123**, 9208 (2001).

[24] N. J. Coville and J. Li, *Catal. Today*, **71**, 403 (2002).

[25] D. J. Duvenhage and N. J. Coville, *Appl. Catal. A*, **233**, 63 (2002).

[26] N. N. Madikizela and N. J. Coville, *J. Mol. Catal. A*, **181**, 129 (2002).

[27] T. R. Motjope, H. T. Dlamini, G. R. Hearne and N. J. Coville, *Catal. Today*, **71**, 335 (2002).

[28] D. J. Duvenhage and N. J. *Coville, Appl. Catal. A*, **289**, 231 (2005).

[29] D. J. Duvenhage and N. J. Coville, *J. Mol. Catal. A*, **235**, 230 (2005).

[30] M. C. Bahome, L. L. Jewell, D. Hilderbrandt, D. Glasser and N. J. Coville, *Appl. Catal. A*, **287**, 60 (2005).

[31] F. Rodriguez-Reinoso, *Carbon*, **36**, 159 (1998).

[32] H. O. Pierson, *Handbook of carbon, graphite, diamond and fullerenes – properties, processing and applications*, William Andrew Publishing (1993).

[33] G. Ertl, H. Knözinger and J. Weitkamp, *Preparation of solid catalysts*, Germany: WileyVCH (1999).

[34] J. H. Knox, B. Kaur and G. R. Millward, *Chromatogr.*, **352**, 3 (1986).

[35] R. Ryoo, S. H. Joo and S. Jun, *J. Phys. Chem. B*, **103**, 7743 (1999).

[36] S. H. Joo, S. Jun and R. Ryoo, *Micropor. Mesopor. Mater.*, **44–45**, 153 (2001).

[37] S. Joo, S. J. Choi, I. Oh, J. Kwak, Z. Liu, O. Terasaki and R. Ryoo, *Nature*, **412**, 169 (2001).

[38] M. Kruk, M. Jaroniec, R. Ryoo and S. H. Joo, *J. Phys. Chem. B*, **104**, 7960 (2000).

[39] S. Jun, S. H. Joo, R. Ryoo, M. Kruk, M. Jaroniec, Z. Liu, *J. Am. Chem. Soc.*, **122**, 10712 (2000).

[40] J. Lee, S. Yoon, S. M. Oh, C.-H. Shin and T. Hyeon, *Adv. Mater.*, **12**, 359 (2000).

[41] J. Lee and T. Hyeon, *J. Am. Chem. Soc.*, **123**, 5146 (2001).

[42] K. P. Gierszal, T.-W. Kim and M. Jaroniec, *J. Phys. Chem. B*, **109**, 2326 (2005).

[43] K. P. Gierszal, M. Jaroniec, *Chem. Commum*., 2576 (2004).

[44] A. B. Fuertes and D. M. Nevskaia, *Micropor. Mesopor. Mater*., **62**, 177 (2003).

[45] Y. Oda, K. Fukuyama, K. Nishikawa, S. Namba, H. Yoshitake and T. Tatsumi, *Chem. Mater*., **16**, 3860 (2004).

[46] J. Lee, S. H. Joo and R. Ryoo, *J. Am. Chem. Soc*., **124**, 1156 (2002).

[47] P. T. Tanev and T. J. Pinnavaia, *Science*, **267**, 865 (1995).

[48] S. B. Yoon, J. Y. Kim and J.-S. Yu, *Chem. Commun*., 1536 (2002).

[49] I. Moriguchi, Y. Koga, R. Matsukura, Y. Teraoka and M. Kodama, *Chem. Commun*., 1844 (2002).

[50] C. H. Kim, D.-K. Lee and T. J. Pinnavaia, *Langmuir*, **20**, 2157 (2004).

[51] T.-W. Kim, I.-S. Park and R. Ryoo, *Angew. Chem. Int. Ed*., **42**, 4375 (2003).

[52] Y. Xia and R. Mokaya, *Adv. Mater*., **16**, 1553 (2004).

[53] M. Kaneda, T. Tsubakiyama, A. Carlsson, Y. Sakamoto, T. Ohsuna, O. Terasaki, S. H. Jun and R. Ryoo, *J. Phys. Chem. B*, **106**, 1256 (2002).

[54] T.-W. Kim, R. Ryoo, K. P. Gierszal, M. Jaroniec, L. A. Solovyov, Y. Sakamoto and O. Terasaki, *J. Mater. Chem.,* **15**, 1560 (2005).

[55] Y. Sakamoto, T.-W. Kim, R. Ryoo and O. Terasaki, *Angew. Chem. Int. Ed.,* **43**, 5231 (2004).

[56] R. Ryoo and S. H. Joo, ***Stud. Surf. Sci. Catal.*** **148**, 241 (2004).

[57] L. A. Solovyov, T.-W. Kim, F. Kleitz, O. Terasaki and R. Ryoo, ***Chem. Mater.*** **16**, 2274 (2004).

[58] T.-W. Kim, I.-S. Park and R. Ryoo, ***Angew. Chem. Int. Ed.*** **42**, 4375 (2003).

[59] H. Darmstadt, C. Roy, S. Kaliaguine, T.-W. Kim and R. Ryoo, ***Chem. Mater.*** **15**, 3300 (2003).

[60] H. Darmstadt, C. Roy, S. Kaliaguine, T.-W. Kim and R. Ryoo, ***Stud. Surf. Sci. Catal.*** **146**, 335 (2003).

[61] O. Terasaki, Z. Liu, T. Ohsuna, T. Kamiyama, D. Shindo, K. Hiraga, S. H. Joo, T.-W. Kim and R. Ryoo, ***Stud. Surf. Sci. Catal.*** **146**, 275 (2003).

[62] J. M. Kim, M. Kang, S. H. Yi, J. E. Yie, S. H. Joo and R. Ryoo, ***Stud. Surf. Sci. Catal.*** **146**, 53 (2003).

[63] Z. Li and M. Jaroniec, *Chem. Mater*., **15**, 1327 (2003).

[64] Z. Li , M. Jaroniec, Y. J. Lee and L. R. Radovic, *Chem. Commun*., 1346 (2002).

[65] Z. Li, G. D. del Cul, W. Yang, C. Liang and S. Dai, *J. Am. Chem. Soc*., **108**, 12782 (2004).

[66] H. Yang, Y. Yan, Y. Liu, F. Zhang, R. Zhang, Y. Meng, M. Li, S. Xie, B. Tu and D. Zhao, *J. Phys. Chem. B*, **108**, 17320 (2004).

[67] D. Walton and P. Lorimer, *Polymers*, Oxford: Oxford University Press (2000).

[68] J. Clayden, N. Greeves, S. Warren and P. Wothers, *Organic chemistry*. Oxford: Oxford University Press (2001).

[69] X-Y. Liu, B-C. Huang and N. J. Coville, *Carbon*, **40**, 2791 (2002).

[70] A. Sakthivel, S-J. Huang, W-H. Chen, Z-H. Lan, K-H. Chen, T-W. Kim, *Chem. Mater.,* **16**, 3168 (2004).

[71] D. Gonzalez, M. A. Montes-Moran, R. J. Young and A. B. Gracia, *Fuel Process Technol*., **79**, 245 (2002).

[72] E. P. Barrett, L. G. Joyner, P. P. Halenda, *J. Am. Chem. Soc*., **73**, 373 (1951).

[73] S. A. Johnson, P. J. Ollivier and T. E. Mallouk, *Science*, **283**, 963 (1999).

[74] G. L. Egan, J. S. Yu, C. H. Kim, S. J. Lee, R. E. Schaak and T. E. Mallouk, *Adv. Mater*., **12**, 1040 (2000).

[75] F. Su, J. Zeng, X. Bao, Y. Yu, J. Y. Lee and X. S. Zhao, *Chem. Mater*., **17**, 3960 (2005).

[76] J. Parmentier, C. Vix-Guterl, P. Gibot, M. Reda, M. Ilescu, J. Werckmann and J. Patarin, *Micropor. Mesopor. Mater*., **62**, 87 (2003).

[77] Y. Kawabuchi, M. Kishino, S. Kawano, D. D. Whitehurst and I. Mochida, *Langmuir*, **12**, 4281 (1996).

[78] G. B. Zheng, K. Kouda, H. Sano, Y. Uchiyama, Y. F. Shi and H. J. Quan, *Carbon*, **42**, 635 (2004).

[79] K. Hata, D. N. Futaba, K. Mizuno, T. Namai, M. Yumura and S. Iijima, *Science*, **306**, 1362 (2004).

[80] T. Kyotani, Z. Ma and A. Tomita, *Carbon*, **41**, 1451 (2003).

[81] F. Ehrburger-Dolle, I. Morfin, E. Geissler, F. Bley, F. Livet, C. Vix-Guterl, S. Saadallah, P. Julien, M. Reda, J. Patarin, M. Ilescu, and J. Werckmann, *Langmuir*, **19**, 4303 (2003).

[82] Y. Xia, Z. Yang and R. Mokaya, *J. Phys. Chem. B*, **108**, 19293 (2004).

PART II: APPLICATIONS OF MESOSTRUCTURED CARBONACEOUS MATERIALS AS SUPPORTS FOR FISCHER-TROPSCH CATALYSTS

Chapter Four

The Fischer-Tropsch Process and Technology: A Review

4.1 Introduction

"*The fifth revolution will come when we have spent the stores of coal and oil that have been accumulating in the earth during hundreds of millions of years… It is to be hoped that before then other sources of energy will have been developed… Whether a convenient substitute for the present fuels is found or not, there can be no doubt that there will have to be a great change in the ways of lifes. This change may justly be called a revolution, but it differs from all the preceding ones in that there is no likelihood of its leading to increases of population, but even perhaps to the reverse.*" Sir Charles Galton Darwin, 1952 [1].

"*Why did you transport that oil halfway across the earth?*" Plinky Fisk II [1].

"*I'd put my money on the sun and solar energy. What a source of power! I hope we don't have to wait 'til oil and coal run out before we tackle that.*" Thomas Edison [1].

So wrote, energy experts many years ago. The truth of the words above can be applied to many situations, but they refer specifically to today's problem with crude oil supply. Indeed, at the present moment, the world's fuel and chemical production is based predominantly on petroleum crude oil even though other fossil fuels such as coal and natural gas can be utilized as feedstock for the chemical industry and the transportation fuels market [2]. Crude oil had been considered an abundant and lasting cheap source of energy until 1949 when studies began to show that oil would not last as long as expected [3]. In 1971, Hubbert predicted that the world oil production would peak due to the progressive depletion of existing resources, decline of proven reserves, and tighter spare capacity of the oil producing countries [4-6]. The Hubbert peak (peak production year) has not yet been accurately predicted; however experts and government agencies (such as the US Energy Information Association, USEIA) generally agree that peaking will occur in the coming decades.

This uncertainty of predicting oil production peaking and continued worldwide oil demand dramatically affects the oil prices as can be observed in Figure 4.1. In addition, the future oil prices are likely to follow an increasing trend due to the following factors:

- Spare capacity is getting tighter [7, 8] in all petroleum producing countries and reserve growth is declining;

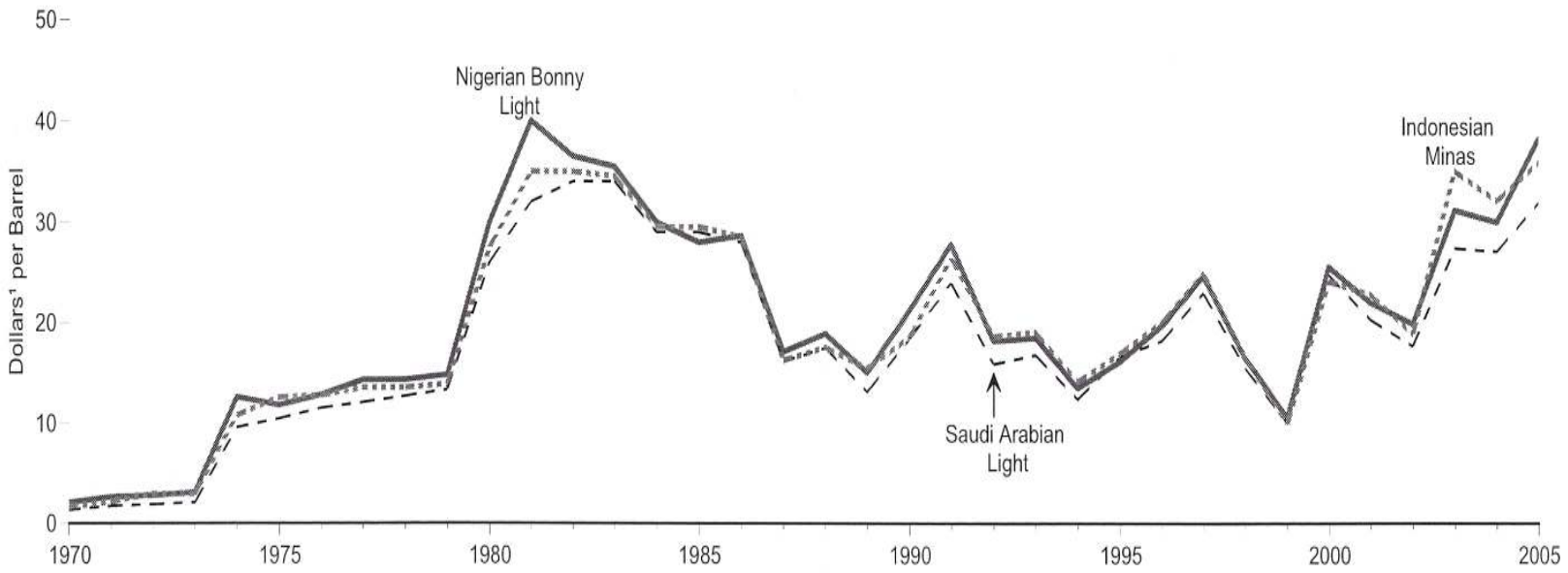

Figure 4.1: Trends in crude oil prices from 1970 to 2005 [6].

Nigerian bonny light: A very light (35 o API) and sweet (low sulfur content) oil which accounts for 65 % of crude oil reserves in Nigeria. API – America petroleum institute.

Saudi Arabian light: One of the five types of Arabian crude oil. The oil and its products are exported via Ras Tanura port on the Arabian gulf and Yanbu' port on the Red sea.

Indonesian minas: One of Indonesia 's onshore based crude oil reserves located in central Sumatra (Indonesia's largest oil producing province). 35 o API gravity.

- Recoverable oil reserves will require much higher capital investments in order to be exploited when compared to low capital cost reserves exploited today [7, 8] (deeper reserves, more expensive areas to drill, poorer oil quality needing more treatment);
- Developing countries, and more specifically China and India with their increasing demand, are likely to worsen the problem. For example, since the early 1990s, China's oil demand has risen faster than anywhere else in the world (around 6 % annual growth) [9], Chinese oil consumption still remains low when compared to other developed or even developing countries leaving plenty of room for growth [7];
- Political unrest in the Middle-east; and
- Tougher environmental laws preventing oil companies from drilling in wild-life reserve regions.

Thus, from the current and future oil supply/demand and increasing prices, it is of prime importance to find alternative fuel sources in order to dampen the economical impact of the energy crunch. To this end, synthetic fuels, mainly produced via Fischer-Tropsch (F-T) synthesis are exhibiting quite interesting features, which make them good candidates as alternative and/or complementary sources of fuel. Moreover, worldwide demand for clean, reliable and affordable energy has never been greater. Due to the large quality of raw materials (coal or

natural gas) which could be used in the F-T process, the intrinsic properties of the produced liquids exhibit the following advantages when compared to crude oil:

- Natural gas and coal needed for the production of the synthesis gas (H_2 and CO) used for the F-T process are plentiful and available at a low cost. Reserves of natural gas are around 50 % more abundant than that of crude oil, and coal reserves also exceed those of oil by about 20 times [10], (see Table 1 provided in Appendix).
- Natural gas, which otherwise would have been flared during oil production can be used as a valuable feedstock in an F-T process [11].
- Natural gas has the largest heat of combustion relative to the amount of CO_2 formed. It produces 45 % less CO_2 than coal for a comparable amount of energy.
- Thus, F-T products are generally cleaner than crude oil [12] and do not require any further treatment to remove undesirable impurities (sulfur compounds, acid gases removal, etc.).
- They have low aromaticity content.
- The F-T process equipment can be installed on-site in large remote natural gas reservoirs which would have been uneconomical to exploit otherwise; and therefore the F-T process can solve expensive transportation costs of liquid natural gas (LNG) [11].

- The kerosene/jet fuel produced has good combustion properties and high smoke points [12]
- The diesel fuel with its high cetane number can be used to upgrade lower quality blend stocks produced from crude oil [12].
- Linear olefins required in the chemical industry can be produced either directly in the FT process or by dehydrogenation of the paraffinic cuts [12].

The gas-to-liquid technology (GTL) with virtually unlimited markets offers a new way to unlock large gas reserves, complementary to other traditional technologies such as Liquefied Natural Gas (LNG) and pipelines [2,12-16]. However, coal or heavy residues can still be used as alternatives on sites where these are available at low costs.

This chapter presents a literature review on the Fischer-Tropsch process. The F-T chemistry, the reactors and catalysts used are described in order to fully understand parameters influencing the overall performance of the F-T process. Furthermore, the objectives of this study in relation to catalytic evaluation of the FTS are outlined at the end of the chapter.

4.2 The Fischer-Tropsch process

In 1897, Losanitsch and Jovitschitsch reported the conversion of CO and hydrogen to liquid products using an electric discharge [13,17]. Not long after that (1902), the synthesis of hydrocarbons from CO hydrogenation over transition metal catalysts was discovered when Sabatier and Senderens produced CH_4 from H_2 and CO mixtures passed over Ni, Fe, and Co catalysts [13,18]. In 1923, Fischer and Tropsch reported the use of alkalised Fe catalysts to produce liquid hydrocarbons rich in oxygenated compounds — termed the Synthol process. Succeeding these initial discoveries, considerable effort went into developing catalysts for this process [13,19].

A precipitated Co catalyst with 100 parts by weight Co, 5 parts by weight ThO_2, 8 parts by weight MgO, and 200 parts by weight kieselguhr (silicious diatomatous earth) became known as the "standard" atmospheric pressure process catalyst for converting CO and H_2 to alkanes. In 1936, Fischer and Pilcher developed the medium pressure (10-15 bar) FTS process [20]. Following this development, alkalized Fe catalysts were implemented into the medium pressure FTS process. Collectively, the process of converting CO and H_2 mixtures to liquid hydrocarbons over a transition metal catalyst has become known as the Fischer-

Tropsch (F-T) synthesis. A brief review of the main events that took place from 1897 to date is summarized in Table A2 provided in Appendix.

The first FT plant was commissioned in Germany in 1938 but was closed down after the end of the Second World War. Then in 1955, Sasol, now a world-leader in the commercial production of liquid fuels and chemicals from coal and crude oil, started Sasol I in Sasolburg, South Africa. Following the success of Sasol I, more Sasol plants, Sasol II and III, came on line in 1980 and 1982, respectively. These three plants as well as several other FT plants abroad produce more than 200 fuel and chemical products. The Mossgas plant which converts natural gas to FT products using a high temperature process and an iron catalyst started up in South Africa in 1992.

Additionally, Shell commissioned a plant in 1993 in Bintuli, Malaysia using the Shell Middle Distillate Synthesis process (SMDS), which is essentially an enhanced FT synthesis. Currently, Syntroleum is building a 10 000 barrels per day (bpd) specialty chemicals and lube oil plant located in Northwestern Australia. The breakthrough to a commercially viable new international industry plants for FT-GLT technology will begin when the 34 000 bpd Oryx plant of Qatar petroleum (51 %) and Sasol (49 %) in Ras Laffan, Qatar, goes on stream. This will be followed (in 2007) by the Nigerian plant, Esctavos Gas to Liquids

(EGTL), which will be owned by Chevron Nigeria (75 %) and Nigeria National Petroleum company (25 %). Both plants will use the Sasol's slurry phase technology [21].

The existing and planned GTL projects are summarised in Table A3 (Appendix section). To this end, FTS has attracted much attention, and an enormous amount of research and development effort is invested in understanding and expanding the technology. To this end, a comprehensive bibliography of FTS literature, including journal and conference articles, books, government reports and patents can be found in the Fischer-Tropsch Archive at www.fischer-tropsch.org.

The commercial FT process involves three main steps, namely: syngas production/formation and purification, FT synthesis, and product upgrading. The steps are described in more detail below and a schematic diagram of the three steps is shown in Figure 4.2.

4.2.1 Syngas production and purification

Given its availability methane is mostly preferred to coal for syngas production. When using natural gas as the feedstock, many authors [21-26] have recommended autothermal reforming or autothermal reforming in combination

with steam reforming as the best option for syngas generation. This is primarily attributed to the resulting H_2/CO ratio and the fact that there is a more favorable economy of scale for air separation units than for tubular reactors (steam methane reforming - SMR). If the feedstock is coal, the syngas is produced via high temperature gasification in the presence of oxygen and steam. The overall schematic diagram of the F-T process is given in Fig. 4.2.

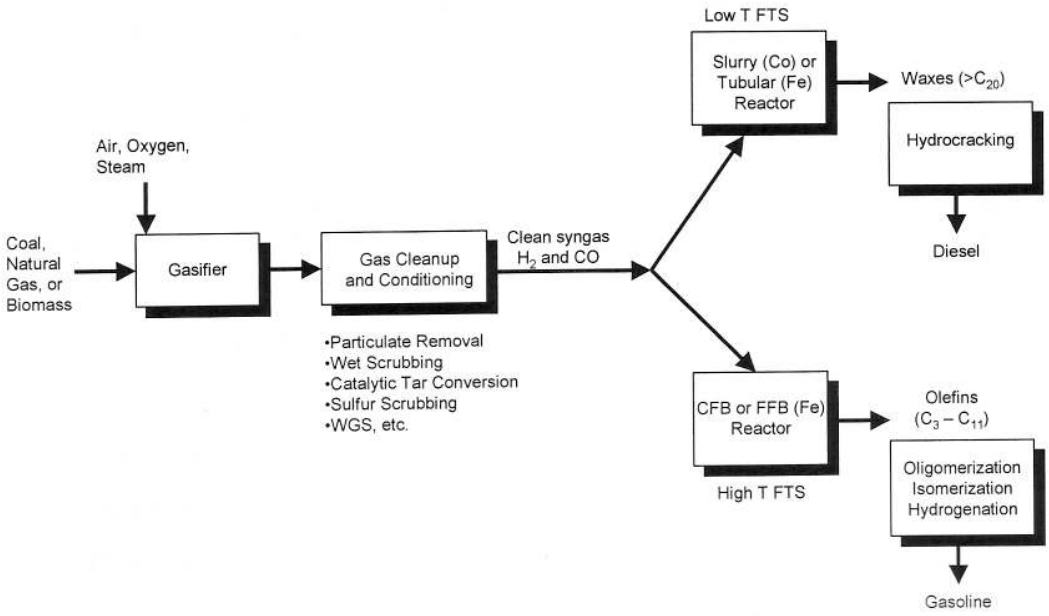

Figure 4.2: The overall Fischer-Tropsch process scheme [27].

4.2.2 The Fischer-Tropsch synthesis

Depending on the types and quantities of FT products desired, either low (200–240 °C) or high temperature (300–350 °C) synthesis is used with either an iron or cobalt catalyst [2, 12, 28-31]. FTS temperatures are usually kept below 400 °C to minimize CH_4 production. Generally, cobalt catalysts are only used at low temperatures. This is because at higher temperatures, a significant amount of methane is produced. Low temperatures yield high molecular mass linear waxes while high temperatures produce gasoline and low molecular weight olefins. If maximising the gasoline product fraction is the key issue, it is best to use an iron catalyst at a high temperature in a fixed fluid bed reactor. If maximizing the diesel product fraction is required, a slurry reactor with a cobalt catalyst is the best choice. The FT reactors are operated at pressures ranging from 10-40 bar.

4.2.3 Product Upgrading and Separation

Conventional refinery processes can be used for the upgrading of Fischer-Tropsch liquid and wax products. A number of possible processes for FT products are: wax hydrocracking, distillate hydrotreating, catalytic reforming, naphta hydrotreating, alkylation and isomerisation [32-34]. Fuels produced by the FT synthesis are of a high quality due their very low aromaticity and zero sulfur

content. The product stream consists of various fuel types: LPG, gasoline, diesel fuel, jet fuel. The diesel fraction has a high cetane number resulting in superior combustion properties and reduced emissions [34]. New and stringent regulations may promote replacement or blending of conventional fuels by sulfur and aromatic free FT products [35,36]. Also, other products besides fuels can be manufactured with Fischer-Tropsch catalyst in combination with upgrading processes, for example, ethene, propene, α-olefins, alcohols, ketones, solvents, specialty waxes, and so forth. These valuable by-products of the FT process have higher added values, resulting in an economically more attractive process economy.

4.3 Fischer-Tropsch Chemistry

FTS has long been recognized as a polymerization reaction [37] with the basic steps of:

1. Reactant (CO) adsorption on the catalyst surface
2. Chain initiation by CO dissociation followed by hydrogenation
3. Chain growth by insertion of additional CO molecules followed by hydrogenation
4. Chain termination
5. Product desorption from the catalyst surface

Chemisorbed methyl species are formed by dissociation of absorbed CO molecules and stepwise addition of hydrogen atoms. These methyl species can further hydrogenate to form methane or act as initiators for chain growth. Chain growth occurs via sequential addition of CH_2 groups while the growing alkyl chain remains chemisorbed to the metal surface at the terminal methylene group. Chain termination can occur at any time during the chain growth process to yield either an α-olefin or an *n*-paraffin once the product desorbs.

The following reaction summarises the FTS reaction:

1. $CO + 2H_2 \longrightarrow --CH_2-- + H_2O$ $\quad \Delta_rH$ (227 °C) = -165 kJ/mol

The water-gas shift (WGS) reaction is a secondary reaction that readily occurs when Fe catalysts are used. Combining reaction one (above) with reaction two (below) gives the net reaction for Fe catalyzed FTS (reaction 3).

2. $CO + H_2O \longrightarrow H_2 + CO_2$ (Water-Gas Shift)

3. $2CO + H_2 \longrightarrow --CH_2-- + CO_2$ (net overall FTS)

The required H_2 to CO ratio for the cobalt catalyst is 2:1 but since the iron catalyst performs WGS in addition to the FT reaction, the H_2 to CO ratio can be slightly lower (1.8) for the iron catalyst [2].

Specific FTS products are synthesized according to the following reactions.

4. $CO + 3H_2 \longrightarrow CH_4 + H_2O$ (Methanation)

5. $nCO + (2n+1)H_2 \longrightarrow C_nH_{2n+2} + nH_2O$ (Paraffins)

6. $nCO + 2nH_2 \longrightarrow C_nH_{2n} + nH_2O$ (Olefins)

7. $nCO + 2nH_2 \longrightarrow C_nH_{2n+1}OH + (n-1)H_2O$ (Alcohols)

Another competing reaction that becomes important in FTS is the Boudouard reaction:

8. $2CO \longrightarrow C(s) + CO_2$

Carbon deposition on the catalyst surface causes catalyst deactivation.

FTS is kinetically controlled and the intrinsic kinetics is stepwise chain growth, in effect the polymerization of CH_2 groups on a catalyst surface. FTS product selectivities are determined by the ability of a catalyst to catalyze chain propagation versus chain termination reactions. The polymerization rates, and therefore kinetics, are independent of the products formed. The probability of chain growth and chain termination is independent of chain length [37]. Therefore, selectivities of various hydrocarbons can be predicted based on simple statistical distributions calculated from chain growth probability and carbon number. The chain polymerization kinetics model known as the Anderson-Shulz-Flory (ASF) model is represented by the following equation:

$$W_n = n(1-\alpha)^2\alpha^{n-1}$$

W_n is the weight percent of a product containing n carbon atoms and α is the chain growth probability. This equation is graphically represented in Figure 4.3. It clearly displays the predicted distributions for several products and product ranges of particular interest [38].

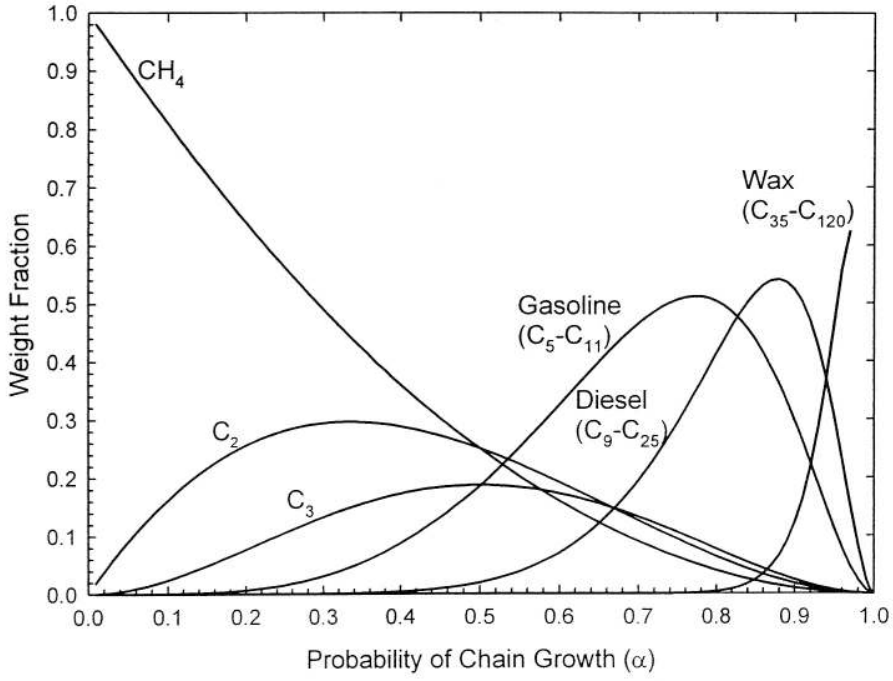

Figure 4.3: Anderson-Shulz-Flory distribution plot. Hydrocarbon selectivity as a function of the chain growth probability factor α, calculated using the above ASF equation.

The variables that influence the product distribution are: reactor temperature, pressure, feed gas composition, catalyst type, and promoters. However, despite the operating conditions, the FT reaction always produces a range of olefins, paraffins, and oxygenated compounds (alcohols, aldehydes, acids, and ketones).

4.4 FTS reactors

For large-scale commercial FTS reactors, heat removal and temperature control are the most important design features to obtain optimum product selectivity and long catalyst lifetimes [39-42]. Over the years, four types of FT reactors (Fig. 4.4) have been designed and used commercially. The fixed bed tubular reactor (Fig. 4.4 b) known as the ARGE reactor operates at 220-260 °C and 20-30 bar. High temperature circulating fluidized bed reactor (Fig. 4.4c), known as Synthol reactors, have been developed for gasoline and light olefin production. They operate at 350 °C and 25 bar.

Recently, the Sasol Advanced Synthol reactor (Fig. 4.4d) has been developed. It is a fixed fluidized bed reactor with similar operating conditions as the Synthol reactor at half the capital cost and size for the same capacity. The fourth reactor design is the low temperature slurry reactor which is a 3-phase reactor (Fig. 4.4a)

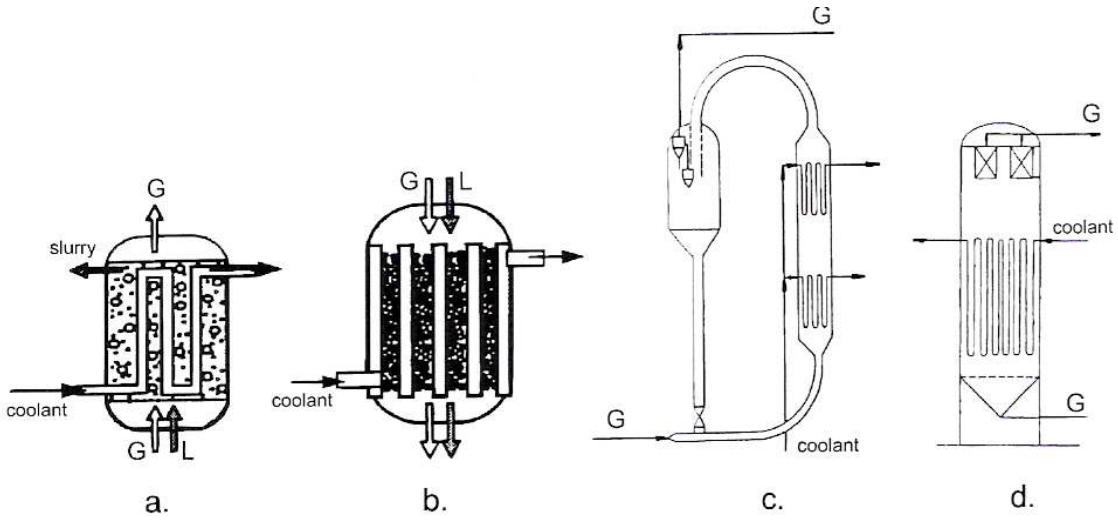

Figure 4.4: Possible reactors for Fischer-Tropsch synthesis. a. Slurry bubble column reactor; b. ARGE Multitubular fixed bed reactor; c. Circulating fluidized bed reactor; d Fluidized bed reactor [39-42]

consisting of a solid catalyst suspended and dispersed in a high thermal capacity liquid (often the FT wax product). Syngas is bubbled through the liquid phase achieving excellent contact with the catalyst while keeping the catalyst particles dispersed. The improved isothermal conditions in slurry reactors allow for higher average reactor temperatures leading to higher conversions to products. These reactors have only recently been put into commercial FT production primarily because one of the technical barriers was reliable catalyst separation from the FT waxes.

4.5 FTS catalysts

Catalysts play a pivotal role in FT synthesis. The basic concept of a catalytic reaction is that reactants adsorb onto the catalyst surface and rearrange and combine into products that desorb from the surface. Only the metals Fe, Ni, Co and Ru have the required FT activity for commercial application. Under practical operating conditions Ni produces too much methane. Although Ru is very active for FTS, the amount available in the world is insufficient for large scale applications considering its very high price. This leaves Fe and Co as viable catalysts [2]. In this thesis, only studies on Fe catalyst have been undertaken and the discussion below has been focused on this catalyst.

The three key properties of F-T catalysts are lifetime, activity and product selectivity [43-45]. Optimizing these properties for desired commercial application has been the focus of FT catalyst research and development since the processes were first discovered. Each one of these properties can be affected by a variety of parameters like:

- Use of promoters

With Fe catalysts, promoters are essential catalyst components [46]. For many years, potassium has been used as a promoter for Fe catalysts to effectively

increase the basicity of the surface. The objective thereof, is to increase the adsorption of CO on the metal surface, which tends to withdraw electrons from the metal, by providing an electron donor. Adding potassium oxide to Fe catalysts, also tends to decrease hydrogenation of adsorbed carbon species, so chain growth is enhanced [47-49], resulting in a higher molecular weight product distribution that is more olefinic. Potassium promotion also tends to increase the WGS activity [50,51] leading to a faster rate of catalyst deactivation because of the increased rate of carbon deposition of the surface of the catalyst.

Copper has also been successfully used as a promoter in Fe FTS [50, 53]. It has been shown to facilitate the reduction of Fe catalysts to active metals. It increases the rate of FTS more effectively than potassium, but decreases the rate of WGS reaction. The average molecular weight of the products increases in the presence of copper but not as much as when potassium is used.

- Catalysts preparation and formulation

Catalyst preparation impacts the performance of Fe catalysts. Fe catalysts can be prepared by precipitation [54-57] onto catalyst supports such as SiO_2 or Al_2O_3, or can be used as fused iron [58, 59] where formulations are prepared in molten iron, followed by cooling and crushing. A good methane selectivy of 7 % is achieved with the fused iron catalyst, and the catalyst produces products that are highly

olefinic [12]. In order to further decrease the undesirable methane selectivity a precipitated catalyst operated at lower temperatures is used. Moreover, to compensate for lower reaction rates at the lower operating temperature, higher surface areas are required; hence supports are used to achieve this.

Supports are essential Fe catalysts components. The advantage of spreading the active phase on a support is to disperse it throughout the pore system, thus making it possible to obtain a large active surface per unit weight used. On the other hand, a supported catalyst facilitates the flow of gases through the reactor and the diffusion of reactants through the pores to the active phase, improving the dissipation of reaction heat, retarding the sintering of the active phase and increasing the poison resistance [60].

Indeed, the selection of the support is based on a series of desirable characteristics: inertness; stability under reaction and regeneration conditions; adequate mechanical properties; appropriate physical form for the given reactor; high surface area (which is usually, but not always, desirable); porosity and chemical nature [60]. Of a wide range of possible supports, in practice only three combine these characteristics optimally, and they account for most industrial supported catalysts: alumina, silica and titania.

The potential of carbon as catalyst support has not yet been fully exploited, even though there is a considerable volume of literature devoted to this field in the last 20 years [58-63]. This large volume of research is mainly due to the fact that carbon has some characteristics that are very valuable and not attainable with any other support, although it is also true that carbon supports cannot be used in hydrogenation reactions > 427 ^{o}C or in the presence of oxygen > 227 ^{o}C, because it may become gasified to yield methane and carbon dioxide, respectively [64].

Although many types of carbon materials have been used to prepare carbon-supported catalysts (graphite, carbon black, activated carbon, activated carbon fibers, carbon-covered alumina, graphite intercalation compounds, glassy carbon, pyrolytic carbon, polymer-derived carbon, fullerenes, nanotubes, etc.), no studies have been reported on high surface area mesoporous carbons. These are the carbons used in this study. The mesoporous carbons have been shown to be graphitized, very porous with a high surface area, and have high thermal stability [64-66]. Most of their outstanding properties and the preparation of these carbons were described in detail in chapter 2 and 3.

4.7 Objectives of the study

Due to our interest in the synthesis of supported catalysts we wished:

- To evaluate the possibility of using mesoporous carbons as catalyst supports in the Fischer-Tropsch synthesis. This will be achieved by introducing Fe metal catalyst onto the surface structure of mesoporous carbons;
- To characterize the Fe/carbon-supported catalyst with TEM and SEM (in order to obtain insight in the dispersion of metal on the support); XRF (to determine the elemental composition of the catalysts); TPR (to determine the reduction behaviour of the catalysts); BET (to obtain textural properties of the catalyst) and XRD (to obtain the structural properties of the catalysts);
- To enhance the catalytic activity of an Fe/mesoporous carbon catalysts by the addition of a promoter (potassium ions);
- To investigate the effect of various amounts of potassium loading on the iron supported catalysts;
- To evaluate and compare the FTS activity, selectivity and productivity of Fe catalysts supported on mesoporous carbons relative to commercial activated carbons and MCM-48 silica under commercial representative reaction conditions in a slurry reactor;

- To compare where possible at a standard set of conditions, the results of this study with those of others' previous studies.

4.7 Conclusion

The information given in this chapter has indicated that the Fischer-Tropsch industry is slowly moving from a position of total dependence on crude oil refining to one which co-exists with natural gas refining, built around GLT technology facilities. In this chapter it has also been shown that catalysts play a pivotal role in FTS. In fact, catalysts in FTS are at the heart of a commercial plant because it is only on the catalyst performance, that the technology providers try to distinguish themselves in the global market. Furthermore, the chain growth probability is a fundamental property of any F-T catalyst, and together with the process operating conditions determines the product distribution.

Fundamental research is essential to achieve new and improved catalysts. Catalysts provide for operation of process modes, and are engineered to improve plant investment and operating costs, e.g., a catalytic slurry system can control heat release and decrease requirements for syngas recycle.

4.8 References

[1] http://www.thelifeaftertheoilcrash.net

[2] M. E. Dry, *Catal. Today*, **71**, 227 (2002).

[3] M. K. Hubbert, M. K., *Science*, **109**, 103 (1949).

[4] M. K. Hubbert, *Energy and Power*, **3**, 31 (1971).

[5] A. J. Cavallo, *Natural Resources Res*., **11**,187 (2002).

[6] http://www.hubbert peak.com

[7] K. Rehaag, "*Is the World Facing a 3rd Oil Shock?*," IEA (International Energy Agency), Workshop, F. I., Rio de Janeiro (2004).

[8] J.-P. Soriano, *Mass Transfer characteristics in an agitated slurry reactor operating under Fischer-tropsch conditions*, MSc. dissertation, University of Pittsburg, USA (2005).

[9] R. Sandrea, *Oil & Gas J*., **102**, 34 (2004).

[10] M. E. Dry, *Appl. Catal. A*, **276**, 1 (2004).

[11] A. C. Vosloo, *Fuel Process. Technol*., **71**, 149 (2001).

[12] A. P. Steynberg and M. E. Dry, *Fischer-Tropsch Technology: Studies in Surface Science and Catalysis*, Elsevier, **152**, (2004).

[13] B. Lutz, *Hydrocarbon Eng*., **6**, 28 (2001).

[14] http://www.chemlink.com.au/gtl.htm

[15] http://gassolutions.conoco.com

[16] http://www.energybulletin.net

[17] I. Kroschwitz and M. Howe-Grant, *Kirk-Othmer encyclopedia of chemical technology*, Wiley & Sons, New York, 4th ed. (1996).

[18] *http://www.pacificrenewables.com*

[19]] F. Fischer, H. Tropsch, *German Patent,* **484337** (1925).

[20] www.world-petroleum.org

[21] D. K. Rider, *Energy: Hydrocarbon Fuels and Chemical Resources*, John Wiley & Sons publication, New York (1981).

[22] B. Jager, M. E. Dry, T. Shingles and A. P. Steynberg, *Catal. Lett.*, **7**, 293 (1990).

[23] P. D. F. Vernon, M. L. H. Green, A. K. Cheetham and A. T. Ashcroft, *Catal. Lett.*, **6**, 181 (1990).

[24] J. Abbott and B. Crewdson, *Oil & Gas J.*, **100**, 70 (2002).

[25] V. R. Choudhary, K. C. Mondal and A. S. Mamman, *J. Catal.*, **233**, 36 (2005).

[26] P. M. Biesheuvel and G. J. Kramer, *AIChE J.*, **49**, 1827 (2003).

[27] P. L. Spath and D. C. Dayton, *Preliminary Screening – Technical and Economic Assessment of Synthetic Gas to Fuels and Chemicals with Emphasis on the Potential for Biomass-Derived Syngas*, NREL/TP-510-34929 [available at www.fischer-tropsch.org].

[28] *www.sasolchevron.com/conceptual_design.htm*

[29] *www.greenhouse.gov.au/transport/comparison/pubs/2ch3.pdf*

[30] *http://www.rentecinc.com*

[31] L. Casale, *British patent*, **274610**, 1927.

[32] G. N. Choi, S. J. Kramer, S. T. Tam, J. M. Fox, N. L. Carr and G. R. Wilson, *Design/economics of a once-through natural gas based Fischer-Tropsch plant with power co-production*, in Coal liquefaction and solid fuels, Pittsburgh (1997).

[33] A. M. Aitani, *14th annual Saudi-Japan Symposium on Catalysts in Petroleum Refining & Petrochemicals*, held at King Fahd University of Petroleum & Minerals (KFUPM), Dhahran, Saudi Arabia, December 5-6 (2004).

[34] G. P. Van der Laan, *Kinetics, Selectivity and Scale Up of the Fischer-Tropsch Synthesis*, Ph.D thesis, University of Groningen, The Netherlands, (1999).

[35] J. M. Fox, III, *Catal. Rev. Sci. Eng*., **35**, 169 (1993).

[36] J. H. Gregor, *Catal. Lett*., **7**, 317 (1990).

[37] R. B. Anderson, *The Fischer-Tropsch Synthesis*, Academic Press, Flodira, USA (1984).

[38] M. M. G. Senden, S. T. Sie, M. F. M. Post and J. Ansorge, *Appl. Sci.*, **225**, 227 (1992).

[39] B. H. Davis, *Catal. Today*, **71**, 249 (2002).

[40] B. Jager, *Stud. Surf. Sci. Catal.,***107**, 219 (1997).

[41] B. Jager, M. E. Dry, T. Shingles and A. P. Steynberg, *Catal. Lett.,* **7**, 293 (1990).

[42] R. L. Espinoza, A. P. Steynberg, B. Jager and A. C. Vosloo, *Appl. Catal. A.*, **186**, 13 (1999).

[43] C. Bartholomew, *Appl. Catal*., **212**, 17 (2001).

[44] N. Sirimanothan, H. H. Hamdeh, Y. Zhang and B. H. Davis, *Catal. Lett*., **82**, 181 (2002).

[45] D. B. Bukur and W.-P. Carreto-Vazquez, *Topics Catal*., **32**, 135 (2005).

[46] M. Luo and B. H. Davis, *Appl. Catal. A*, **246**, 171 (2003).

[47] A. G. Sault, *J. Catal*., **140**, 136 (1993).

[48] D. A. Wesner, F. P. Coenen and H. P. Bonzel, *Langmuir*, **1**, 478 (1985).

[49] D. J. Dwyer, J. H. Hardenburg, *Appl. Surf. Sci*., **19**, 14 (1984).

[50] D. B. Bukur, D. Mukesh, S. A. Patel, *Ind. Eng. Chem., Res*., **29**, 194 (1990).

[51] M. Luo, R. J. O'Brien, S. Bao, B. H. Davis, *Appl. Catal. A.*, **239** 111 (2002).

[52] G. P. Van der Laan and A. A. C. M. Beenackers, *Ind. Eng. Chem. Res*., **38**, 1277 (1999).

[53] D B. Bukur and C. Sivaraj, *Appl. Catal. A.*, **231**, 201 (2002).

[54] D. J. Duvenhage and N. J. Coville, *Appl. Catal. A.*, **298**, 211 (2006).

[55] T. C. Bromfield and N. J. Coville, *Appl. Catal. A,* **186**, 245 (1999).

[56] T. C. Bromfield and N. J. Coville, *Appl. Surf. Sci.*, **119**, 19 (1997).

[57] M. C. Bahome, L. L. Jewell, D. Hilderbrandt, D. Glasser and N. J. Coville, *Appl.Catal. A*, **287**, 60 (2005).

[58] Z. Kowalczyk, M. Krukowski, W. Rarog-Pilecka, D. Szmigiel and J. Zielinski, *Appl. Catal. A* , **248**, 67 (2003).

[59] Z. Liu, Q. Dong and Y. Chen, *Mater. Chem. Phys*., **53**, 67 (1998).

[60] F. Rodriguez-Reinoso, *Carbon*, **36**, 159 (1998).

[61] A. Dandekar, R. T. K. Baker and M. A. Vannice, *J. Catal.,* **183**, 131 (1999).

[62] J. M. Martin-Martinez and M. A. Vannice, *Ind. Eng. Chem. Res*., **30**, 2263 (1991).

[63] Van Steen and F. F. Prinsloo. *Catal. Today*, **71**, 327 (2002).

[64] C. N. Mbileni, F. F. Prinsloo, M. J. Witcomb and N. J. Coville, *Carbon*, In Press.

[65] H. Darmstadt, C. Roy, S. Kaliaguine, S. H. Joo and R. Ryoo, *Micropor. Mesopor. Mater.*, **60**, 139 (2003).

[66] H. Darmstadt, C. Roy, S. Kaliaguine, S. J. Choi and R. Ryoo, *Carbon*, **40**, 2673 (2002).

Chapter Five

Experimental Section

5.1 Introduction

Iron catalysts have been used for many decades in the synthesis of liquid hydrocarbons from syngas (Fischer-Tropsch reaction) because of their low cost, low methane selectivity, flexible product slate, and robustness at low H_2/CO ratios, and high water gas shift activity [1-4]. These catalysts can be prepared by different techniques such as impregnation, deposition precipitation and sol-gel procedures [5]. As already discussed in Chapter 4, unlike fused and sol-gel Fe catalysts, precipitated Fe catalysts operated at lower FTS temperatures are preferred as they tend to decrease the undesirable methane selectivity. Moreover, to compensate for lower reaction rates at the lower operating temperature, higher surface areas are required; hence supports are used to achieve this.

Owing to their interesting features such as high surface area, porosity, thermal stability, mechanical stability and inertness, carbon supports have recently attracted much attention in catalysis and nanotechnology [6]. However, the

potential of carbon as catalyst supports have not been fully exploited even though there has been a considerable volume of literature devoted to this field in past two decades. Many types of carbon have been used to prepare supported catalysts, such as graphite, activated carbon, carbon nanotubes, fullerenes, etc. [6]. However, the use of mesoporus carbons as supports for Fe catalysts is a new concept in the FTS field. Thus, we wish to prepare such carbons; impregnate the porous structure of the carbon support with an Fe catalyst using a deposition precipitation technique; characterise the catalyst precursors and finally evaluate their performance in FTS.

Continuous laboratory reactors are used to measure reaction kinetics and product distributions of the Fischer-Tropsch synthesis. Slurry phase FT experiments are performed in slurry reactors using either a liquid batch of FT-wax or a high boiling solvent. These reactor systems, are perfectly mixed recycle reactors with turbine impellers or gas inducers [7].

In this chapter we describe the procedures and techniques used to prepare and characterise the prepared precipitated Fe/K/carbon catalysts for FTS. The pretreatment method used in this study is compared to other methods used in the literature. The equipment used to perform experiments (gas-slurry Fischer-

Tropsch synthesis) as well as the experimental procedures and product analyses are also described below.

5.2 Preparation of supported iron catalyst

In this study, catalysts containing 15 wt. % Fe and various potassium loadings were prepared by a deposition precipitation method [8-11] followed by subsequent colloidal impregnation of the support. Three different supports were used, namely: activated carbon (used as received, 100 mesh, Darco G-60, GFS chemicals), mesoporous carbon and MCM-48 silica (both laboratory synthesized, see chapter 3 for detailed preparation methods) supports. Typically, a 0.2 M solution of $Fe(NO_3)_3.9H_2O$ (The Shepherd Chemical Co., USA) was stirred vigorously and then precipitated with an appropriate amount of 4 M NH_4OH (Aldrich). The amount of the precipitating agent was determined by the amount required to achieve a pH between 7.5 and 9 [12-14]. The precipitate was then separated from the liquid avoiding agglomeration; this was achieved by using a centrifuge (International equipment inc., USA). The precipitate was re-slurried in sufficient ethanol (denatured 94-96%, Alfar Aesar) to fill the pores of the individual support. The support was then added (physically mixed) to the precipitate slurry. The amount of support added guaranteed a metal loading of 15 wt.%. The catalyst precursor was spread thinly on a plate and dried overnight at

125 °C in a static oven, and then calcined at 250 °C for 6.5 h in an inert atmosphere (carbon supports) or in air (MCM-48 silica) using a heating rate of 5 °C/minute. The flow rate was maintained at 45 ml (STP)/minute per gram of support material.

The calcined precipitated iron catalysts were then impregnated (incipient wetness impregnation) with various amounts of K_2CO_3 (99.99%, Aldrich) to locate the maximum effect of the potassium promotion. Catalysts with three potassium loadings relative to the iron content i.e 100Fe/2K, 100Fe/5K and 100Fe/10K (atomic ratio) were prepared for comparative FTS studies. In this context the catalysts are referred to as 15%Fe/2%K/AC, 15%Fe/5%K/AC and 15%Fe/10%K/AC, respectively for metal catalysts supported on activated carbon and 15%Fe/2%K/MC, 15%Fe/5%K/MC and 15%Fe/10%K/MC, respectively for metal catalysts supported on mesoporous carbon. Furthermore, a 15%Fe/2%K/MCM-48 catalyst was also prepared in order to evaluate the catalytic performance of the catalyst precursor and also to compare the FTS of the oxidic supported Fe catalyst with the carbonaceous supported Fe catalysts.

5.3 Reactor set up

A one litre bolted autoclave **(1)** with an internal diameter of 6.7 cm, [manufactured by Pressure Product Industries Inc., PA] was used and a 2 μm internal sintered metal filter **(2)** was installed to remove wax samples from the catalyst slurry. The reactor is rated for a maximum working pressure of 41.4 MPa at a maximum temperature of 350 ^{o}C. A schematic diagram of the reactor set-up is presented in Fig. 5.1 and details of the reactor dimensions are summarized in Table 5.1. The reactor is equipped with an external heating jacket as well as a heating tape and thermal insulation **(3)** wrapped around the upper part of the reactor to achieve better temperature control. A hollow shaft connected to a six blade impeller **(4)** is used for mixing. Four holes **(5)** of 0.24 cm diameter drilled at each end of the hollow shaft enable the reactor to be operated in a gas-inducing mode. Thus, this enabled the vapour in the reactor to be recycled by the impeller.

The agitator **(6)** was always magnetically driven at 750 rpm to ensure complete mixing of the liquid phase, uniform distribution of the catalysts, and high mass and heat rates. A gas feed tube **(7)** was used to deliver reactant gas to the bottom of the reactor, flowing down through the catalyst slurry **(8)**. A three bladed baffle **(9)** was inserted into the

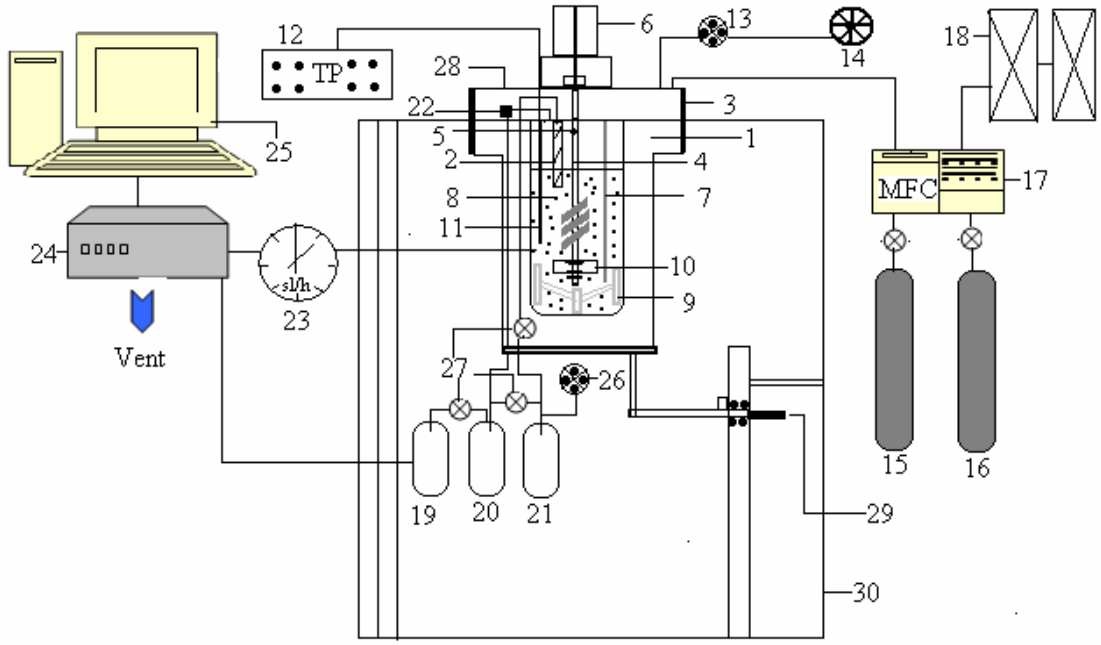

Figure 5.1: Schematic diagram of the CSTR reactor set up.

1: Autoclave; 2: internal sintered metal filter; 3: heating tape; 4: impeller; 5: holes; 6: magnetic agitator; 7: gas feed tube; 8: catalyst slurry; 9: three bladed baffle, 10: stirrer blades; 11: K-type thermocouple; 12: temperature programmer; 13: Bourdon tube type pressure gauge; 14: back pressure regulator; 15: CO gas cylinder; 16: H_2 gas cylinder; 17: Brookes mass flow controller; 18: purifying columns; 19: 0 ^oC cold trap (oil and water); 20: 100 ^oC warm trap (light wax); 21: 200 ^oC hot trap (heavy wax); 22: external sintered metal filter; 23: volumetric flow rate meter; 24: gas chomatrograph; 25: personal computer; 26: hot trap pressure regulator; 27: valves; 28: reactor cover; 29: elevating assy and 30: reactor stand.

Table 5.1: Reactor dimensions

Reactor internal diameter	6.7 cm
Reactor external diameter	11.1 cm
Internal length	26.0 cm
Impeller diameter	3.2 cm
Baffle width	5.8 cm
Reactor geometry	Cylindrical
Lower impeller clearance from the bottom	4.5 cm
Number of impellers	1
Number of blades on the impeller	6
Impeller type	Flat blade disk turbine
Hollow shaft length	17.8 cm
Shaft hole diameter	2.4 cm
Reactor internal depth	23.8 cm
Volume of reactor	0.98 litres
Reactor's material of construction	316 SS

autoclave, occupying a 5.8 cm diameter of the autoclave and leaving enough opening for the stirrer blades **(10)**. The baffle was used to prevent the formation of vortices.

The temperature inside the reactor was measured by a K-type thermocouple **(11)** inserted in the reactor vessel and a ramp soak temperature controller **(12)** (Omega, PPI, USA) was used to program the desired temperature. The liquid products were removed via a 2 μm internal sintered metal filter, which maintained the reactor catalyst inventory. The reactor pressure was measured with a Bourdon tube type pressure gauge **(13)** and kept constant at 2.0 MPa using a back pressure regulator **(14)**. CO **(15)** and H_2 **(16)** gases (both 99.9 % purity, Scott Gross inc., USA) were metered using a Brookes mass flow controller **(17)** with a flow of 2.5 sl/min. Two purification columns **(18)** were used to remove possible catalyst poisons like iron carbonyls, sulfides, and oxygen. The columns were packed with a calsicat 20 % wt. PbO_2 on Al_2O_3 catalyst at room temperature.

Product gas continuously exited the reactor to the warm trap **(20)** kept at 100 ^oC and the hot trap **(21)** kept at 200 ^oC through an externally mounted 7 μm sintered metal filter **(22)**, whereas the liquid reactor products were removed once daily via the 2 μm internal sintered metal filter **(2)**. The remaining gaseous stream was reduced to atmospheric pressure. The volumetric flow rate of the gaseous stream

was determined with a thermostated flow meter (DTM-200A, American Meter Company, USA) **(23)**. A small sample flow was split from the main flow and led to a heated injection valve of an on-line gas chromatograph **(24)**. Finally, the product stream was transported to a low-pressure condenser at 0 ^{o}C. The condensed products collected from the cold **(19)**, warm **(20)** and hot traps **(20**) were separated manually into an aqueous and oil phase.

5.3 In situ activation of the catalysts

Activation of catalysts prior to FTS is generally considered to be necessary as it directs the activity and productivity of the catalyst under study [15]. It has been reported that activation of fused magnetite catalysts with H_2 at a high temperature >500 ^{o}C and a linear flow rate is necessary to produce a substantial surface area necessary for good activity, however, activation with syngas or CO is ineffective [11]. In contrast, many studies have shown that precipitated iron catalysts need to be activated with H_2, CO or synthesis gas prior to F-T synthesis [8, 12-14, 16-20].

Davis *et al*. investigated the performance of precipitated Fe catalysts after activation in CO, H_2 and syngas [14, 16]. They found that activation in CO gave highly active and stable catalysts, while the FTS performance of catalysts activated with syngas was found to be dependent upon the partial pressure of

hydrogen in the activating gas. Furthermore, Luo and co-workers [12, 13] reported that catalysts activated with CO yielded higher amounts of long-chain hydrocarbons than catalysts activated with syngas or H_2. Bukur *et al*. [17] observed higher initial activity and a heavier product with precipitated Fe catalysts activated in CO or syngas than activated with hydrogen. However, activation with hydrogen has been reported to result in more stable catalysts [17].

The reduction of Fe_2O_3 with CO gas is reported to occur in 2 steps [12]:

$$3Fe_2O_3 + CO \longrightarrow 2Fe_3O_4 + CO_2$$

$$5Fe_3O_4 + 32CO \longrightarrow 3Fe_5C_2 + 26CO_2,$$

In addition CO_2 may be formed by the Boudouard reaction:

$$2CO \longrightarrow C + CO_2.$$

Consequently, there is a bone of contention as to which is the active phase in Fe catalysts used for FTS. One of the reasons is that the reduced phases are moisture and air sensitive, thus characterisation results vary widely. Datye *et al*. [21] reported that the active phase of an iron catalyst for FTS is represented by a mixture of carbides (Fe_2C, Fe_7C_3, Fe_5C_2 and Fe_3C) while Davis and co-workers [12, 16] proposed that Fe_5C_2, Fe_3O_4 and α-Fe are the active phases for FTS. The authors further elaborated that approximately 50-100% more carbon was present in the activated catalyst mass than was needed to form Fe_5C_2. Gradual oxidation

of Fe_5C_2 to Fe_3O_4 was observed when the iron catalyst was used in FTS. It is believed that the reaction system becomes more oxidizing and magnetite is usually formed at a high CO conversion.

On the other hand, carbon supported catalysts have been previously pretreated in a hydrogen atmosphere at temperatures as high as 420 - 450 ^oC [23-25]. Van Steen and Prinsloo [22] reported *in situ* activation of Fe catalyst supported on carbon nanotubes in hydrogen at a GHSV = 1860 ml/(h. g) by ramping the fixed reactor temperature at 0.2 ^oC/min up to 70 ^oC followed by a heating rate of 0.3 ^oC/min to 220 ^oC, which was kept for 16 h. Consequently, the authors reported a low degree of reduction with the procedure and hence very low activity of the catalyst was observed. In contrast, Ma *et al*. activated Fe catalyst supported on activated carbon with H_2 at 420 °C, 6.4 MPa, for 16 h [22].and found that the catalysts were reasonably active in FTS.

In another report, Bahome and co-workers, employed an in situ activation of Fe catalysts supported on carbon nanotubes at 350 ^oC for 24 h under a stream of H_2 flowing at 20 ml/min and a pressure of 0.2 MPa [24]. The catalysts were reported to be stable and active in FTS. Mulay *et. al*., [25] have reported the reduction of Fe/C in a H_2 atmosphere at a constant temperature of 120 ^oC for 30 minutes before continuing to heat to 450 ^oC for 16 h, at a pressure of 0.1 MPa using a

micro-fixed bed reactor. Although the authors claimed that they achieved a higher throughput per unit volume as a consequence of higher dispersions and/or metal-support interaction than unsupported Fe catalysts and higher olefin selectivity, the FTS over this catalyst was performed using non-typical FT conditions, i.e. atmospheric pressure and so it is difficult to determine whether the reduction process was really successful.

In this study the activation procedure reported by Luo and co-workers [12] was used. The precipitated and K promoted iron catalysts were pretreated with CO gas at 270 °C for 24 hours. The stirring speed of the CSTR was set at 750 rpm before the pressure was increased to 2.0 MPa with the CO at a flow rate of 24 sl/hr. The CO flowed through the catalyst slurry containing 15 % solids suspended in 310 ml Ethylflow 164 oil (C_{30}) [Ethyl Corp., USA].

5.4 Fischer-Tropsch synthesis

The FTS conditions were 250 °C, 2.0 MPa with a H_2/CO ratio of 2. CO and H_2 gas mass flow controllers were used to provide a simulated synthesis gas of the desired composition, and the syngas was introduced at a rate of 3.6 sl/hr. g Fe. The wax sample was extracted through an internal filter and collected in a hot trap

held at 200 °C. A warm trap (100 °C) and cold trap (0 °C) were used to collect light wax and the water plus oil samples respectively.

5.5 Product sampling and analysis

Daily gas, water, oil, light, and heavy wax samples were collected and analysed. Tail gas from the cold trap was analysed with an online HP Quad Series Micro GC, providing molar compositions of C_1–C_7 olefins and paraffins as well as for H_2, CO, and CO_2. The gas chromatograph was equipped with a heated (200 ^oC) 10-port gas injection valve, with a sample loop and a loop for the Deferred Standard (DS), methane. The DS method for on-line gas chromatographic analysis was reported by Marsman *et al*. [26]. The relative DS technique improves the reliability of the analysis and reduces the calibration efforts. Sample injection on the column was performed after the injection of the DS. The DS and sample were subsequently injected at an initial temperature of the GC of 30 ^oC. The initial temperature was maintained for 8 min, after which the oven temperature was increased to 120 ^oC at the rate of 6 ^oC/min. After 5 min at 120 ^oC the temperature was increased to 180 ^oC. After another 5 min the temperature was increased to the final temperature of 250 ^oC. This temperature was maintained until all the components of interest had eluted. The complete on-line analysis time was 60 min. The components were separated on a capillary column (25 m x 0.53

mm i.d. coated with 0.020 mm Poraplot Q, carrier flow, 0.017 ml/s). H_2, CO, CO_2, and H_2O were detected with a Thermal Conductivity Detector (TCD) and the hydrocarbon products (alcohols, acids, ketones, etc.) with a Flame Ionization Detector (FID, see Fig. 5.2). Both detectors were connected to an integrator and a personal computer for peak integration and data storage. The oil and light wax samples were mixed before analysis and separated on an HP-SIL 5-CB capillary column using an HP-5790A GC. For these components the mass response factors of the flame ionization detector were taken as constant.

The heavy wax of the high-pressure condenser contained C_{15+} hydrocarbons and were analyzed with a 10 m HT-SimDist column on a HP-5890 Series II Plus GC while the water sample was analyzed using an Hewlett-Packard-5890 GC. Table 5.2 presents a summary of the instruments and detectors used for analysis of FTS products. The wax samples were dissolved in ortho-xylene and were injected to the column to prevent splitter discrimination at an initial temperature of 40 ^{o}C. The temperature was raised with an optimized programme to 400 ^{o}C to elute components until C_{40} (see Fig. 5.2). Peak identification was performed using injection of pure components.

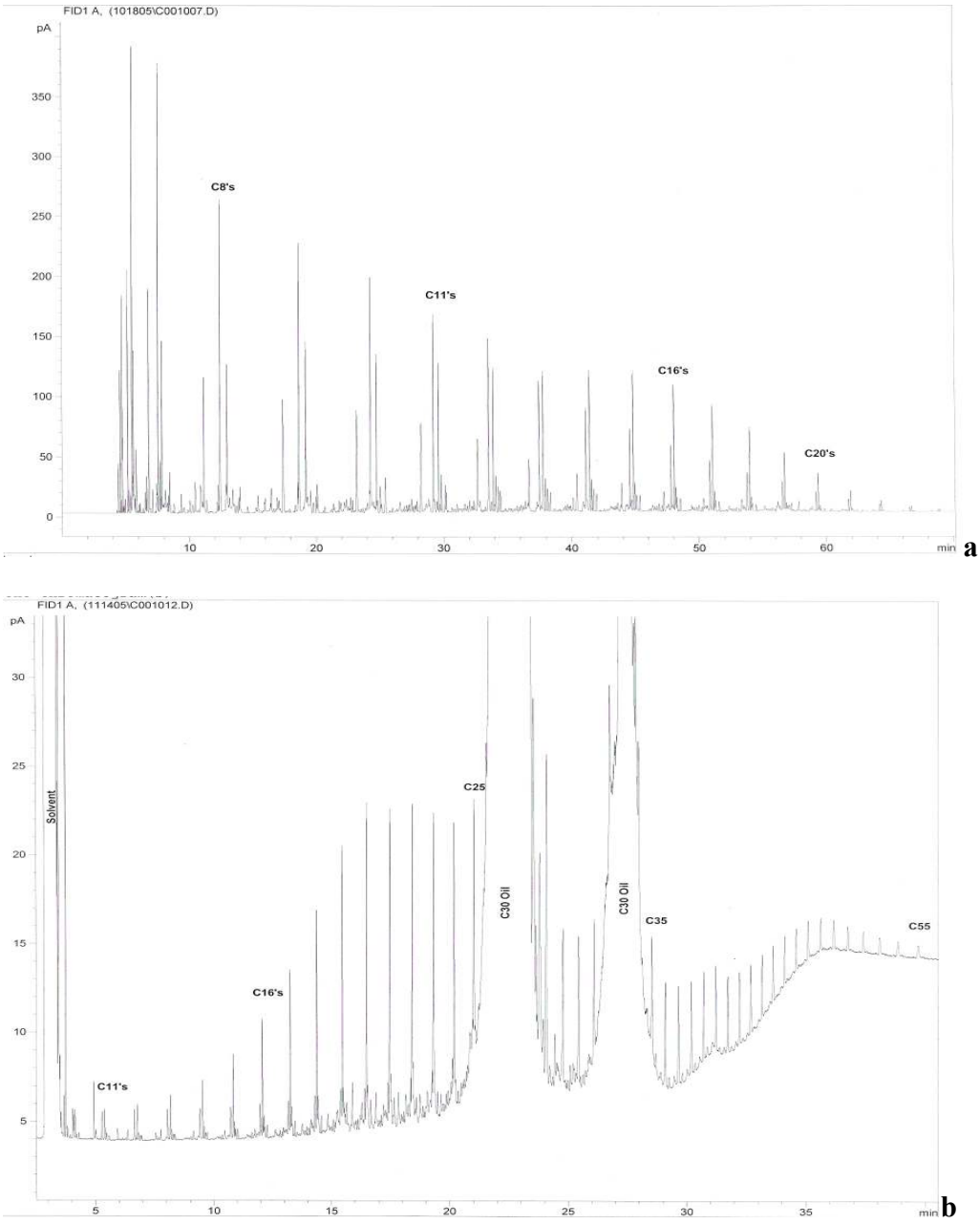

Figure 5.2: Typical on-line gas chromatograms for hydrocarbon products. (a) Oil and (b) wax FID signals.

5.2: Instruments used for the analysis of FTS products

Instrument	Sample	GC detector
HP Quad Series Micro GC	Gas	TCD
HP5890 GC	Water	FID
HP5790A GC	Oil + light wax	TCD
HP5990 Series II Plus	Heavy wax	FID

5.6 Fischer-Tropsch data calculations

The FTS data and calculations can be broken into several major groups, these being the conversions, rates, selectivity's and finally product distributions. All the data was stored in raw form in a Microsoft Access database. Any conversions, scaling, and further manipulation of the data was done entirely by SQL query of the database system with the single exception of the curve fitting for the calculation of alpha values. This curve fitting is primarily done with the SAS system of Statistical Software. The system has a Microsoft Visual Basic 5.0 front end for data entry with reporting by Crystal Reports Professional Version 6.

Hydrogen, carbon monoxide and syngas conversions were calculated based on the gas product GC analysis results and the gas flow measured at the reactor outlet. Thus, the conversions were obtained using the following formula:

$$\text{Conversion } (\%) = \frac{N_{in} - N_{out}}{N_{in}} \times 100$$

Selectivity of component x_i (%) = (moles component x_i/ Σx_i) x 100

Where N is the number of moles of CO, H_2 and syngas; and x_i represents any hydrocarbon of interest.

5.8 Characterization of the Fe supported catalysts

Powder diffractograms of calcined catalysts were recorded using a Phillips X'Pert diffractometer. The scans were taken over the range from 2 theta of 10 to 70 ^{o} using the scanning step of 0.01, a scan speed of 0.0025 sec^{-1}, and a scan time was 4sec. The surface area, pore volume and average pore radii of the supports and the catalysts were measured by BET using a Micromeritics Tri-Star system. Prior to measurements, the samples were slowly ramped to 160 ^{o}C and evacuated for approximately 0.67 MPa. Elemental analysis was performed with a PW 2404 X-ray fluorescence spectrometer. The TPR profiles of catalysts were measured utilizing a Zeton-Altamira AMI-200 unit. Calcined samples were purged in flowing inert gas to remove water traces. A liquid nitrogen trap was used to

prevent water generated by reduction from interfering with the signal of the thermal conductivity detector (TCD). TPR was performed using a 10% H_2/Ar mixture at 39 ml/min using Ar as the reference to maximize the signal to noise ratio. The sample was heated from 50 ^{o}C to 800 ^{o}C using a heating ramp of 5 ^{o}C/min.

High resolution (HR) TEM images were aquired using a JEOL 2010-F Fas TEM Field Emission Electron Microscope which was operated at 200 kV. Sample preparation required the placement of small amount of powdered material onto the lacy-carbon coated copper grid (200 mesh). To avoid contamination with a carbon-based solvent, the powder was sonicated dry to break up larger particle agglomerates, spread over a clean surface and then coated onto a support tip which was rolled across the copper grid. This method delivers enough particles onto the lacy-carbon support. High resolution imaging (HR-TEM) was applied to obtain information on the size and shape of the support particles including activated carbon, pyrolyzed mesoporous carbon and MCM-48 as well as the iron nanopartilces. All images were obtained with a point-to-point resolution of 0.2 nm. A high voltage finely focused electron beam with a minimum beam size of 0.5 nm was passed through the sample material.

5.8 References

[1] J. Xu, C. H. Bartholomew, *ICC2004.catalyse.cnrs.fr*

[2] D.B. Bukur, L. Nowichi, X. Lang, *Eng. & Fuels*, **9**, 620 (1995).

[3] M. E. Dry, *Catalysis Today*, **71**, 227 (2002).

[4] A. P. Steynberg and M. E. Dry, *Fischer-Tropsch Technology: Studies in Surface Science and Catalysis*, Elsevier, **152**, (2004).

[5] G. Neri, G. Rizzo, S. Galvagno, G. Loiacono, A. D. Onato, M. G. Musolino, R. Pietropaolo and E. Rombi, *Appl. Catal. A*, **274**, 243 (2004).

[6] F. Rodriguez-Reinoso, *Carbon*, **36**, 159 (1998).

[7] G. P. Van der Laan, *Kinetics, Selectivity and Scale Up of the Fischer-Tropsch Synthesis*, Ph.D Thesis, University of Groningen, The Netherlands, (1999).

[8] T. R. Motjope, H. T. Dlamini, G. R. Hearne, N. J. Coville, *Catal. Today*, **71**, 335 (2002).

[9] M. Khoudiakov, M. C. Gupta and S. Deevi, *Nanotech*., **15**, 987 (2004).

[10] I. P. Silverwood, *Synthesis and Characterisation of Au/Fe_2O_3 Catalysts,* MSc. Dissertation, University of Edinburg, (2002).

[11] M. E. Dry, "*Catalysis: Science and Technology,"* (J. R. Anderson and M. Boudart, eds.), **1**, (1981).

[12] M. Luo, R. J. O'Brien, S. Bao, B. H. Davis, *Appl. Catal. A*, **239**, 111 (2003).

[13] B.H. Davis, *Technology Development for Iron Fischer–Tropsch Catalysts*, Final Report DoE/PC90056-T17 (1996) [available at www.fischer-tropsch.org].

[14] http://crtc.caer.uky.edu/pubs/final98/task4.pdf

[15] M. S. Spencer, M V. Twigg, *Annual Rev. Mater*., **35**, 427 (2005).

[16] R. J. O'Brien, L. Xu, R. L. Spicer and B. H. Davis, *Eng. & Fuels*, **10**, 921 (1996).

[17] D. B. Bukur, X. Lang, J. A. Rossin, W. H. Zimmerman, M. P. Rosynek, E. B. Yeh and C. Li,. *Ind. Eng. Chem. Res.*, **28**, 1130 (1989).

[18] D. B. Bukur, M. Koranne, X. Lang, K. R. P. M. Rao, and G. P. Huffman, *Appl. Catal.*, **126**, 85 (1995).

[19] H. W. Pennline,M. F. Zarochak, J. M. Stencel and J. R. Diehl, *Ind. Eng. Chem. Res.*, **26**, 595 (1987).

[20] V. K. Jones, L. R. Neubauer and C. H. Bartholomew, *J. Phys. Chem*., **90**, 4832 (1986).

[21] A. Datye, Y. Jin, L. Mansker, R. Motjope, T. Dlamini and N. J. Coville, *Stud. Surf. Sci. Catal*., **130**, 1139 (2000).

[22] E. van Steen, F. F. Prinsloo. *Catal. Today*, **71**, 327 (2002).

[23] W-P. Ma,Y-J. Ding, J. Yang, X. Liu and L-W. Lin, *React. Kinet. Catal. Lett*., **84**, 11 (2005).

[24] M. C. Bahome, L. L. Jewell, D. Hilderbrandt, D. Glasser and N. J. Coville, *Appl. Catal. A.*, **287**, 60 (2005).

[25] L. N. Mulay, A. V. P. Rao, P. L. Walker Jr., K. J. Yoon and M. A. Vannice, *Carbon*, **23**, 501 (1985).

[26] J. H. Marsman,C. J. Van Ede, B. B. Breman, E. J. Stamhuis, E.J and A. A. C. M. Beenackers, *Anal. Chim. Acta*, **238**, 129 (1990).

Chapter Six

The Characterization of the Supported Iron Catalysts

6.1 Introduction

Iron has been the principal Fischer-Tropsch catalyst for many years, typically in the form of reduced, promoted bulk oxides placed on various supports [1]. The size of the catalyst particles can be made to vary and the particle size will affect the CO hygrogenation ability. Small iron particles dispersed on various oxides although catalytically active, usually give strong interactions with many oxide surfaces and this can thus prevent the complete reduction of all the iron [1,2]. Thus, the support limits the use of particles with smaller sizes. However, it is not necessary to use oxidic supports and indeed the use of carbon as a support would potentially overcome the strong metal-support interaction (SMSI) effect when Fe is used in FT reactions.

The metal-support interactions were reported for the first time in 1978 [3], and it was primarily interpreted as a morphological effect, where the reduced support produces an expansion in its ionic crystal lattice due to the decrease in the

electrostatic attraction, after reduced species were formed. However, an electronic interpretation was also made, in this case that the metal-support interaction is considered as a charge transference from the reduced support to the dispersed metal. This effect produces an increase in the electronic density in the *d* subshell of the dispersed metal [3].

Although a number of Fe/C supported materials in catalytic reaction have been examined, the support used has typically been activated carbon. Additional studies of other carbons such as mesoporous carbons [see chapter 3] and carbon nanotubes with supported iron catalyst have also been reported. The ordered mesoporous carbons are characterized by uniform pores, controllable pore diameters, high specific surface areas and large pore volumes when compared to carbon nanotubes and graphitic carbon.

In this chapter three different supported Fe catalysts i.e. 15%Fe/2%K/support (support = activated carbon (AC), mesoporous carbon (MC) and /MCM-48 (preparation of these catalysts is reported in detail in chapter 5)) have been characterized by XRF, BET, TPR and XRD in order to generate the physico-chemical information about the catalysts, while SEM and TEM were used to obtain information about the structural morphology and dispersion of the metal crystallites on the supports.

6.2 Results and discussion

6.2.1 Elemental analysis of Fe-supported catalyst precursors

Table 6.1 gives the results of the analysis of the 15%Fe/supported catalysts with different K loadings, using XRF. The XRF analysis of dried and calcined samples revealed that the metal ratios obtained were close to those predicted from

Table 6.1: Supported catalysts composition (atomic wt%)

Catalyst	Fe content	K content
15%Fe/2%K/AC	14.81	2.07
15%Fe/5%K/AC	13.98	5.32
15%Fe/10%K/AC	14.76	9.88
15%Fe/2%K/MC	14.45	1.93
15%Fe/5%K/MC	14.03	4.89
15%Fe/10%K/MC	14.62	10.33
15%Fe/2%K/MCM-48	14.51	2.19

the catalyst preparation data. The iron content gave values 0.2–1 % values lower than expected. This can be attributed to the loss of some of iron during the multi-

step catalyst preparation procedure. In contrast, potassium promoter was added by incipient wetness impregnation (after calcination of the Fe loaded support precursor) onto the supported catalyst. The results are very close (± 0.3 %) to the calculated values.

6.2.2 Textural properties of Fe-supported catalyst precursors

The determination of surface area is considered to be an important requirement in the characterization of a catalyst, although the catalytic activity may only be indirectly related to the total surface area. In addition, it is usually necessary to specify the pore content and structure since this parameter may control the transport of the reactants and products of a catalytic reaction [4].

Table 6.2 shows the BET data for the three supports used (activated carbon, mesoporous carbon, MCM-48) and the corresponding supported catalyst precursors. A comparison of the BET surface areas of the supports before and after metal impregnation, shows that the surface areas of the supported Fe catalysts were remarkably reduced after impregnation. The corresponding pore volumes of the supported catalysts were also reduced. This was expected as the

Table 6.2: Textural properties of supported catalysts

Sample	Surface area (m^2/g)	Pore volume (cm^3/g)	Pore diameter (nm)
MCM-48	1293	1.00	2.9
15%Fe/2%K/MCM-48	527	0.82	3.2
Activated carbon	811	0.66	1.6
15%Fe/2%K/AC	694	0.57	1.7
Mesoporous carbon	748	0.59	2.3
15%Fe/MC	398	0.55	2.4
15%Fe/2%K/MC	303	0.51	2.6

pores in the supports were filled and/or the pores were blocked during the slurry impregnation step [5]. Although the surface area of the mesoporous carbon became smaller as the Fe metal loading increased, it was further decreased when potassium was added to the catalysts precursor. This could be attributed to the covering of the support by potassium during the precipitation process. As expected, the potassium promoter generally increased the pore diameter of the catalyst precursor. It can be hypothesized that the metal catalyst crystallites have increased in size in the presence of potassium.

This data can be compared with the effect of potassium loading on other Fe catalysts. For example, Dry [6] investigated the effect of potassium loading over a fused iron catalyst and concluded that the higher the alkali loading, the greater the loss in surface area. Such a result was ascribed to the ability of potassium to improve the agglomeration of the FeOOH precursor and further enlarge the crystallite size of α-Fe_2O_3 after calcination. This would induce a decrease in surface area. On the contrary, Li *et al*. [7] have found an opposite result for a precipitated Fe/Cu catalyst. In their method potassium was added after the thermal treatment of the Fe/Cu catalyst. Presumably the FeOOH had transformed to the stable α-Fe_2O_3 phase before potassium addition. These differences may thus be related to the different catalyst preparation procedures.

In a related study, Yang and co-workers [8] used XRD to study the effect of potassium on Fe crystallites size. It was revealed that the samples containing potassium had larger Fe crystallites than the samples without potassium. The pore diameter of the support simultaneously increased with the increase of the potassium content. The authors further reported that the loss of surface area is hence due to crystallite growth and not due to pore blocking after potassium addition.

6.2.3 Reduction behaviour of the Fe-supported catalyst precursors

Although the TPR technique provides useful information on the relative reducibility of different catalysts and the energetics of the reduction process, it is not always representative of the actual FT reduction procedure employed. However, this procedure allows for the generation of "relative" data and permits trends to the observed in a series of catalysts.

The reducibility of bulk iron oxides by TPR is well documented in the literature, but it is worth noting that the literature data diverge to some extent. This might be due to the presence of different oxides that exist in the starting material (Fe_2O_3, Fe_3O_4 and FeO) and moreover, that these materials can contain impurities and dopants [9]. For example, Unmuth *et al*. [10] studied the reduction of Fe catalysts supported on silica gel, and found that the corresponding reduction profiles consisted of two peaks at 307 ^oC due to hematite and at 447 ^oC corresponding to magnetite. Feng *et al*. [11] reported that the reduction of an Fe catalyst gave a TPR profile with a sharp peak at 380 ^oC and a broad peak at 700 ^oC corresponding to the reduction of Fe_2O_3 to Fe_3O_4, FeO and possibly Fe^o [12]. Indeed, from the data above, it is postulated that the reduction of bulk hematite (α-Fe_2O_3) proceeds via magnetite (Fe_3O_4) and wustite (FeO) to metallic iron. However, the formation of FeO is not always observed, because wustite is metastable below 570 ^oC at

which temperature disproportionation into Fe_3O_4 and Fe proceeds. With supported iron catalysts the purely divalent state of iron can be stabilized well below the critical temperature by interaction with the support due to the formation of mixed oxides [4].

Bahome *et al*. [13] and Van Steen and Prinsloo [14] reported the reduction of Fe catalysts supported on carbon nanotubes (CNTs). Two peaks were present in all Fe/CNTs TPR profiles. The authors hypothesized that since transition metals can act as catalysts for the formation of methane through reaction of hydrogen with carbon nanotubes when T > 600 ^{o}C, the peak that was observed at 550 ^{o}C in all Fe/CNTs was attributed partly to the gasification of CNTs support. The carbon gasification was substantiated by passing the outlet gas from the TPR reactor through a GC. Methane was detected in the outlet gas at temperatures above 550 ^{o}C. This suggested that gasification of the carbon nanotubes occurred at higher temperatures, presumably catalyzed by the Fe, even in the absence of oxygen. The same phenomenon was also observed by Jones *et al*. [15] on the reduction behaviour of an Fe/C catalyst.

The reduction behaviour of 15%Fe/2%K supported on activated carbon, mesoporous carbon and MCM-48 was studied and the corresponding TPR profiles of the three catalyst precursors are presented in Fig. 6.1. It can be seen that the

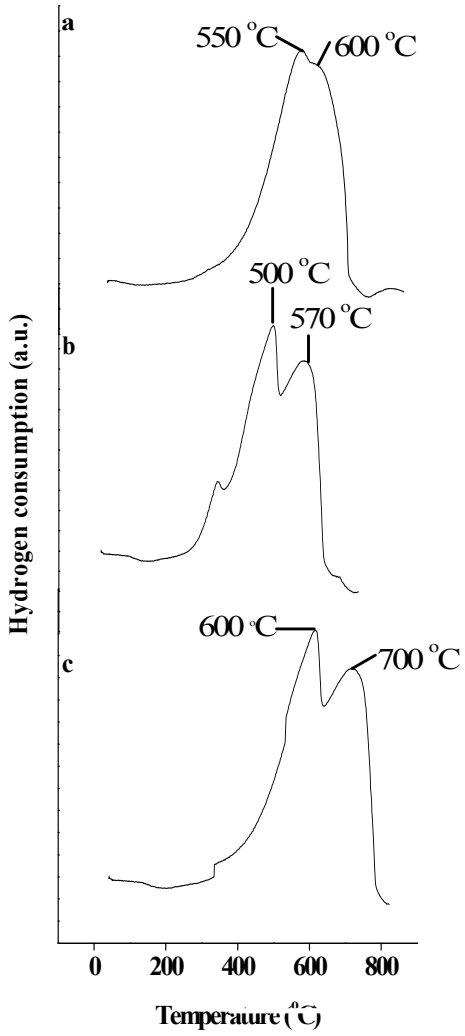

Figure 6.1: TPR spectra of (a) 15%Fe/2%K/AC; (b) 15%Fe/2%K/MC and (c) 15%Fe/2%K/MCM-48.

reduction of 15%Fe/2%K/MC and 15%Fe/2%K/AC occurred at lower temperatures than the reduction of Fe on MCM-48. This is due to the role/effect the type of support has on the catalytic reduction of the catalyst metal. The 15%Fe/2%K/MC catalyst precursor has a shoulder at 350 ^{o}C which was also observed with 15%Fe/2%K/MCM-48 catalyst. The observed shoulder peaks are speculated to have been due to an instrumental issue. The TPR profiles of all the three catalyst precursors are very similar and have well defined peaks.

The peaks at around 500 ^{o}C for 15%Fe/2%K/MC, 550 ^{o}C for 15%Fe/2%K/AC and 600 ^{o}C for 15%Fe/2%K/MCM-48 are attributed to the reduction Fe_2O_3 to Fe_3O_4 which proceeds via the equation given below:

$$3Fe_2O_3 + H_2 \longrightarrow 2Fe_3O_4 + H_2O$$

The peaks whose maxima were located at 570 ^{o}C for 15%Fe/2%K/MC, 600 ^{o}C for 15%Fe/2%K/AC and 700 ^{o}C for 15%Fe/2%K/MCM-48 were due to the second reduction step from Fe_3O_4 to the metallic iron:

$$Fe_3O_4 + 4H_2 \longrightarrow 3Fe + 4H_2O$$

From the data above, it can be concluded that the catalytic reduction of the precipitated iron catalyst occurs at lower temperatures when the catalyst is supported on mesoporous carbon, followed by activated carbon and lastly, MCM-

48 silica. Thus, enhanced reduction in the case of carbon based materials can be assumed and it could be due not only to the reductive properties of the carbon but also to the weaker iron oxide−support interaction in this case. The data are consistent with the graphite-like character and presence of few functional groups on the mesoporous carbon [16].

Even though it was not used in this study, Mossbauer is believed to be a very powerful spectroscopic technique that could be used to determine the extent of reduction of Fe catalysts. Interestingly, Van Steen and Prinsloo [14], and Valiant and co-workers [17], used the technique to distinguish between different iron phases of an Fe/C catalyst. The data provided evidence of the existence of two major phases in the reduced Fe/C catalysts. It was noted that the Mossbauer spectra were best fitted with a singlet for super paramagnetic Fe(0) and a six-line pattern characteristic of magnetic Fe(0), a singlet and a doublet for Fe(II), and an Fe(III) doublet.

6.2.4 Structural properties of Fe-supported catalyst precursors

XRD was used to identify iron oxide peaks in the three calcined catalyst precursors studied (Fig. 6.2). Most peaks present in the XRD patterns of the catalysts are assigned to haematite (α-Fe_2O_3) and either magnetite (Fe_3O_4) or γ-

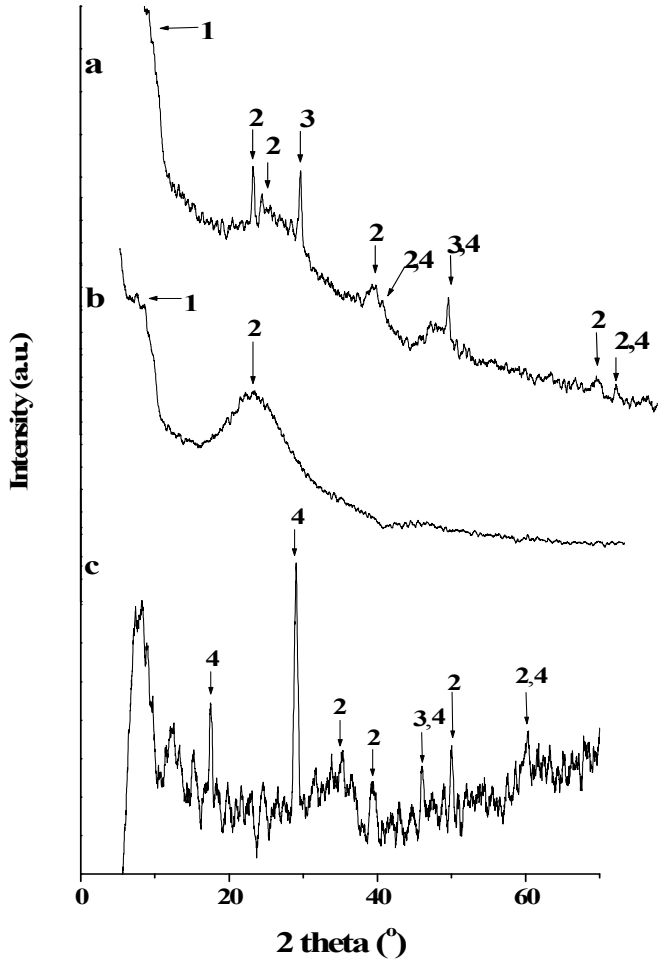

Figure 6.2: XRD patterns of (a) 15%Fe/2%K/MC, (b) 15%Fe/2%K/MCM-48 and (c) 15%Fe/2%K/AC. Peaks: 1 - mesoporous materials; 2 - α-Fe_2O_3; 3 - Carbon and 4 - α-Fe_3O_4 and γ-Fe_2O_3.

Fe_2O_3 [8,18]. As magnetite and γ-Fe_2O_3 have very similar diffraction patterns, a definitive assignation is not possible with these materials. From the appearance of the peaks it is possible to infer the relative crystallinity of the support material [8].

The XRD patterns of 15%Fe/2%K/MC and 15%Fe/2%K/MCM-48 have one peak [**(1)** in Fig. 6.2a and b] that is common in both catalyst precursors, the peak is a characteristic feature of mesoporous materials and appears at 2-theta = 2-3 ^{o}. The peak is not observed in the 15%Fe/2%K/AC sample. The graphitic nature of 15%Fe/2%K/MC is revealed by small narrow peaks at 2-theta = 27 and 54° shown in Fig. 5.4a **(3)** corresponding to the *002* and *101* planes associated with graphitic pore walls [19]. A peak due to carbon at 27° 2 theta is also observed in 15%Fe/2%K/AC. In all the patterns, α-Fe_2O_3 is observed and mainly the phase appears in the carbon supported catalysts. The XRD pattern of 15%Fe/2%K/MCM-48 indicates no sign of long-range ordered iron oxide.

Only two small peaks at 2-3° 2 theta and one broad peak at 2-theta = 22° ascribed to mesoporous silica materials (**1**) are observed. There is no obvious distinction of the Fe peaks on the MCM-48 catalyst peaks but it can be speculated that they overlap with the silica peak. This observation is unusual and it may only be speculated that potassium has suppressed the iron oxide peaks in the oxidic

support. Kim *et al*. [20] conducted a similar study using SBA-15 Fe catalysts and found that the iron oxide peaks disappeared after the addition of potassium dopants to an SBA-15 Fe catalyst.

6.2.5 Electron microsopy studies

a) Activated carbon catalyst

SEM and TEM images of catalysts after calcination (prior to the FT synthesis) are shown below. The SEM image of the activated carbon is shown in Fig. 6.3 and revealed that the carbon is irregularly shaped and contains non uniform particles/fibers that exhibit sizes between 20-100 nm. The high resolution TEM image showed that the activated carbon has a fine porous structure.

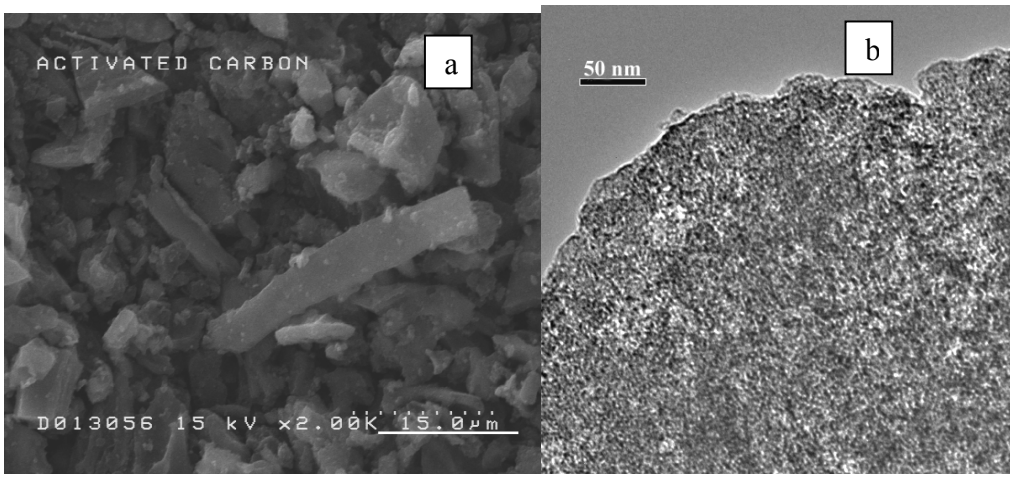

Figure 6.3: Electron microscopy of activated carbon support; a – SEM image and b – high resolution TEM image.

The fine structure of the activated carbon is distinguishable from the iron particles (Fig. 6.4a). The iron particles are clustered and as a result form agglomerates. Most of the metal particles were widely dispersed on the surface of the activated carbon, this was expected considering the microporosity of the activated carbon support.

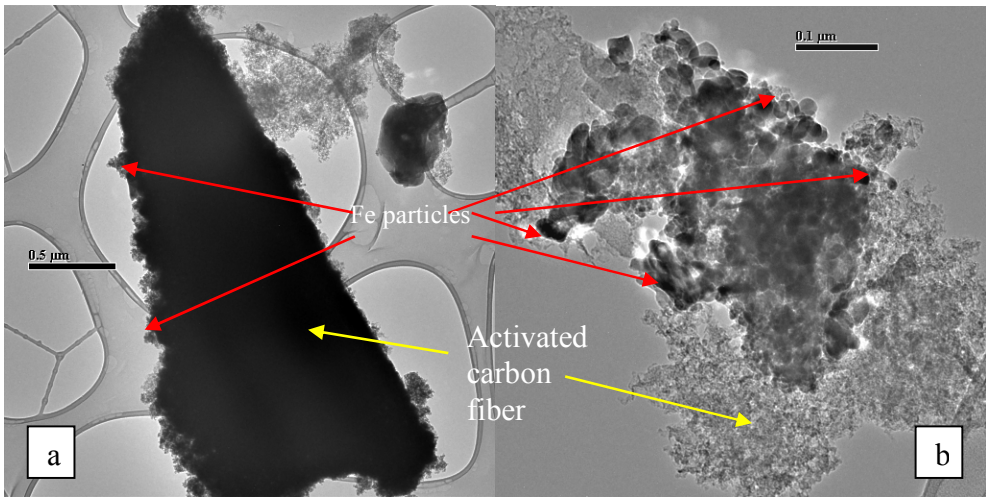

Figure 6.4: The HR-TEM images of two 15%/2%/AC samples; a – Fe particles on the surface of the carbon fiber and Fe particles dispersed on the surface of the activated carbon.

Moreover, Fig. 6.4b shows that nanostructured materials that look like fine carbon particles can be formed on the outer surface of the activated carbon. In essence, activated carbon aggregates are transformed into a fine carbon scaffold by selectively removing the "soft" parts of the activated carbon. This is speculated to have been achieved by catalytic burning of carbon during calcination of the Fe/AC catalysts precursor. The image in Fig. 6.4b also shows that the iron particles are observed on the surface of the activated carbon support.

Looking at Fig. 6.5a, it seems like the iron particles nucleate (see red arrows) and then grow bigger and overlap with each other forming semi-spherical nano-

particles with sizes ranging from 10–50 nm. Fig. 6.5b revealed that the Fe-nanoparticles have good crystallinity clearly seen at a higher manification. However it is difficult to discern whether the morphology of the nanoparticles is hexagonal or spherical.

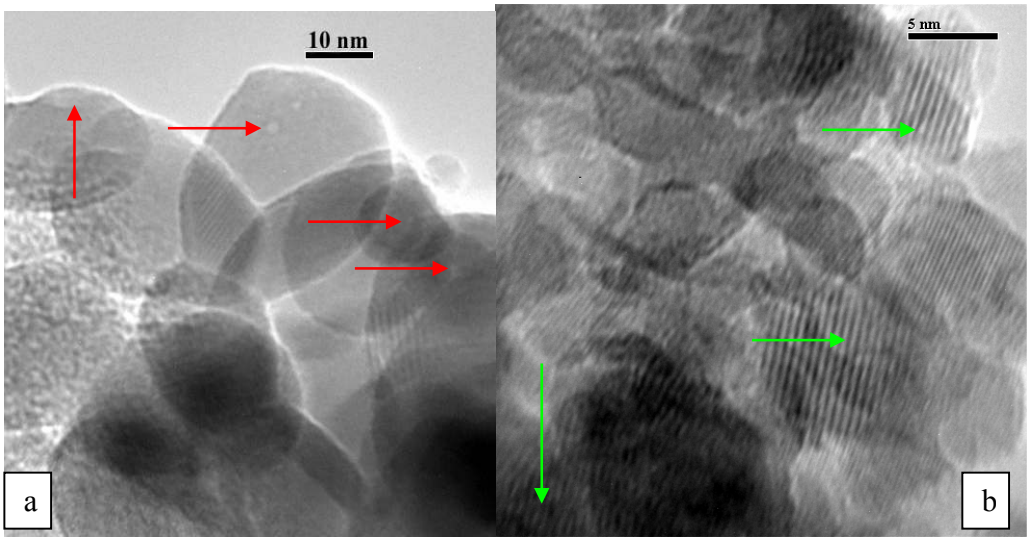

Figure 6.5: HR-TEM images of Fe nanoparticles; a - nucleation of Fe nanoparticles and b - crystallinity of the Fe nanoparticles.

b) Mesoporous carbon catalyst

Addition of the metal ions (Fe and K) did not affect the morphology of the MCs (compare Fig. 6.6a and b). However, when Fe metal was supported on mesoporous carbon, the structure of the carbon appeared to have small and dark

particles that follow an elongated line-like pattern (see inside circles and arrows in Fig. 6.7). These particles were ascribed to Fe nano-particles.

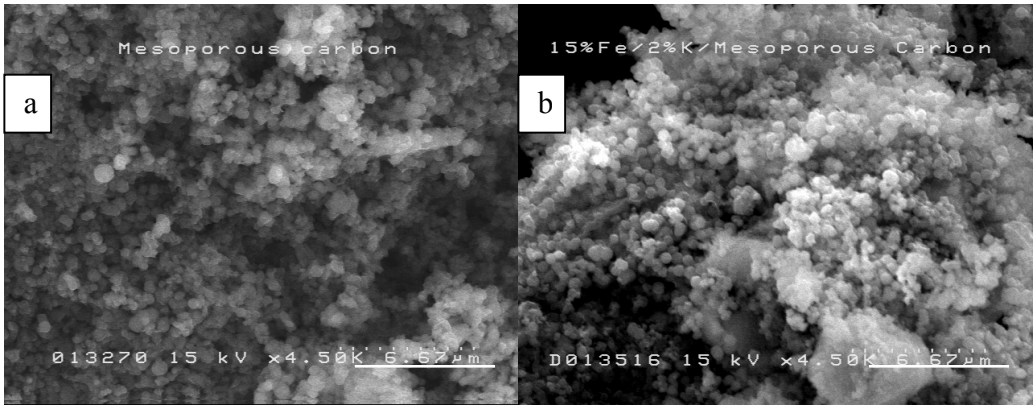

Figure 6.6: SEM images images of (a) mesoporous carbons and (b) 15%Fe/2%K/MC.

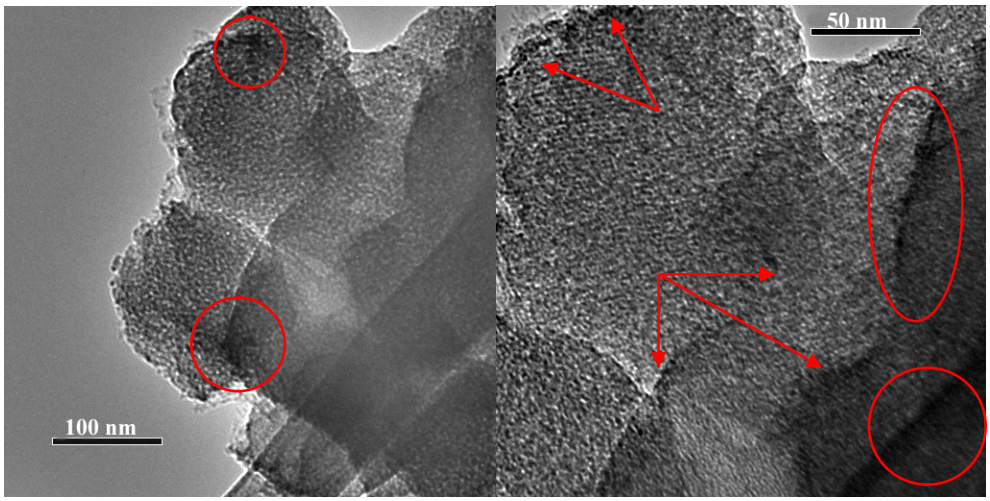

Figure 6.7: High resolution TEM images of 15%Fe/2%K/MC samples.

It is further revealed that these Fe-particles are not evenly distributed on the support material. This is speculated to arise from the deposition precipitation method used for the preparation of the catalyst. In general, the particles concentrate and then follow the structure of the channels of the mesoporous carbon.

Most Fe particles were shown to have been dispersed on the surface of the support material. TEM images of mesoporous carbons revealed that the iron particles are very big with diameters ranging from 10–40 nm in size. The Fe nano-particles appeared to form agglomerates from smaller particles that fuse with other neighbouring particles thus resulting in nano-clustered particles. Individual globules link with neighbouring particles to form non-ordered structures.

c) MCM-48 catalyst

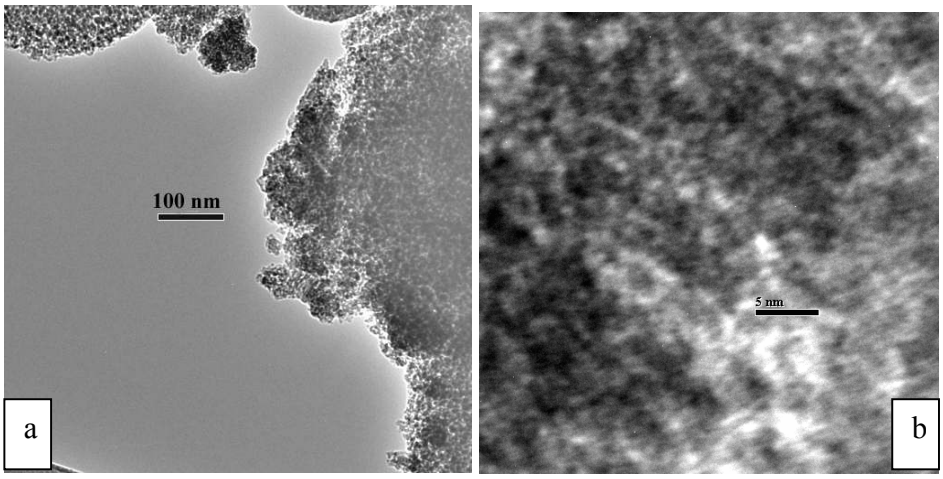

Figure 6.8: HR-TEM images of 15%Fe/2%K/MCM-48 taken from different angles.

The TEM micrograph of the 15%Fe/2%K/MCM-48 showed that the iron particles produced by precipitation were not well dispersed on the silica surface, and further indicated that these materials are porous aggregates of small clusters of 10-20 nm particles. The Fe particles appear (Fig. 6.8) to be on the surface of the silica template, and in addition, they form nano-clusters. However, when the image was taken at a different spot, it revealed that the iron particles were homogeneously dispersed on the silica material (Fig. 6.8 b).

6.3 Conclusion

In this study precipitated iron catalysts supported on activated carbon, mesoporous carbon and MCM-48 were prepared and characterized by XRF, BET, TPR, XRD, SEM and TEM. It was found that the elemental composition of the catalysts were comparable to the calculated values. The BET surface area of the supports were reduced after impregnation with Fe metal catalyst. A decrease of surface area was further observed when potassium was introduced to the porous structure of the supported catalysts. Although potassium seemed to decrease the surface area of all the supports in this study, it also had a positive effect in that it increased the pore diameters of the catalysts precursors.

Reduction of iron oxide was monitored by TPR studies and the data revealed that the supported precipitated catalysts reduce in two steps as reported in the literature. Enhanced reduction in the case of mesoporous carbon based materials could be assumed and it could be due not only to the reductive properties of the carbon but also to the weaker iron oxide−support interaction in this case. Different iron oxide phases were observed and identified from the XRD data provided. Characterization with electron microscopy revealed that the iron was found on the surface of the supports and in most cases the Fe nano-particles aggregated with neighbouring particles to form Fe nano-clusters.

6.4 References

[1] J. M. Martin-Martinez and M. A. Vannice, *Ind. Eng. Chem. Res*., **30**, 2263 (1991).

[2] M. E. Dry, The Fischer-Tropsch synthesis, In Catalysis, Science and Technology, eds. J. R. Anderson and M. Boudart, Springer: Berlin, **1** (1981).

[3] F. Faccin, F. F. Guedes, E. V. Benvenutti, *Eclet. Quim*, **27**, Sao Paolo (2002) [available at www.scielo.br].

[4] E. M. Mokoena, *Synthesis and use of silica materials as supports for the Fischer-Tropsch reaction*, PhD thesis, University of the Witwatersrand, Johannesburg (2005).

[5] D. B. Bukur and C. Sivaraj, *Appl. Catal. A: Gen*., **231**, 201 (2002).

[6] M.E. Dry, G.J. Oosthuizen, *J. Catal*., **11**, 18 (1968).

[7] C. Li, *Effect of Potassium and Copper Promoters on Reduction Behavior of Precipitated Iron Catalysts*, Ph.D. Thesis, Texas A & M University, (1998).

[8] Y. Yang, H.-W. Xiang, Y.-Y. Xu, l. Bai and Y.-W. Li, *Appl. Catal. A: Gen*., **266**, 181 (2004).

[9] A. Luengnaruemitchai, S. Osuwan, E. Gulari, *Catal. Commun.*, **4**, 215 (2003).

[10] E. E. Unmuth, L. H. Schwartz and J. B. Butt, *J. Catal*., **61**, 242 (1980).

[10] X. B. Feng and W. K. Hall, *J. Catal*., **166**, 368 (1998).

[12] L. J. Lobree, I.C. Hwang, J.A. Reimer and A. T. Bell, L. *J. Catal*., **186**, 242 (1999).

[13] M. C. Bahome, L. L. Jewell, D. Hilderbrandt, D. Glasser and N. J. Coville, *Appl. Catal. A: Gen.*, **287**, 60 (2005).

[14] E. van Steen and F. F. Prinsloo. *Catal. Today*, **71**, 327 (2002).

[15] V. K. Jones, L. R. Neubauer and C. H. Bartholomew, *J. Phys. Chem*., **90**, 4832 (1986).

[16] H. Darmstadt, C. Roy, S. Kaliaguine, S. J. Choi and R. Ryoo*, Carbon 2001*, International Conference on Carbon, Lexington, Kentucky, USA (2001).

[17] K. J. Valiant, L. R. Neubauer and C. H. Bartholomew, *J. Phys. Chem*., **90**, 4832 (1986).

[18] A. Iljinas, R. Brucas, V. Stakus and J. Dudonis, *Mater. Sc. Eng*., **25**, 590 (2005).

[19] Y. Xia and R. Mokaya, *Adv. Mater*., **16**, 1553 (2004).

[20] D. J. Kim, B. C. Dunn, M. Kang, J. E. Yie and E. M. Eyring, *CFFS Annual Technical Meeting*, West Virginia, (2005) [available at www.cffs.uky.edu].

Chapter Seven

Fischer-Tropsch Synthesis over an Iron Catalyst Supported on Activated Carbon: Effect of Potassium Loading

7.1 Introduction

The Fischer-Tropsch synthesis (FTS), which is regarded as a clean route for the conversion of coal or natural gas to transportation fuels and petrochemical substitutes, has received considerable attention since its discovery in 1923 [1,2]. Over the past decades, extensive efforts have been made to develop FTS catalysts with high activity and high C_{5+} selectivity [1]. Most of these studies have been performed with iron or cobalt catalysts supported on silica [3-5], alumina [6-8] and titania [9,10]. In recent years, other supports have been investigated for use in the FTS, and one of these is carbon. Carbon materials are attractive supports in catalytic processes owing to their inertness and to in their ability to be tailored to meet specific needs [11].

In the last twenty years, activated carbon has been widely used as a heterogeneous catalyst support because of features that include: stablity at high temperatures in

an inert atmosphere, resistant to acidic or basic media, and its ability to be tailored with regard to pore structure and the chemical nature of the surface. [12-14]. A series of studies by Vannice and co-workers [15-17] in the 1980's reported on the use of activated carbon supported organometallic iron complexes. From their findings, only CH_4 and C_2-C_4 olefins were produced from syngas with very low conversions. It was further mentioned that Fe/C catalysts have a higher throughput per unit volume as a consequence of higher dispersions and/or metal–support interactions than unsupported iron catalysts. In these studies the FTS was performed at atmospheric pressure which in not an ideal and typical condition for the FT reaction. It is to be noted, however, that Dry [18] reported that the total pressure has little or no effect on the selectivity on iron based catalysts.

Jones *et al*. [19] used a fixed bed reactor for the CO hydrogenation of iron catalysts supported on activated carbon using the following conditions: H_2/CO ratio of 2, T = 177 - 257 ^{o}C and P = atmospheric pressure. The activity of the well dispersed Fe/carbon catalyst decreased very significantly with time. On the other hand, Jung *et al*. [16,17] reported that poorly dispersed Fe/carbon catalysts are more active for CO hydrogenation than Fe/alumina and that well dispersed iron on porous carbon black has a high activity and stability at atmospheric pressure and a H_2/CO ratio of 3. Sommen and co-workers [20] also observed high olefin selectivity for Fe/carbon catalysts, but also found a strong tendency

for these catalysts to deactivate due to the formation of carbon deposits at a H_2/CO ratio of 1.

Ma *et al*. [21] have studied FTS with activated-carbon supported iron catalysts in a slurry-phase reactor under conditions of 304 °C, 3.0 MPa, 1.1 sl/g-cat/h, and $H_2/CO = 2$. It was found that catalyst activity increased with increase in reduction temperature between 350 and 420 °C, and gas and liquid hydrocarbons were formed on the catalysts with a C_{5+} weight percentage of about 35 % but a high CH_4 selectivity of 15 % was observed. A summary of some reaction conditions used for the FTS of Fe/carbon catalysts is given in Table 7.1 below.

Over the past 80 years efforts have been expended in the FTS for developing catalysts that maximized conversion of syngas to high molecular weight hydrocarbons. Indeed, precipitated iron catalysts on oxidic supports have been proven as ideal commercial FTS catalysts [21]. These types of catalysts preferentially yield high molecular weight hydrocarbons. By contrast, Fe/AC (AC = activated carbon) catalysts have rarely been shown to be capable of producing high molecular weight products. Others [21] have claimed that the nature of the Fe/AC catalyst, producing only gas and liquid hydrocarbons, might be related to the carbon pore structure and/or metal particle size of the catalyst supported on the carbon.

Table 7.1: Summary of reactions conditions used for the FTS of Fe/carbon catalysts

Catalyst	**FTS Conditions**	**Comments**	**Reactor type**	**Reference**
Activated carbon organometallic iron complexes	T = 227 ^{o}C, H_2:CO ratio = 3, P = atm.	Only CH_4 and C_2-C_4 olefins were produced from syngas with very low conversions	Fixed bed reactor	Vannice and co-workers [15-17]
Fe/activated carbon	H_2/CO = 2, T = 177 – 257 ^{o}C and P = atm	The activity of the well dispersed Fe/carbon catalyst decreased very significantly with time.	Fixed bed reactor	Jones *et al*. [19]
Fe/activated carbon	T = 304 ^{o}C, P = 3.0 MPa, H_2/CO = 2, 1.1 sl/g-	Gas and liquid hydrocarbons were formed on the catalysts with a C_{5+} weight percentage of about 35 % but	Slurry phase reactor	Ma *et al*. [21]

	cat/h	a high CH_4 selectivity of 15 % was observed		
Fe/activated carbon	T = 397 ^oC, H_2:CO = 1-2, P = 1 atm	Observed high olefin selectivity for Fe/carbon catalysts, but also found a strong tendency for these catalysts to deactivate due to the formation of carbon deposits	Fixed bed reactor	Sommen *et al*. [20]
Fe/activated carbon	T = 227 ^oC, P = 1 atm, H_2/CO ratio = 3.	Reported that poorly dispersed Fe/carbon catalysts are more active for CO hydrogenation than Fe/alumina and that well dispersed iron on porous carbon black has a high activity and stability.	Fixed bed reactor	Jung *et al*. [16,17]

It is well known that the FTS product spectrum can be manipulated by modifying traditional F-T catalysts (Fe, Co, Ni and Ru) [18, 23-26] by means of promoters [27-33]. Many FTS studies have been conducted with potassium-promoted iron catalysts [28,30,31,34-42]. Indeed, the potassium promoter has been shown to increase the alkene yield, provide a decrease in the fraction of methane that is produced [28,30,31], and in some cases has resulted in the preferential production of long chain products [27] in FTS. It has also been reported that potassium can increase the CO activation rate and the rate of carburization of Fe_3O_4 (thus increasing the catalytic activity for FTS) and enhance the water gas shift reaction [32,34,38,39]. Nonetheless, some have found potassium to be an inhibitor for the activity of the catalyst [21, 42]. Furthermore, Davis [43] reported that the addition of potassium without a binder increased the deactivation rate as compared to a catalyst containing only iron (i.e. an unsupported and unpromoted catalyst).

Dry [17] has reported that when acidic oxides are used as supports, they may react with basic alkali and thereby reduce the promotional effect of potassium. Also the use of high surface area supports tends to reduce direct contact between iron and potassium since the metal covers only a small fraction of the support surface [44]. This would also render the potassium promotion less effective. As a result, both Davis [43] and Dry [17] emphasised that there is a synergism in the

maintenance of FTS activity on addition of both support/binder and potassium promoter.

In the work reported in this chapter, a standard commercial activated carbon has been used as a reference material in FTS. It has been previously applied as a catalyst support in the CO hydrogenation of iron based catalysts [15-17,19-21]. Therefore, it would be interesting to evaluate the FT performance of this type of carbon as a support for precipitated and promoted iron catalysts. In addition, the overall FT performance of the catalyst precursor will be compared with our own prepared mesoporous carbon supported iron catalyst (see Chapter 8 and 9). Thus, in this chapter, we report the catalytic investigation of the effect of potassium promotion on three precipitated iron catalysts supported on activated carbon for FTS in a slurry bubble CSTR reactor.

7.2 Experimental

The precipitated and promoted iron catalyst precursors used in this chapter 15%Fe/2%K/AC, 15%Fe/5%K/AC and 15%Fe/10%K/AC were synthesized and characterized as reported in detail in chapter 5. Activity is expressed in terms of CO conversion for a constant mass of the catalyst. The conversions for different catalysts are compared at the same synthesis gas space velocity (3.6 NL/h g-Fe

i.e. standard litres of synthesis gas per gram of iron in the reactor) Reaction conditions used were: temperature = 250 ^{o}C, pressure = 2.0 MPa and H_2/CO ratio = 2:1.

7.3 Results and discussion

7.3.1 The Fischer-Tropsch activity of the Fe/AC catalyst precursors

The data presented for CO (Figure 7.1) and syngas (Figure 7.2) conversions for the three catalysts using 3 different potassium loadings indicate that the catalyst went through an induction period before they stabilised. The length and extent of the activity change depended upon the catalyst composition and the reaction conditions. Furthermore, previous studies [45] have shown that the induction period tends to be longer at lower temperatures and it is also longer for catalysts with higher alkali content.

All catalysts under study started at a high CO (~90%) and syngas (~60%) conversion and went through a period of bedding-in until the conversions stabilised after 191 h, 213 h and 240 h for the 10, 2 and 5% K loaded precipitated Fe/AC catalysts, respectively. Therefore, from this data it can be seen that

stabilisation of the catalysts is nearly independent on the amount of the K loading with respect to CO and syngas conversions.

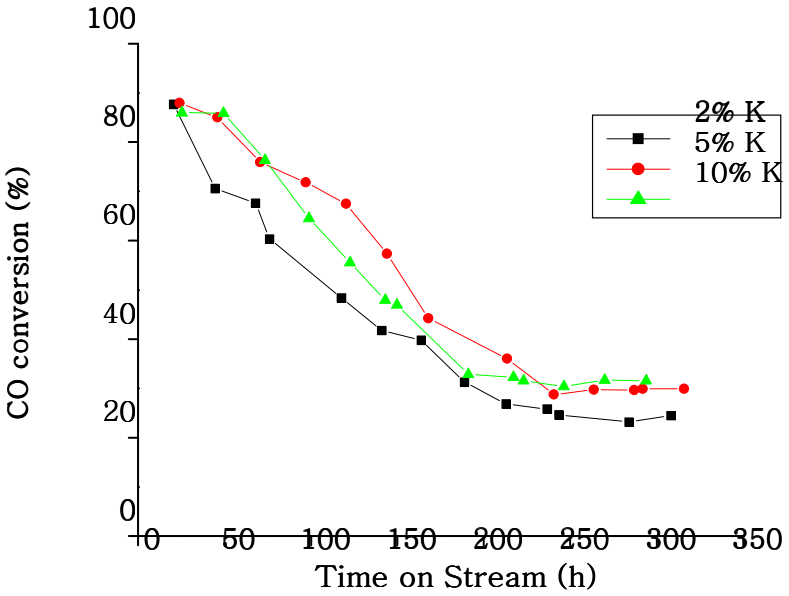

Figure 7.1: CO conversion as a function of time on stream for 15% Fe /AC promoted with 2, 5 and 10% K.

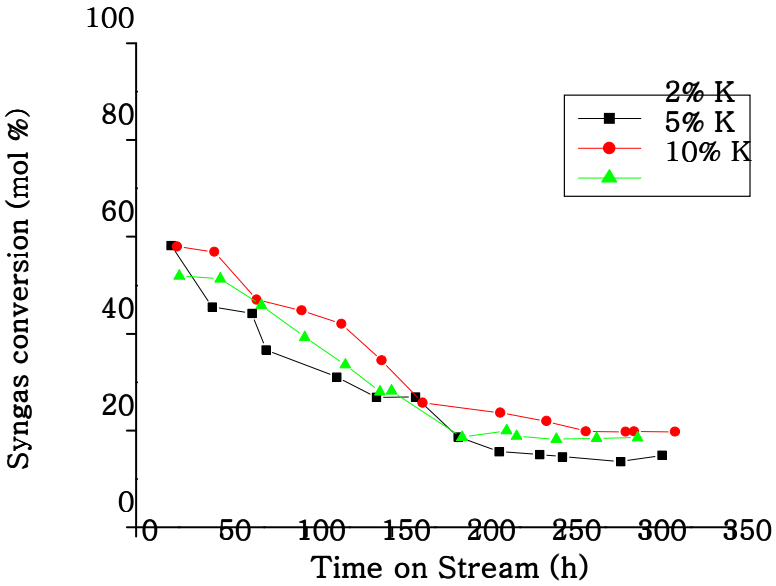

Figure 7.2: Syngas conversion as a function of time on stream for 15% Fe/AC promoted with 2, 5 and 10% K.

The catalysts reached stable CO conversions of 25, 30 and 31%; and syngas conversions of 16, 20 and 19 % for the 2, 5 and 10 % K loaded Fe catalysts, respectively. It was found that the 5% K promoted catalysts was more active than the 2% K promoted catalyst. However, when potassium was added at levels higher than 5% it did not increase the CO and syngas conversions. This shows that potassium promotion effect for an Fe/AC catalyst activity reached a maximum at a loading with the 5% K. Although, potassium enhanced the FTS activity, high potassium loadings may cover too large of a fraction of the surface

of the iron catalyst, resulting in a limited promotion effect or even a decrease in FTS conversions [30]. Yang *et al*. [46] also observed the same trend. They reported that the CO conversion of Fe/Mn/K catalyst increased significantly with the increase of potassium content and passes through a maximum at the potassium content of 0.7 wt.%. Beyond this potassium concentration, a monotonic decrease in catalyst activity is observed with the increase of potassium.

7.3.2 Deactivation of the Fe/AC catalysts

The detail of the mechanism for the deactivation of iron catalysts has been a bone of contention for many years. Many factors have been shown to impact on the deactivation process. Bartholomew [47] reported that supported precipitated Fe catalysts undergo attrition which is usually observed in slurry reactors due to mechanical and chemical stresses. Duvenhage and Coville [48] reported that the deactivation effect of the precipitated Fe catalyst in a fixed bed reactor resulted predominantly from sulfur poisoning in the top of the reactor and magnetite formation and crystallite growth in the bottom of the reactor bed. Spencer and Twigg [49] postulated that in general the deactivation of an Fe catalyst could be due to fouling, sintering and even adsorption of poisons. Davis [43] has reported that the rate of deactivation of the precipitated iron catalysts is also dependent on

the presence/absence of promoters such as potassium and/or binders such as silica.

It is noteworthy that deactivation has been observed for other reported Fe/AC catalysts [18-20]. However there is not sufficient data in the literature to explain this interesting phenomena for the carbon supported iron catalysts. Ma *et al*. [20] reported the selective FTS of C_1-C_{20} complexes with an Fe/AC catalyst prepared by a vacuum impregnation method and promoted with Cu and K. The authors observed that the syngas conversion reached a maximum value of 60.6% after 43 h on stream; between 44-115 h and thereafter it decreased quickly with a syngas conversion loss of 0.21%/h. During the last portion of the test (116-166 h) catalyst activity still decreased but the deactivation rate (0.022%/h) was quite low. However, the detail of the mechanism of the deactivation of their catalysts was not mentioned.

The deactivation process appears to be similar for all the catalysts studied, and a summary of deactivation rates for the three catalysts is presented in Table 7.2 below. From Table 7.2 it can be seen that the CO conversion started at a high value of ~90 % after ~20 h on stream for all three K loaded catalysts, between 20 - 240 h on stream it decreased quickly with a CO conversion loss rate of 0.30 ± 0.02%/h for all three K loaded catalysts. During the last portion of the test (190 –

294 h), catalyst activity still decreased with time on stream but the deactivation rate (0.03 and 0.01%/h) was quite low for the 2 and 10% K loaded catalysts, respectively. Interestingly, the 5% K loaded catalyst deactivation rate was nearly, if not, zero.

Table 7.2 Changes in deactivation rate as a function of time on stream

Catalyst	CO conversion (mol %)	Time on stream (h)	Loss rate (%/h)
15%Fe/2%K/AC	87 – 26 26 – 24	20 – 212 212 - 308	0.32 0.03
15%Fe/5%K/AC	88 – 36 28 – 29	24 – 240 240 - 316	0.27 0
15%Fe/10%K/AC	86 – 32 32 – 31	25 – 191 191 - 294	0.32 0.01

The observed deactivation of the catalysts can be speculated to be due to the following factors:

a) Loss of the active metal from the FT reaction

In this study it was found that the wax product collected contained a small amount of Fe. In order to determine the extent of the loss of the Fe catalyst, samples of the wax were collected and the elemental composition of the Fe catalyst in the

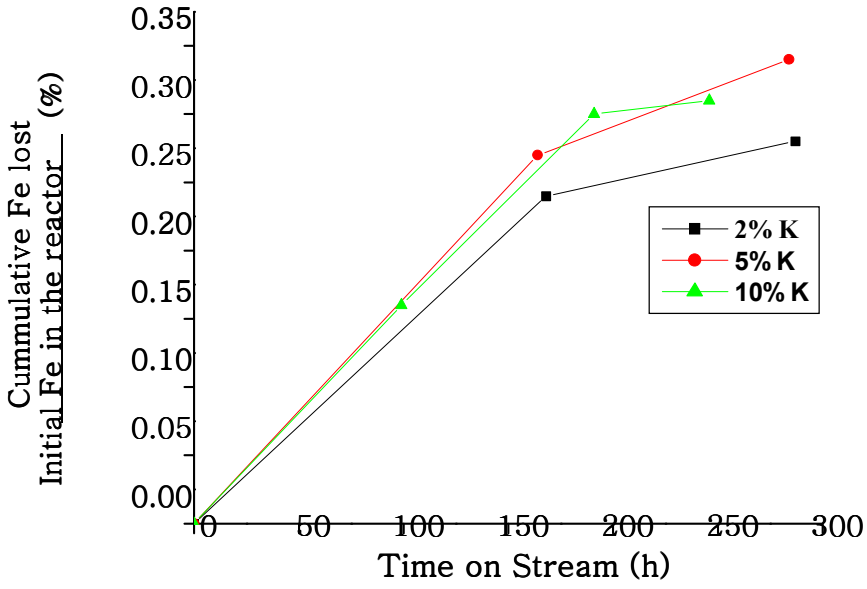

Figure 7.3: Deactivation for 15% Fe on activated carbon with 2, 5 and 10% K promotion as a function of time on stream.

wax product collected was determined by XRF analysis. From the results it was found that on average 0.02% Fe was lost a day for all the three catalysts over the time of study. The cumulative amount of Fe lost compared to the initial amount of Fe in the reaction as a function of time-on-stream for the three catalysts is plotted in Figure 7.3. The cumulative amount of Fe lost is almost the same for the three catalysts and appears to slow down with time. Since the amount of Fe lost was very small for all the catalysts, it therefore can be concluded that the deactivation of the catalysts in this study was not due to the loss of the active metal from the F-T reaction.

b) Sulfur poisoning

Energy dispersive X-ray (EDX) was used to determine the elemental composition of the activated carbon (prior to the addition of Fe). Fig. 7.4 shows a typical EDX pattern of the activated carbon support used. It is evident from Fig. 7.4 that the support contained silicon and sulfur as impurities as has been reported by others [50-53]. To remove the impurities from a related activated carbon, Rioux and co-workers [50-53] washed the activated carbon in refluxing nitric acid at 90 ^{o}C for 12 h. This not only removed the impurities but also made the surface of the carbon rich in oxygen-containing functional groups. Vannice *et al*. used carbon black as a support for organometalic Fe complexes and heated the carbon in

flowing hydrogen for 12 h at 950 ^{o}C to remove residual sulphur [50-53]. The authors reported that without sulfur removal the catalyst was inactive. However, it is worth noting that the procedures used above compromised the interesting structural features of the carbon material and also resulted in the loss of some of the carbon materials. The EDX spectrum in Fig. 7.4 shows that the amount of sulfur found on the carbon support was very small (0.5-0.7 g of total sulphur content/100g activated carbon). Sulfur has been reported to be a poison for Fe catalysts [53-55].

c) Phase changes

While it is recognized that Fe carbides are formed during activation of Fe catalysts in CO and during the F-T reaction [29,30], the presence of iron carbides is not sufficient to ensure high and stable CO and syngas conversions. Luo and co-workers [29,30] reported that gradual oxidation of Fe_5C_2 to Fe_3O_4 was observed when the precipitated iron catalyst was used in FTS after activation in a CO atmosphere. It is believed that the reaction system becomes more oxidizing and magnetite is usually formed at a high CO conversion. Because the same activation procedure was used for all three Fe catalysts, it can be speculated that part of the deactivation observed in this study could be also related to the formation of the inactive magnetite.

Sommen *et al*. [20] have investigated the activity of Fe catalysts supported on activated carbon. They found that the Fe/C catalysts inherently possess the tendency to form graphitic carbon deposits in the form of fibers. The observed deactivation was possibly mainly caused by plugging of catalyst pores. The high initial rate of deactivation was due to the relatively large surface area present in small pores. Since we also observed a rapid bedding in/initial deactivation of our catalysts, the deactivation is probably also due to complete filling or blockage of catalyst pores and not to gradual coverage of the iron surface by (inactive) carbon.

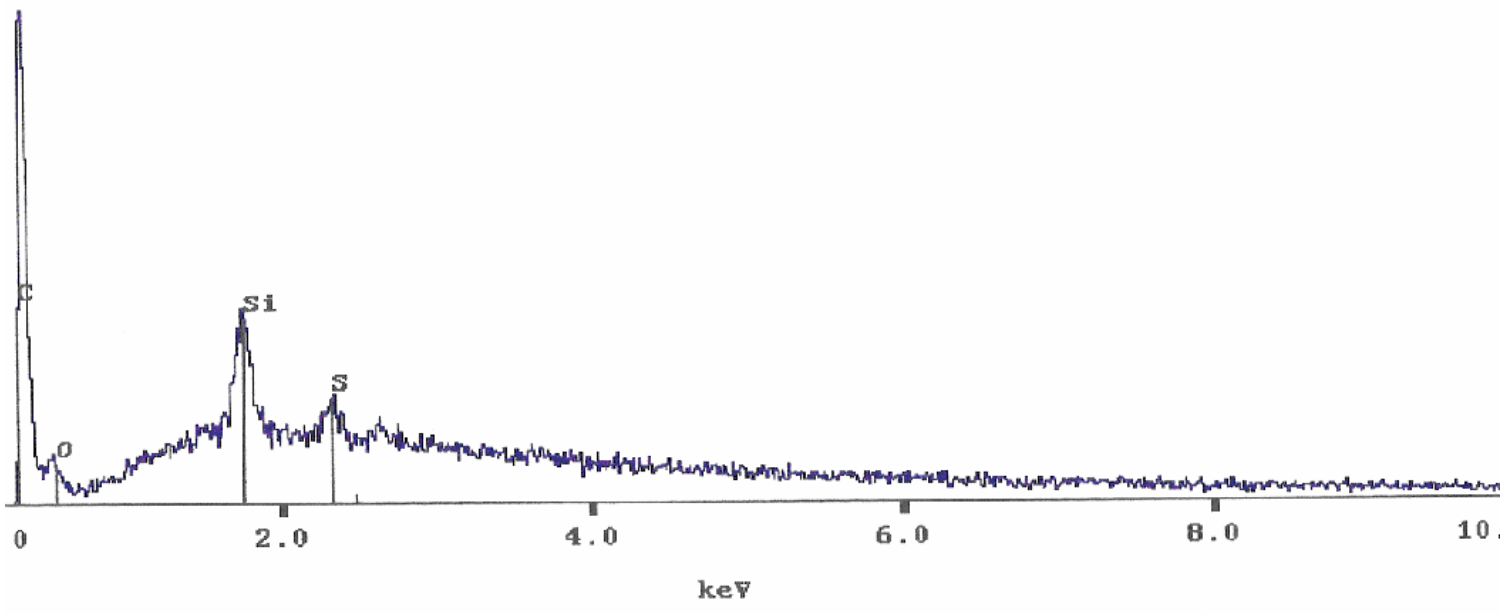

Figure 7.4: EDX spectrum of activated carbon support.

7.3.3 Selectivity of the Fe/AC catalysts

Table 7.3 shows the selectivity and productivity of the three catalysts. It can be seen that the methane selectivity was only slightly influenced by the potassium content as the potassium loadings were increased. Thus, a slight decrease, if any, in methane selectivity was observed when the potassium content was increased from 2 to 5% and the methane content then decreased with the 10 % K loaded catalyst. Figure 7.5 shows the effect of K loading with respect to methane selectivity as a function of time on stream and the methane selectivity for all catalysts is seen to be stable with time on stream even while the catalysts were bedding in. This contrasts with results of Fe/SiO_2 and Fe/Al_2O_3 catalysts, in which case the methane fraction generally increases as deactivation proceeds [20]. Furthermore, the addition of K to the Fe/AC catalysts showed an expected overall (moderate) decrease in methane selectivity compared to the other reported Fe/C catalysts with [21] and without [15-19] potassium addition.

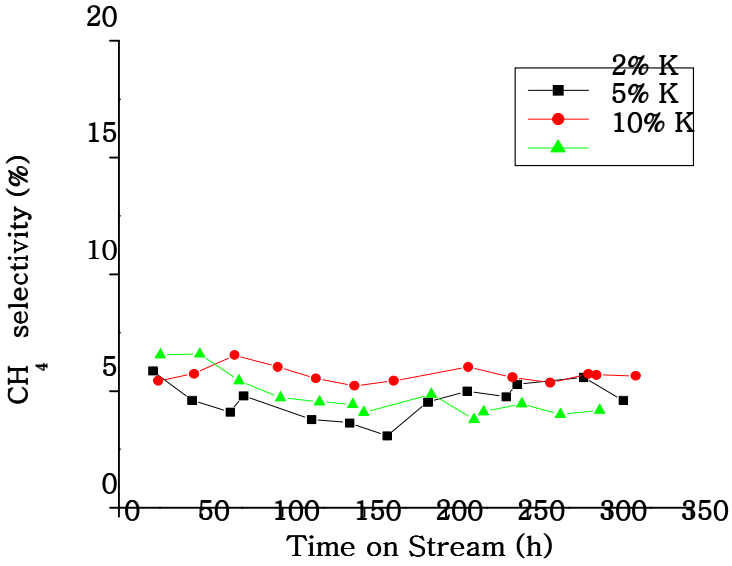

Figure 7.5: Methane selectivity as a function of time on stream for 15% Fe on activated carbon after 2, 5 and 10% K promotion

The water gas shift (WGS) reaction is an important reaction in FTS when an iron catalyst is used [29]. In this reaction CO reacts with water, which is generated from FTS, and produces CO_2 and H_2. Figure 7.6 shows the influence of K loading on CO_2 selectivity for the three catalysts. The variation in the WGS activity with potassium loading has a similar trend with that of the FTS reaction reactivity.

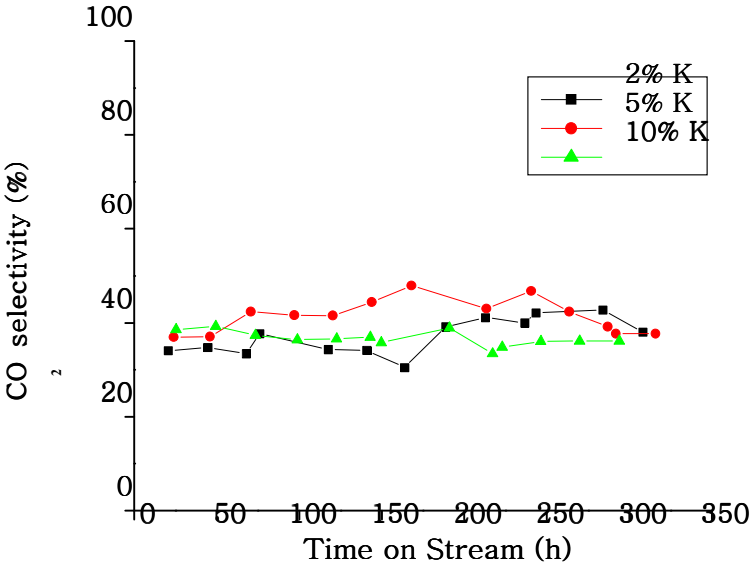

Figure 7.6: CO_2 selectivities as a function of time on stream for 15% Fe/AC catalysts after 2, 5 and 10% K loadings.

Generally, potassium can promote WGS activity [31,42]. The CO_2 selectivities of the catalysts were found to show a decrease with increasing K promotion and were almost stable with time on stream.

Sommen *et al*. [20] reported that the presence of CO_2 may increase the coverage of iron sites by CO, hinder adsorption and reaction of hydrogen, and consequently reduce the overall activity. On the other hand, Schulz *et al*. [56] found that the

presence of K in Fe-FT catalysts enhanced carbon deposition and hence, enhanced the high CO_2 selectivity, as observed in this study.

7.3.4 Productivity of the catalyst

The data shown in Table 7.3 below were recorded under steady state (i.e. when the CO conversion was stable, ~250 h). It is interesting to note that the olefin selectivity for the three catalysts were comparable despite the various K loadings. In general the olefinity fraction of all the catalysts was found to be high and ranged from 0.48 (with C_5 being the lowest for all catalysts) to 0.87. The hydrocarbon productivity for the 5% K is slightly higher than the other two catalysts. The overall H_2/CO usage was low.

Table 7.3: FTS conversion, Productivity and Selectivity for potassium promoted Fe catalysts

15% Fe Catalyst	**2% K**	**5% K**	**10% K**
Process conditions at steady state for all catalysts			
T = 250 ^{o}C, P = 2.0 MPa, H_2/CO ratio = 2:1, SV = 3.6 sl/hr g-Fe			
Conversion[a]			
CO	25.0	29.6	30.4
H_2	8.9	14.8	12.2
Syngas	13.63	19.74	18.2
H_2/CO usage[b]	0.77	1.00	0.80
Productivity			
Hydrocarbon (g/h/g-Fe)	0.16	0.22	0.14
C_1 (mol/h)	0.27	0.38	0.33
C_2 (mol/h)	0.22	0.29	0.28
C_3 (mol/h)	0.22	0.28	0.27
C_4 (mol/h)	0.13	0.16	0.15
C_5 (mol/h)	0.05	0.07	0.07
C_6 (mol/h)	0.03	0.05	0.04
C_7 (mol/h)	0.01	0.02	0.01

Selectivity (mol %)			
CH_4[c]	5.58	5.53	4.45
CO_2[d]	42.79	39.13	36.05
Olefin fraction[e]			
C_2	0.79	0.72	0.80
C_3	0.85	0.77	0.85
C_4	0.87	0.84	0.86
C_5	0.48	0.48	0.48
Product composition (wt. %)			
C_1-C_4	25.84	22.95	25.54
C_5-C_{11}	28.78	25.14	20.38
C_{12}-C_{18}	14.71	14.17	11.89
C_{19+}	30.67	37.73	42.18
α-1	0.83	0.81	0.79
α-2	0.85	0.86	0.88

[a]Conversion = (*N*in – *N*out / *N*in) x 100

[b]Usage = r_{H2}/r_{CO}

[c]CH_4 (mol %) = CH_4/ all hydrocarbons

[d]CO_2 (mol %) = CO_2 formed/ CO converted

[e]Olefin fraction = olefin/ (olefin + paraffin)

7.3.5 Product distribution

All the catalysts under study showed a medium carbon chain distribution with the products ranging from carbon numbers, C_1 to C_{55}. By contrast, Vannice et *al*. [15-17], Ma *et al*. [21] and others [19, 20] observed a limited chain growth with Fe/AC catalysts using fixed bed reactors. Carbon numbers only up to C_{20} were produced. It was claimed that the observed poor chain growth ability of the catalyst might have be due to the microporosity of the activated carbon support.

The 2 and 5% K loaded catalysts produced a slightly higher percentage of liquid organic products when compared to the 10% loaded catalyst (see Table 7.3). Larger molecular products were dominant in the catalyst with the highest K loading. The product spectrum was broadly distributed, with the C_{19+} products being more dominant than any other products for all the catalysts. Dry [21] reported that the level of alkali promoter for an iron catalyst influences the product spectrum. Thus, the higher the K_2O content, the greater is the shift to the higher carbon number products. This was shown to be true in the study; the highest potassium loaded (10%) catalyst produced more solid organic products than the other two catalysts.

Figure 7.7 shows the ASF plot of the hydrocarbon product distribution for the three catalysts.

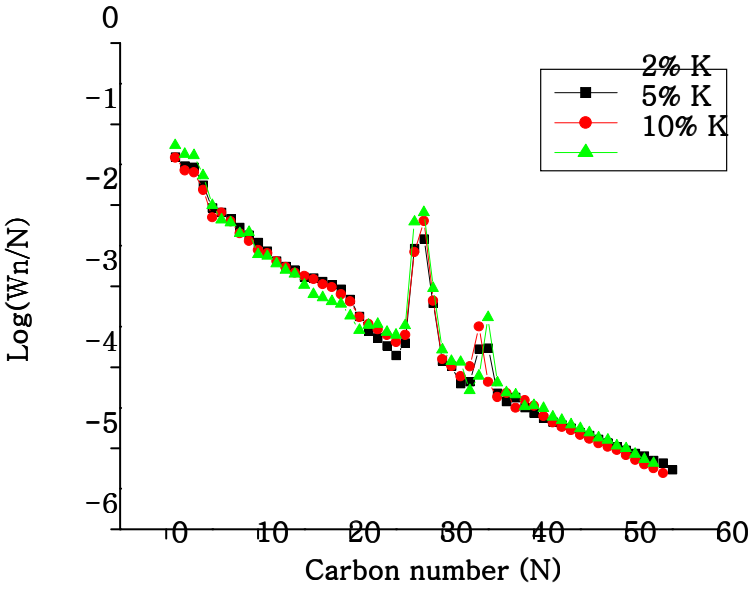

Figure 7.7: ASF product distribution for the 15%Fe/AC catalyst impregnated with various amounts of potassium.

The hydrocarbon after C_3, obey the ideal ASF law, ($\log(Wn/N) = n\log\alpha + \log((1 - \alpha)^2/\alpha)$ [1,57] used for calculating the α-1 values. As expected, very slight deviation (excess) occurs at C_1 indicating a slight enhanced concentration of the methyl species on the catalyst surface. Another deviation occurs at C_2 showing a slightly lower percentage yield. This is said to be caused by a higher rate of

ethene secondary reactions which take place simultaneously during the FT reaction [56,57]. Deviations between C_{28}-C_{32} and C_{35}-C_{37} are due to the wax used as a solvent in the reaction (refer to Fig. 5.2 in chapter 5).

When disregarding the deviations observed for the solvent used in the reaction, the three catalysts gave similar α-1 and α-2 values between 0.79 and 0.88.

7.4 Conclusion

In this study, the effect of potassium promotion on precipitated iron catalysts supported on activated carbon was investigated. It was observed that the three promoted and precipitated Fe/AC gave initially high rate of conversion that then decreased with time on stream. The deactivation was consistent for all the catalysts and was speculated to have been due to a possible contribution of sulfur poisoning and phase changes. More importantly, the deactivation is probably due to complete filling or blockage of catalyst pores with time and not to gradual coverage of the iron surface by (inactive) carbon. The catalysts eventually reached stable CO conversions (25, 30 and 31 with the 2, 5 and 10% K loaded catalysts, respectively). The results suggested that a further increase in K loading will not enhance the activity of these FTS catalysts.

The methane selectivity was low (below 6%) and stable, and the overall olefin fraction was found to be high for all three catalysts. On average, a CO_2 yield of ~40% was obtained for all the three catalysts, indicating similar water gas shift reaction behaviour. From the study it was shown that middle alpha (α-1 and α-2 ranged between 0.79 and 0.88) catalysts were prepared and that the potassium promoter increased the hydrocarbon chain growth during the FT synthesis up to C_{55}. Increasing the amount of promoter from 5 to 10% K did not show any significant increase in activity of the studied catalysts.

7.5 References

[1] W.-P. Ma, Y.-J. Ding, and L.-W. Lin, *Ind. Eng. Chem. Res.*, **43***,* 2391 (2004).

[2] B. H. Davis, *Catal. Today*, **84**, 83 (2003).

[3] D. B. Bukur and C. Sivaraj, *Appl. Catal. A*, **231**, 201 (2002).

[4] C. Aaserud, A-M. Hilmen, E. Bergene, S. Eric, D. Schanke, A. Holmen, *Catal. Lett.*, **94**, 171 (2004).

[5] S. L. Soled, E. Iglesia, R. A. Fiato, J. E. Baumgartner, H. Vroman, S. Miseo, *Topics in Catal*., **26**, 101 (2003).

[6] G. Jacobs, J. A. Chaney, P. M. Patterson, T. K. Das, J. C. Maillot, B. H. Davis, *J. Synchroton Rad*., **11**, 414 (2004).

[7] R. J. O'Brien, L. Xu, A. Raje, B. H. Davis, *Appl. Catal*., *A,* **196**, 173 (2000).

[8] J. Van De Loosdrecht, A. J. Van Dillen, D. Reinders, A. A. Van Der Horst, E. Boellaard, A. M. Van Der Kraan, J. W. Gues, *Stud. Surf. Sc. Catal*., **107**, 201 (1997).

[9] V. Curtis, C. P. Nicolaides, N. J. Coville, D. Hildebrandt, D. Glasser, *Catal. Today*, **49**, 33 (1999).

[10] J. L. Li, G. Jacobs, T. Das, Y. Q. Zhang and B. Davis. *Appl. Catal. A.*, **236**, 67 (2002).

[11] F. Rodriguez-Reinoso, *Carbon*, **36**, 159 (1998).

[12] R. Giordano, P. Serp, P. Kalck, y. Kihn, J. Schreiber, C. Marhic and J-L. Duvail, *Eur. J. Inorg. Chem*., 610 (2003).

[13] R. R. A. Rios, D. E. Alves, I. Dalmazio, S. F. V. Bento, C. L. Donnici and R. M. Lago, *Mat. Res*., **6**, 129 (2003).

[14] F. P. Van der Zee, I. A. Bisschops, G. Lettinga and J. A. Field*, Environ Sci, Technol*., **37**, 402 (2003).

[15] H.-J. Jung, P.L. Walker Jr. and M.A. Vannice, *J. Catal*., **75**, 416 (1982).

[16] H.-J. Jung, M.A. Vannice, L.N. Mulay, R.M. Stanfield and W. N. Delgass, *J. Catal*., **76** (1982) 208.

[17] A.A. Chen, M.A. Vannice and J. Phillips, *J. Phys. Chem*., **91**, 6257 (1987).

[18] M. E. Dry, *Catal. Today*, **71**, 227 (2002).

[19] V. K. Jones, L. R. Neubauer and C. H. Bartholomew, *J. Phys. Chem*., **90**, 4832 (1986).

[20] A. P. B. Sommen, F. Stoop and K. Van der Wiele, *Appl. Catal*. *A*, **14**, 227 (1985).

[21] W.-P. Ma,Y-J. Ding, L-W. Lin. *Ind. Eng. Chem. Res*., **43**, 2391 (2004).

[22] M. E. Dry, *Appl. Catal. A.*, **276**, 1 (2004).

[23] G. P. Van der Laan and A. A. C. M. Beenackers, *Catal. Rev.*, **41**, 255 (1999).

[24] B. Jager and R. Espinoza, *Catal. Today*, **23**, 17 (1995).

[25] P.C. Das, N. C. Pradhan, A. K. Dalai and N. N. Bakshi, *Catal. Today*, **98**, 153 (2004).

[26] D. J. Duvenhage and N. J. Coville, *Appl. Catal. A*, **153**, 43 (1997).

[27] M-S. Luo, R. J. O'Brien, S. Bao and B. H. Davis. *Appl. Catal. A*, **239**, 111 (2003).

[28] J. Li, G. Jacobs, T. Das and B. H. Davis, *Appl. Catal. A*, **233**, 255 (2002).

[29] M.-S. Luo and B. H. Davis. *Fuel Process. Technol.*, **83**, 49 (2003).

[30] M.-S. Luo, S. Bao and B. H. Davis, *Appl. Catal. A*, **239**, 111 (2003).

[31] B. D. Bukur, D. Mukesh and S. A. Patel*, Ind. Eng. Chem. Res.*, **29**, 194 (1990).

[32] G. Jacobs, T. K. Das, Y. Zhang, J. Li, G. Racoillet and B. H. Davis, *Appl. Catal. A*, **233**, 263 (2002).

[33] L. Senzi, K. Sundaram, L. Anwu, M. George and D. I. Enrique, *J. Catal.*, **206**, 202 (2002).

[35] S. A. Eliason and C. H. Bartholomew. *Appl. Catal., A*, **186**, 229 (1999).

[36] M. E. Dry, "*Catalysis: Science and Technology,"* (J. R. Anderson and M. Boudart, Eds.), **1**, (1981).

[37] D. B. Bukur, D. Mukesh and S. A. Patel. *Ind. Eng. Chem. Res*., **29**, 921 (1990).

[38] A. P. Raje, R. J. O'Brien and B. H. Davis. *J. Catal.*, **180**, 36 (1998).

[39] S. Li, G. D. Meitzner and E. Iglesia, *Stud. Surf. Sc. Catal.*, **136**, 387 (2001).

[39] W.-P. Ma,Y.-J. Ding, L.-W. Lin. *Ind. Eng. Chem. Res*., **43**, 2391 (2004).

[40] J. Van de Loosdreght, A. J. Van Dillen, D. Reinders, A. A. Van der Horst, E. Boellaard, A. M. Van der Kraan and J. W. Geus, *Stud. Surf. Sc. Catal.*, **107**, 201 (1997).

[41] J. W. Dun, E. Gulari and K. Y. S. Ng, *Appl. Catal. A*, **15**, 247(1985).

[42] H. Arakawa and A. T. Bell, *Ind. Eng. Chem. Proc. Des. Dev.* **22**, 97 (1983).

[43] B. H. Davis, *Technology development for iron catalysts*, Final report DoE/PC94055-13 (1999) [available at www.fischer-tropsch.org].

[44] G. B. McVicker and M. A. Vannice, *J. Catal*., **63**, 25 (1980).

[45] B. H. Davis, *Catal. Today*, **84** , 83 (2003).

[46] Y. Yang, H.-W. Xiang, Y.-Y. Xu, L. Bai and Y.-W. Li, *Appl. Catal. A*, **266**, 181 (2004).

[47] C. H. Bartholomew, *Appl. Catal. A,* **212**, 17 (2001).

[48] D. J. Duvenhage and N. J. Coville, *Appl. Catal. A*, **298**, 211 (2006).

[49] M. S. Spencer and M. V. Twigg, *Ann. Rev. Mater*., **35**, 427 (2005).

[50] R. M. Rioux, M. A. Vannice, *J. Catal*., **233**, 147 (2005).

[51] R. M. Rioux, M. A. Vannice, *J. Catal*., **216**, 362 (2003).

[52] M. H. Kim, J. R. Ebner, R. M. Friedman and M. A. Vannice, *J. Catal*., **208**, 381 (2002).

[53] M. A. Vannice, P. L. Walker, H.-J. Jung, C. Morena-Castilla and O. P. Mararaj, *Proceedings of the VII International Congress of Catalysis*, Tokyo, Paper **A31**, July (1980).

[54] A. P. Steynberg and M. E. Dry. *Stud. Surf. Catal.***, 152***, Fischer-Tropsch technology*, 1st ed., Elsevier, Amsterdam, (2004).

[55] I. Prasetyo and D. D. Do, *Carbon*, **37**, 1909 (1999).

[56] H. Schulz, *Erdöl und Kohle*, **30**, 123 (1977).

[57] H. Schulz and M. Claeys, *Appl. Catal. A*, **186**, 91 (1999).

Chapter Eight

Fischer-Tropsch Synthesis over an Iron Catalyst Supported on Mesoporous-Carbon: Effect of Potassium Loading

8.1 Introduction

Carbon supported iron catalysts have been the subject of recent scientific interest owing to the weak chemical interaction of the carbon with the deposited active phase (providing a high active phase efficiency), their low cost and the formation of highly dispersed supported metal particles due to their high surface areas [1-3]. Carbon materials such as graphite, carbon black and activated carbon [1,2] have also been used as supports for iron catalysts in a number of other catalytic processes such as CO and CO_2 hydrogenation [4], desulfurisation and dehalogenation [5,6], ozone or hydrogen sulfide decomposition [7,8], catalytic removal of SO_2, NO and HCl [9], and in the Fischer-Tropsch synthesis (FTS), even though only a few reports have appeared on the use of carbons for FTS [10-16]. In addition, Fe catalysts supported on carbon have been reported to produce high selectivites for olefins in the FTS [17], compared to conventional inorganic supports.

Activated carbon is anticipitated to have some serious drawbacks when applied in FTS. For instance, these carbons may have a poor mechanical strength (resulting in crushing when packed in an industrial reactor) and a high degree of microporosity (causing diffusion limitations for large reactant molecules) [3]. Thus, carbon supports that might not be subjected to these drawbacks can be advantageous. Indeed, carbon nanotubes and ordered mesoporous carbons that have recently been prepared show promising features for catalytic applications.

Since carbon the discovery of nanotubes [18], few reports have appeared on the use of this type of carbon as a support for catalytic reactions [19-22] and especially for the FT reaction [23,24]. Van Steen and Prinsloo [23] published their findings on the synthesis of C_1-C_{15} hydrocarbons on Fe/carbon nanotube supported catalysts. Unfortunately, the activity of their catalyst was very low and declined quickly from 45% to almost 10% within 70 h of testing. Later on, Bahome *et al*. [24] reported higher yields of CO_2 and C_2 olefins with a potassium promoted iron catalyst supported on carbon nanotubes using a microscale fixed bed reactor at 275 ^{o}C, 0.8 MPa and $H_2/CO = 2$. Even though the FTS results on carbon nanotubes are interesting, these carbons have been reported to exhibit broad pore size distribution in the micropore and mesopore ranges, and relatively small surface areas, the latter being attributable to adsorption inside the tubes, and to adsorption on the external surface of the tubes [25].

In a different study, Bezemer *et al*. [26,27] used an unpromoted cobalt supported on carbon nanofiber catalyst prepared by high pH (8) deposition precipitation technique in FTS. The FTS was performed using the conditions: H_2/CO ratio = 2, pressure = 0.1 MPa, T = 220 ^{o}C at 2% CO conversion. It was found that the selectivity to methane was 20 wt% and the catalyst produced remarkably high and stable C_{5+} selectivity of around 53 wt %.

The recent discovery of ordered mesoporous carbons (MC) provides a new generation of carbonaceous supports for catalytic applications [28-49]. Only a few reports have been published on ordered mesoporous carbons loaded with metal nanoparticles and their corresponding catalytic performance. A notable example was reported by Ryoo and co-workers [29,34]. They reported the synthesis of a Pt-loaded CMK-3 mesoporous carbon prepared by impregnation with chloroplatinic acid solution, followed by hydrogen reduction at 300 ◦C. The Pt/CMK-3 catalyst has very good performance for oxygen reduction, but only for small area microelectrodes submerged in a solution [34,35].

In another study, the authors prepared CMK-5 nanoporous carbon and used it as a suppot for Pt and Ru metal catalysts which were loaded onto a carbon support via incipient wetness impregnation of $H_2PtCl_6.6H_2O$ and $RuCl_3.xH_2O$, and subsequently reduced at 300-400 ^{o}C in H_2 flow [36]. The nanoporous carbons

were characterized by TEM and gas chemisorption and a showed high metal dispersion of Pt and Ru clusters, when compared with conventional porous carbons. In addition, Minchev *et al*. [2] prepared a series of iron oxide supported CMK-1 and CMK-3 materials for the catalytic decomposition of methanol.

Palladium supported on mesoporous carbon has shown high catalytic activity in liquid phase hydrogenation [33] and Heck iodobenzene [34] reactions. Ding and co-workers [35] described platinum, ruthenium and palladium modified CMK carbons as materials with remarkably high catalytic activity when compared to their analogues obtained on other carbons or inorganic supports. Zhang *et al*. [36] reported the synthesis and application of CuO/Mn_3O_4-mesoporous composite for the reduction of tar, CO and tobacco in cigarette smoke. Recently, Lee *et al*. [37] reported the synthesis of a magnetically separable ordered mesoporous carbon (M-OMC) containing magnetic nanoparticles embedded in the carbon walls. The sysnthesis of poly(pyrrole) with residual Fe^{2+} ions was converted to a carbon material containing super-paramagnetic nanoparticles. The sizes of the magnetic nanoparticles obtained were restricted by the channel size of the SBA-15 silica template, which resulted in the generation of super-paramagnetic nanoparticles embedded in the carbon rods.

Although there is a substantial literature on the synthesis of mesoporous carbons, these carbons are yet to be evaluated for FTS. Due to our interest in iron-supported catalysts, we wish to report on the evaluation of the performance of some mesoporous carbons as supports for FTS iron catalysts. Thus, in this chapter, we report the catalytic investigation of the effect of potassium promotion on three precipitated iron catalysts supported on mesoporous carbons in the FTS reaction in a slurry bubble CSTR.

8.2 Experimental section

In order to establish the catalytic properties and to assess the effect of potassium promotion, three 15%Fe loaded metal catalysts supported on mesoporous carbon were studied and compared in the FT synthesis reactions. The preparation, reduction procedure, characterisation techniques, etc. for the precipitated and promoted iron catalyst precursors 15%Fe/2%K/MC, 15%Fe/5%K/MC and 15%Fe/10%K/MC used in this chapter are reported in detail in Chapter 5. All catalysts were activated under the same conditions (CO at 270 ^{o}C and 2.0 MPa for 24 h), and tested at process conditions of 250 ^{o}C, 2.0 MPa, 3.6 sl/(g-Fe h) and $H_2/CO = 2$.

8.3 Results and discussion

8.3.1 The Fischer-Tropsch activity of the precipitated and promoted Fe/MC catalysts

The effect of potassium on the FTS activity measured by CO and syngas conversions is shown in Fig. 8.1 and 8.2, respectively. For all the three catalysts, the CO conversion started at a moderate values (~60 mol% at 50 h on stream). During the first 50-100 h on stream, the CO (Fig. 8.1) and syngas (Fig. 8.2) conversions decreased with time. The 2% K loaded catalysts declined quickly with a loss rate of 0.34%/h between 50-120 h on stream; thereafter no deactivation of the catalyst was observed. The conversion of the 5 and 10% K rapidly declined at a rate of 0.19 %/h between 50-160 h; and further deactivated at 0.06 and 0.04%/h between 150 - 290 h on stream. Beyond the 5% K loading concentration, a decrease in the catalyst activity was observed with an increase in potassium loading.

The 10% loaded K catalysts showed slightly lower CO conversion when compared to the other two catalysts. It has been previously postulated by Luo *et al*. [49] that high potassium loadings may result in the potassium covering too large of a fraction of the surface of the iron catalysts, resulting in a decrease in

CO conversion or even decreased FTS conversions. Yang *et al*. [50] also observed the same phenomena with an increase in potassium loading. This was proposed to be due to increased carbon deposition as well as sites being blocked on the catalysts surface. After 100 h TOS the catalyst activity became stable.

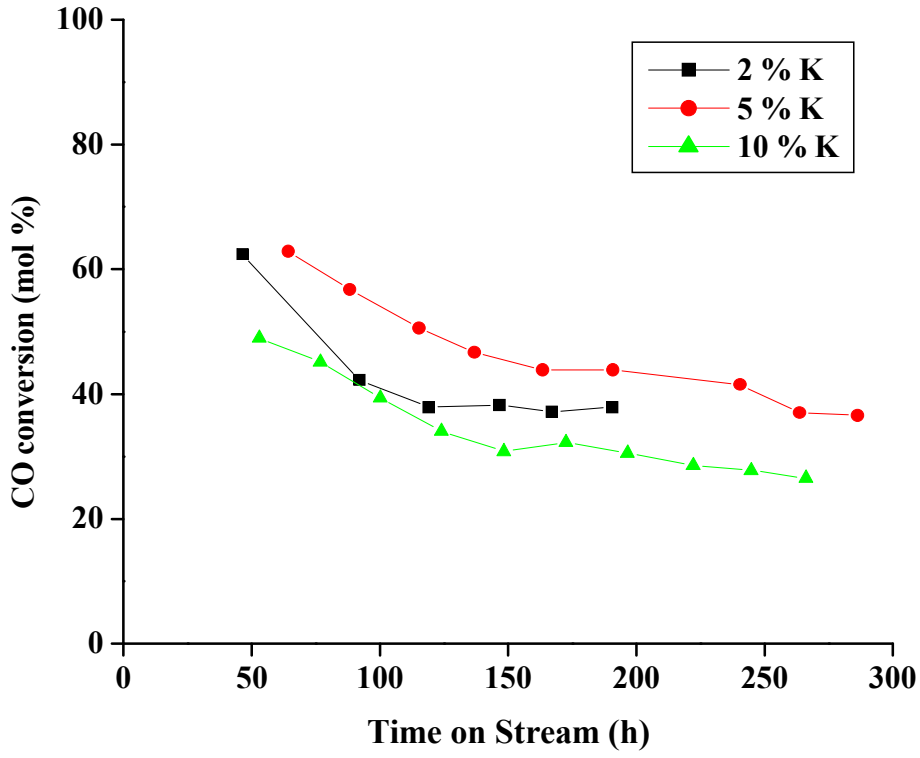

Figure 8.1: CO conversion as function of time on stream for 15 %Fe/mesoporous carbon loaded with different amounts of potassium.

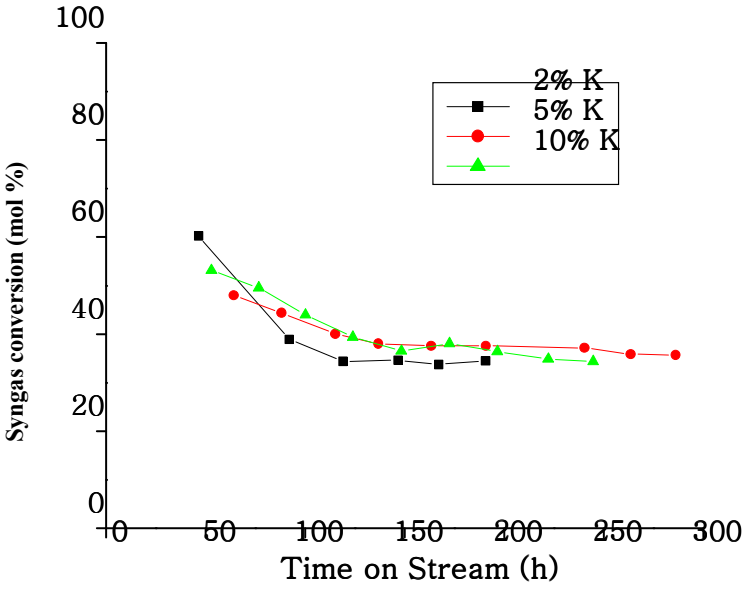

Figure 8.2: Syngas conversion function of time on stream for 15 %Fe/mesoporous carbon loaded with different amounts of potassium.

Van Steen and Prinsloo [23] used a deposition precipitation method to prepare an Fe/Cu/K catalyst supported on carbon nanotubes. The catalyst was tested for FTS using a fixed bed reactor under these conditions: T = 220 ^{o}C, P = 2.4 MPa, H_2/CO = 1.7. They found that the catalysts had a very low activity with a CO conversion of 12.1% even though it was promoted with potassium. However, it was not clear whether the potassium was associated with the Fe or with the residual acidic sites

on the carbon nanotubes. When they compared this result to the ones they found on other catalysts prepared by an incipient wetness impregnation method with Cu and without K, it was observed that the CO conversion of the incipient wetness method declined from 48% to about 15% within 70 hours of testing. The authors speculated that the origin of the difference in activity was related to the difference in metal crystallite size distribution in the two catalysts, which would result in a different percentage of the phases present in the active FT catalysts.

Bahome *et al*. [24] reported their findings on the FT synthesis over Fe catalysts supported on carbon nanotubes using a microscale fixed bed reactor at 275 ^{o}C, 0.8 MPa and $H_2/CO = 2$. The activity for the catalyst prepared by the deposition precipitation method and impregnated with potassium was initially low (60%) but increased significantly to 85% within 15 h on stream and became stable for the entire experiment (20-120 h). Chin *et al*. [53] reported on the performance of a FeCrAlY/carbon nanotube modified structured FTS engineered catalyst support in a microchannel reactor. Co-Re/Al_2O_3 was then further deposited to generate the FT catalyst. The CO conversion at 150 h on stream was 42% with a 27% methane selectivity using these conditions: GHSV = 14,400 h^{-1}; T = 266 ^{o}C, P = 1.5 MPa.

The differences in trends (activity *vs* TOS data) in Van Steen and Prinsloo's [23], Bahome *et al*.'s [24], Chin *et al.*'s [51] studies and the present study may be due to the differences in the methods of catalyst preparation, the activation procedures used and process conditions employed. It is thus not possible to comprehensively compare the data from the different studies.

8.3.2 Selectivity of the precipitated and promoted Fe/MC catalysts

The effects of potassium promotion on the selectivity of Fe/MC catalysts to methane selectivity are shown in Fig. 8.3. The high methane selectivity on the 15%Fe/2%K/MC catalyst is speculated to have been caused by hydrogenation of additional active carbon species generated by oxygen containing groups on the mesoporous carbon [51]. However, when the K loading was increased to 5% and 10% the selectivity to methane was suppressed to 0.80 and 0.71 mol%, respectively, at steady state conditions. By contrast Bahome *et al*. [24] reported a methane selectivity of 11% for the FTS of Fe/carbon nanotubes. Van Steen and Prinsloo [23] reported that the methane selectivity seemed to be in the range of what is usually reported for iron based catalysts under similar reaction conditions (methane selectivity was not shown; due to the large methane content of the synthesis gas used, the exact methane selectivity determination was associated with large errors).

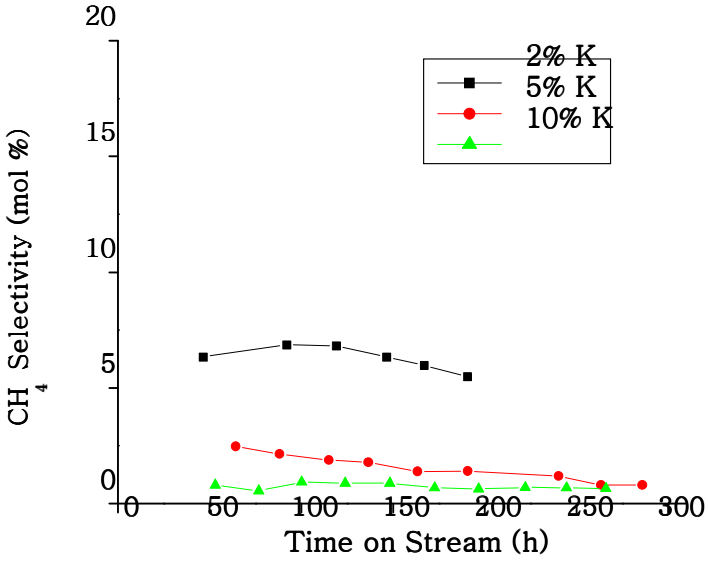

Figure 8.3: Methane selectivity function of time on stream for 15%Fe/mesoporous carbon loaded with different amounts of potassium.

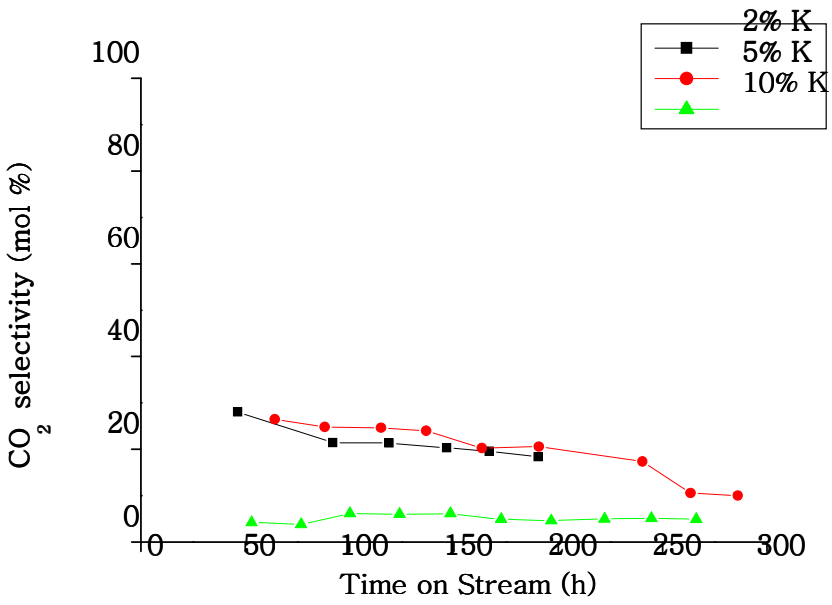

Figure 8.4: CO_2 selectivity function of time on stream for 15%Fe/mesoporous carbon loaded with different amounts of potassium.

It has already been mentioned in the previous chapter that the selectivity to CO_2 represents a measure of the water-gas shift activity. All catalysts under study exhibited a low water gas shift activity. However, the use of differently loaded K catalysts had a remarkable effect on the WGS activity. Selectivity to CO_2 was fairly stable but at the late stage of the run decreased quickly with the 2% K loaded catalyst and more slowly with the 5% K loaded catalyst.

The low level of CO_2 selectivity is well below expectation. However, the observed trend in the variation of the CO_2 selectivity and potassium level has a similar trend to that of the methane selectivity. From this observation it could be speculated that carbon dioxide and water favour the formation of methane for the Fe/K/MC catalysts. On the contrary, Dry [52] reported that the formation of methane is inversely proportional to the concentration of water and carbon dioxide. Luo and co-workers [53] suggested that the surface structure and/ or composition of an Fe/K catalyst changes in the FTS reaction so that it favours the formation of CO_2 and inhibits the formation of methane.

Although potassium is known to increase the rate of the WGS activity, the highest (10 % K) loaded catalysts gave a very low CO_2 selectivity followed by the 5% K loaded catalyst, indicating that K suppressed the WGS activity. The lower level of carbon dioxide production can be understood from the higher partial pressure of hydrogen, which leads to more hydrogenation of adsorbed oxygen to water and less reaction of carbon monoxide with adsorbed oxygen [54].

For the FT synthesis over Fe catalysts supported on carbon nanotubes, Van Steen and Prinsloo [23] reported that a high CO_2-selectivity (45% C) was obtained initially with the catalyst prepared by the deposition/precipitation method with Cu and without potassium. After 96 h on stream the CO_2-selectivity for all catalysts

was found to be rather low (10 – 20% C). Similar results were found by Bahome *et al*. [24] who reported a CO_2 selectivity of 12.6 %.

8.3.3 Productivity of the catalyst

The results reported in Table 8.1 represent steady state conditions when the conversions were stable for all the catalysts. The increase in average molecular weight of the hydrocarbon products is due to the fact that the CO/H concentration ratio on the catalyst surface can be increased by potassium addition. Therefore the presence of potassium enhances the probability of continued chain growth to form higher molecular weight products. In the present study it was found that this effect of potassium on the formation of methane and gaseous products is significant with the 10% K loaded catalyst. However, it was found that there is no obvious change in the selectivity to olefins between the three catalysts under study. By contrast, Yang *et al*. [50] reported that the olefin content increases with an increase in potassium loading for precipitated and unsupported Fe/Mn catalysts. Van Steen and Prinsloo [23] reported lower olefinity of their catalyst compared to what Bahome *et al*. [24] have reported on carbon nanotube supported Fe catalyst (0.72 fraction). However, both authors observed a shortened hydrocarbon chain length of up to C_{20} when using Fe/carbon nanotube catalysts loaded with potassium.

Table 8.1: FTS conversion, Productivity and Selectivity for potassium promoted Fe catalysts

15% Fe Catalyst	**2% K**	**5% K**	**10% K**
Process conditions at steady state for al catalysts			
T = 250 ^{o}C, P = 2.0 MPa, H_2/CO ratio = 2:1, SV = 3.6 sl/hr g-Fe			
Conversion[a]			
CO	37.89	36.58	28.62
H_2	32.90	35.29	34.02
Syngas	34.56	35.72	34.89
H_2/CO usage[b]	1.7367	1.9295	2.6576
Productivity			
Hydrocarbon (g/h/g-Fe)	0.15	0.20	0.13
C_1 (mol/h)	0.24	0.36	0.31
C_2 (mol/h)	0.22	0.26	0.25
C_3 (mol/h)	0.19	0.26	0.25
C_4 (mol/h)	0.11	0.15	0.14
C_5 (mol/h)	0.04	0.06	0.05
C_6 (mol/h)	0.03	0.05	0.04
C_7 (mol/h)	0.01	0.02	0.1

Selectivity (mol %)			
CH_4[c]	5.49	0.80	0.71
CO_2[d]	7.9	10.02	5.02
Olefin fration[e]			
C_2	0.42	0.78	0.75
C_3	0.76	0.85	0.83
C_4	0.74	0.79	0.76
C_5	0.46	0.47	0.48
Product composition (wt. %)			
C_1-C_4	36.21	22.06	20.86
C_5-C_{11}	27.15	27.97	20.96
C_{12}-C_{18}	11.42	15.93	17.65
C_{19+}	24.40	34.04	40.53
α-1	0.79	0.82	0.83
α-2	0.84	0.88	0.90

[a]Conversion = (*N*in – *N*out / *N*in) x 100

[b]Usage = r_{H2}/r_{CO}

[c]CH_4 (mol %) = CH_4/ all hydrocarbons

[d]CO_2 (mol %) = CO_2 formed/ CO converted

[e]Olefin fraction = olefin/ (olefin + paraffin)

Figure 8.5 shows the ASF plot of the hydrocarbon product distribution for the three catalysts. When disregarding the deviations observed for the solvent used in the reaction, the three catalysts gave increased α-1 and α-2 values between 0.79 and 0.90. The 2 and 5% K loaded catalysts produced a slightly higher percentage of

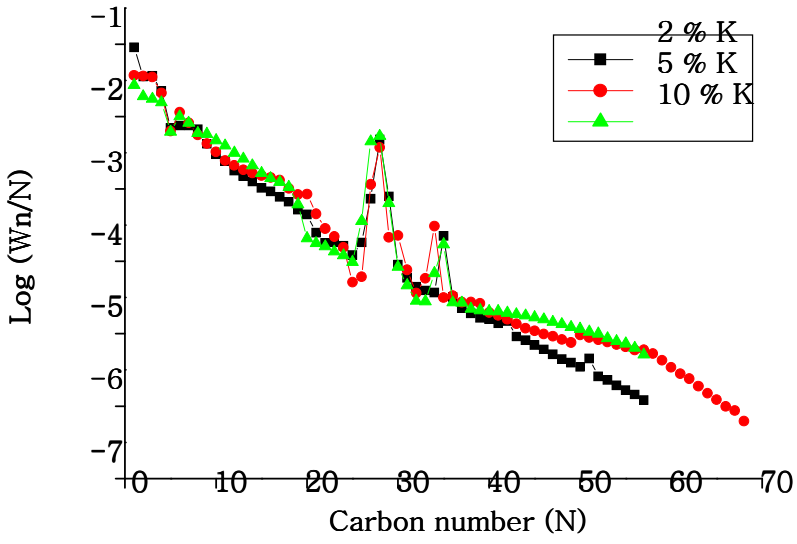

Figure 8.5: ASF- product distribution of 15%Fe/MC impregnated with various amounts of potassium.

gaseous and liquid organic products when compared to the 10 % loaded catalyst (see Table 8.1). Larger molecular products were dominant in the catalyst with the

highest K loading. However, the alpha values for the 5% and 10% K loaded catalysts are similar.

8.4 Conclusion

To the best of our knowledge, this is the first reported FTS activity data obtained for an Fe/MC catalyst. Extensive research still needs to be conducted in order to optimize the catalytic behaviour of Fe/MC by varying FTS process variables.

The activity of the catalysts, measured in terms of CO conversion as a function of time on stream, was found to be similar for the 2 and 5% K loaded catalysts. The 10% K loaded catalyst by contrast showed slightly lower CO conversion when compared to the other two catalysts. The methane selectivity of all three catalysts was low compared to other reported Fe/C catalysts. The 2% K loaded catalyst exhibited a low methane selectivity of 5 mol% and it was interesting to note that the selectivity to methane was further decreased with increases in potassium loading. The use of differently loaded K catalysts had a remarkable effect on the CO_2 selectivity. The CO_2 selectivity for all three catalysts was found to be low with the 10% K loaded catalyst exhibiting a significant decrease (~5 mol %) compared to 2% K loaded catalyst (~20 mol%) and 5% K loaded catalyst (~10 mol%).

It was interesting to see the positive effect potassium had on Fe/MC catalysts. Potassium is thus an effective promoter to restrain the formation of methane and gaseous products and to shift selectivity to higher molecular weight hydrocarbons on Fe/mesosoporous carbons. The catalysts under study were able to suppress the methane selectivity and also produced a high fraction of light olefins.

8.5 References

[1] F. Rodriguez-Reinoso, *Carbon*, **36**, 159 (1998).

[2] C. Minchev, H. Huwe, T. Tsoncheva, D. Paneva, M. Dimitrov, I. Mitov and M. Fro¨ba, *Micropor. Mesopor. Mater*., **81**, 333 (2005).

[3] C. K. Groot, V. H. J. de Beer, R. Prins, M. Stolarski and W. S. Niedzwiedz, *Ind. Eng. Chem. Prod. Res. Dev*., **25**, 522 (1986).

[4] C. Moreno-Castilla, M.A. Salas-Peregrin and F.J. Lopez-Garzon, *Fuel*, **74**, 835 (1995).

[5] J. Ma, Zh. Liu, Sh. Liu and Zh. Zhu, *Appl. Catal. B*, **45**, 301(2003).

[6] D. Santoro, V. de Jong and R. Louw, *Chemosphere*, **50**, 1255 (2003).

[7] C. Heisig, W. Zhang and S. Oyama, *Appl. Catal. B*, **14**, 117 (1997).

[8] Yu.V. Maksimov, M.V. Tsodikov and M.A. Prerderi, *Surf. Interf. Anal*., **30**, 74 (2000).

[9] Hui-Hsin Tseng, Ming-Yen Wey, Yu-Shen Liang and Ke-Hao Chen, *Carbon*, **41**, 1079 (2003).

[10] H. Juntgen, *Fuel*, **65**, 1436 (1986).

[11] H.-J. Jung, P.L. Walker Jr. and M.A. Vannice, *J. Catal*., **75**, 416 (1982).

[12] H.-J. Jung, M.A. Vannice, L.N. Mulay, R.M. Stanfield and W.N. Delgass, *J. Catal*., **76** (1982) 208.

[13] A.A. Chen, M.A. Vannice and J. Phillips, *J. Phys. Chem*., 91, 6257 (1987).

[14] V. K. Jones, L. R. Neubauer and C. H. Bartholomew, *J. Phys. Chem*., **90**, 4832 (1986).

[15] A. P. B. Sommen, F. Stoop and K. Van der Wiele, *Appl. Catal*., **14**, 227 (1985).

[16] W-P. Ma,Y-J. Ding, L-W. Lin. *Ind. Eng. Chem. Res*., **43**, 2391 (2004).

[17] K. J. Valiant, L. R. Neubauer and C. H. Bartholomew, *J. Phys. Chem*., **90**, 4832 (1986).

[18] S. Iijima, *Nature*, **354**, 56 (1991).

[19] X-Y Liu, B-C. Huang and N. J. Coville, *Carbon*, **40**, 2791 (2002).

[20] M. L. Mabudafhasi, R. Bodkin, C. P. Nicolaides, X-Y. Liu, M.J. Witcomb and N. J. Coville, *Carbon*, **40**, 2737 (2002).

[21] X. Y. Liu, B. C. Huang and N. J. Coville, *Carbon*, **40**, 2791 (2002).

[22] X. Y. Liu, B. C. Huang and N. J. Coville*, Fullerenes, Nanotubes, Carbon Nanostruct*., **10**, 339 (2002).

[23] E. van Steen and F. F. Prinsloo. *Catal. Today*, **71**, 327 (2002).

[24] M. C. Bahome, L. L. Jewell, D. Hilderbrandt, D. Glasser and N. J. Coville, *Appl. Catal. A*, **287**, 60 (2005).

[25] R. Ryoo, S. H. Joo, M. Kruk and M. Jaroniec, *Adv. Mater*., **13**, 677 (2001).

[26] G. L. Bezemer, P. B. Radstake, V. Koot, A. J. Van Dillen, J. W. Geus and K. P. de Jong, *J. Catal*., **237**, 291 (2006).

[27] G. L. Bezemer, A. van Laak, A. J. Van Dillen and K. P. de Jong, *Stud. Surf. Sci. Catal*., **147**, 259 (2004).

[28] S. Jun, S. H. Joo and R. Ryoo, *J. Am. Chem. Soc*., **122**, 19712 (2000).

[29] S. Han and T. Hyeon, *Carbon*, **37**, 1645 (1999).

[30] L. A. Solovyov, T.-W. Kim, F. Kleitz, O. Terasaki and R. Ryoo, *Chem. Mater*., **16**, 2274 (2004).

[31] A. B. Fuertas and D. M. Nevskaia, *J. Mater. Chem.,* **13**, 1843 (2003).

[32] M. Kuno, T. Naka, E. Negishi, H. Matsui, O. Terasaki, R. Ryoo and N. Toyota, *Synthetic Metals*, **135**, 721 (2003).

[33] B. H. Han, W. Zhou and A. Sayari, *J. Am. Chem. Soc*., **125**, 3444 (2003).

[34] C. Vix-Guterl, S. Boulard, J. Parmentier, J. Werckmann and J. Patarin, *Chem. Lett*., 1062 (2002).

[35] Z. Li and M. Jaroniec, *J. Phys. Chem. B*, **108**, 824 (2004).

[36] Z. Li and M. Jaroniec, *Chem. Mater*., **15**, 1327 (2003).

[37] P. M. Barata-Rodrigues, T. J. Mays and G. D. Moggridge, *Carbon*, **41**, 223 (2003).

[38] S. Han, M. Kim and T. Hyeon, *Carbon*, **41**, 1525 (2003).

[39] D. Kawashima, T. Aihara, Y. Kobayashi, T. Kyotani and A. Tomita, *Chem. Mater*., **12**, 3397 (2000).

[40] J. Pang, Q. Hu, Z. Wu, J.E. Hampsey, J. He and Y. Lu, *Micropor. Mesopor. Mater*., **74**, 73 (2004).

[41] S.H. Joo, S.J. Choi, I. Oh, J. Kwak, Z. Liu, O. Terasaki and R. Ryoo, *Nature*, **412**, 169 (2001).

[42] R. Ryoo, S.H. Joo, M. Kruk and M. Jaroniec, *Adv. Mater*., **13**, 677 (2001).

[43] J.S. Lee, S.H. Joo and R. Ryoo, *J. Am. Chem. Soc.,* **124**, 1156 (2002).

[44] J. Lee, J. Kim and T. Hyeon, *Chem. Commun*., 1138 (2003).

[43] Q. Hu, J. Pang, N. Jiang, J. E. Hampsey and Y. Lu, *Micropor. Mesopor. Mater.,* **81**, 149 (2005).

[45] J. Solla-Gull´on, F.J. Vidal-Iglesias, V. Montiel and A. Aldaz, *Electrochim. Acta*, **49**, 5079 (2004).

[46] J. Ding, K.-Y. Chana, J. Rena and F.-S. Xiao, *Electrochim. Acta*, **50**, 3131 (2005).

[47] S. H. Joo and R. Ryoo, *Photon Factory Activity report B*, 20 (2003) [available at http://pfwww.kek.jp/acr2002pdf].

[48] J. Lee, S. Jin, Y. Hwang, J.-G. Park, H. M. Park and T. Hyeon, *Carbon*, **43**, 2536 (2005).

[49] M-S. Luo and B. H. Davis. *Fuel Process. Technol.*, **83**, 49 (2003).

[50] Y. Yang, H.-W. Xiang, Y.-Y. Xu, l. Bai and Y.-W. Li, *Appl. Catal. A*, **266**, 181 (2004).

[51] Y.-H. Chin, J. Hu, C. Cao, Y. Gao and Y. Wang, *Catal. Today*, **110**, 47 (2005).

[52] M.E. Dry, *Catal. Sci. Technol*., **1**, 159 (1981).

[53] M. Luo, R. J. O'Brien, S. Bao and B. H. Davis, *Appl. Catal. A*, **239**, 111 (2003).

[54] F. R. Van den Berg, ZirconiaSupported *Iron-Based Fischer-Tropsch Catalysts*, PhD thesis, Utrecht University, Netherlands (2001).

Chapter Nine

Comparative Studies of Fe Catalysts Supported on Activated carbon, Mesoporous Carbon and MCM-48 Silica Template

9.1 Introduction

In this chapter the Fischer-Tropsch synthesis (FTS) catalytic performance of three precipitated and promoted Fe catalysts supported on activated carbon (15%Fe/2%K/AC), mesoporous carbon (15%Fe/2%K/MC) and mesoporous silica MCM-48 template (15%Fe/2%K/MCM-48) are compared. The FTS data for the 15%Fe/2%K/AC and the 15%Fe/2%K/MC was reported in Chapter 7 and 8, respectively.

9.2 Experimental section

The preparation, reduction procedure, characterisation techniques, etc, of the precipitated and promoted iron catalyst precursors used in this chapter are reported in detail in chapter 5. In order to compare the FTS performance of 2 % K loading, three Fe catalysts supported on activated carbon, mesoporous carbon

and MCM-48 were studied and compared during FT synthesis. All catalysts were activated under the same conditions (CO at 270 ^{o}C and 2.0 MPa for 24 h), and tested at process conditions of 250 ^{o}C, 2.0 MPa, 3.6 sl/(g-Fe h) and $H_2/CO = 2$.

9.3 Results and discussion

9.3.1 The Fischer-Tropsch activity of the precipitated and promoted Fe/MCM-48 catalysts

The activity and stability of the three catalysts, measured by CO conversion as a function of time on stream are shown in Fig. 9.1. The 15%Fe/2%K/AC catalyst was initially more active than the other two catalysts and started at a higher CO conversion, however, the activity declined quickly and stabilized in the later portion of the run after about 200 h on stream. The 15%Fe/2%K/MCM-48 started at a lower conversion but was the most stable catalyst at 50 % CO conversion. The catalyst deactivated slowly at a loss rate of 0.16%/h. The 15%Fe/2%K/MC catalysts started at a CO conversion of 60% and declined at a loss rate of 0.3%/h before 100 h on stream and then stabilized at 40% CO conversion. From the data above, it can be concluded that once bedded in (settled), the MC catalyst was the most stable of the three catalysts. The syngas conversions (Fig. 9.2) of the three catalysts followed the same trend as the CO conversions.

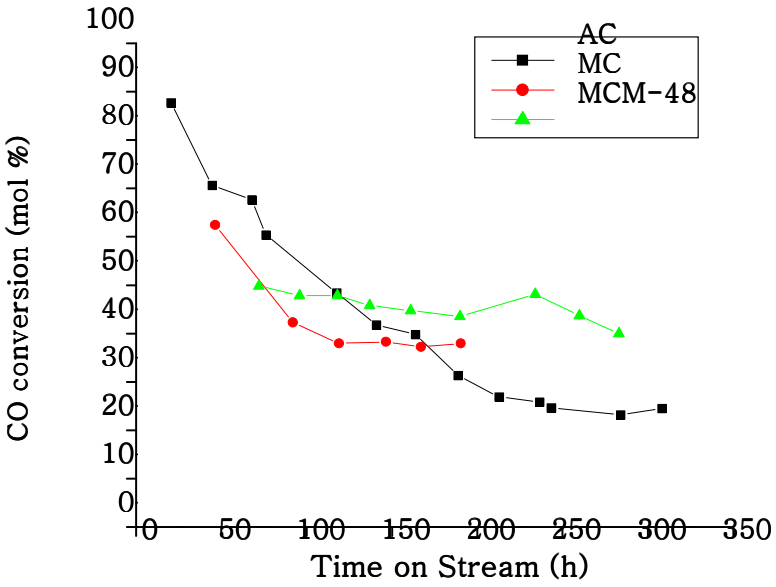

Figure 9.1: CO conversion as a function of time on stream of the 15%Fe/2%K catalyst on different supports.

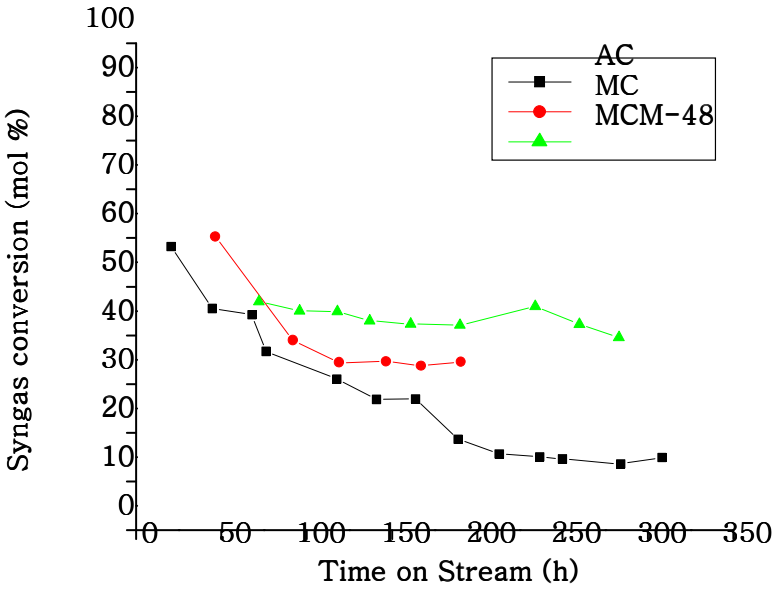

Figure 9.2: Syngas conversion as a function of time on stream of 15%Fe/2%K catalyst on different supports.

9.3.2 Selectivity of the precipitated and promoted Fe catalysts on different supports.

The methane selectivity of the three catalysts shown in Fig. 9.3 is lower (between 4 and 6 mol%) than other reported Fe/C catalysts [1-9]. The selectivity to methane as a function of time on stream for the 15%Fe/2%K/MCM-48 also did not vary with time on stream.

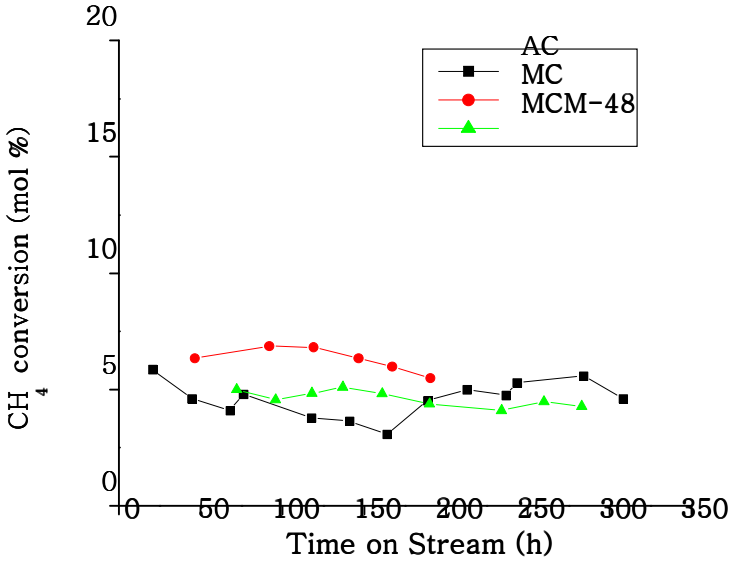

Figure 9.3: Methane selectivity of 15%Fe/2%K on different supports as a function of time on stream.

It can be seen that the methane selectivity was only slightly influenced by the different supports used, however CO_2 selectivity was affected. Thus, a decrease in CO_2 selectivity was observed when the supports were varied; with 15%Fe/2%K/AC catalyst giving ~40 mol% CO_2 with the selectivity decreasing to ~20 mol % when 15%Fe/2%/MC was used. The CO_2 selectivity was further decreased with 15%Fe/2%K/MCM-48 catalyst. Fig. 9.4 also shows that the three catalysts were stable with time on stream.

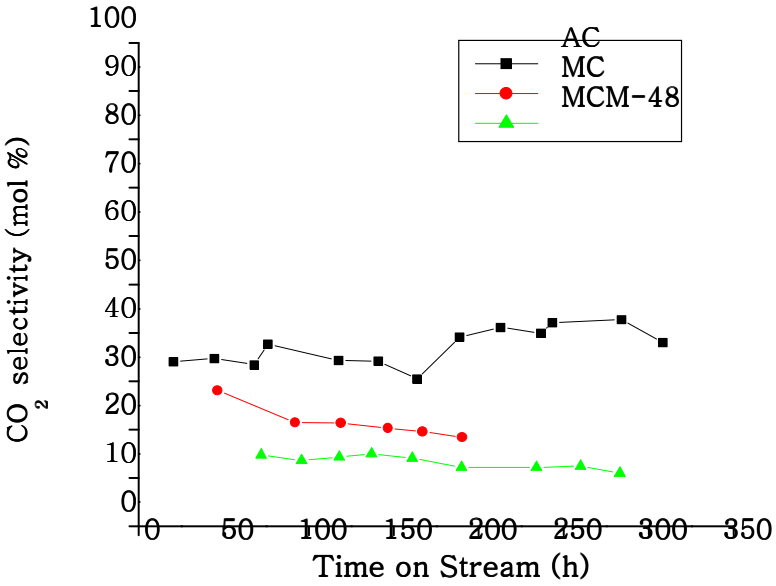

Figure 9.4: CO_2 selectivity as a function of time on stream of the 15%Fe/2%K catalyst on different supports.

9.3.3 Productivity of the precipitated and promoted Fe catalysts on different supports.

A summary of the productivity and selectivity data of the three catalysts is presented in Table 9.1. The results represent steady state condition when the conversions were stable for all the catalysts. It appears that the type of the support used had a marked effect on the product selectivities and product distributions. Both the 15%Fe/2%K/carbon supported catalysts produced higher

Table 9.1: FTS conversion, Productivity and Selectivity for potassium promoted Fe catalysts

15% Fe Catalyst	**15%/Fe/2% K/MC**	**15%/Fe/2% K/AC**	**15%/Fe/2% K/MCM-48**
Process conditions at steady state for all catalysts			
T = 250 ^{o}C, P = 2.0 MPa, H_2/CO ratio = 2:1, SV = 3.6 sl/hr g-Fe			
Conversion[a]			
CO	38	25	40
H_2	33	9	39
Syngas	35	14	40
H_2/CO usage[b]	1.7367	0.7671	1.9705
Productivity			
Hydrocarbon (g/h/g-Fe)	0.15	0.16	0.23
C_1 (mol/h)	0.24	0.27	0.28
C_2 (mol/h)	0.22	0.22	0.24
C_3 (mol/h)	0.19	0.22	0.25
C_4 (mol/h)	0.11	0.13	0.15
C_5 (mol/h)	0.04	0.05	0.06
C_6 (mol/h)	0.03	0.03	0.04

C_7 (mol/h)	0.01	0.01	0.02
Selectivity (mol %)			
CH_4[c]	5.49	5.58	4.28
CO_2[d]	7.9	42.79	12.43
Olefin fration[e]			
C_2	42	79	44
C_3	76	85	77
C_4	74	87	73
C_5	46	48	45
Product composition (wt. %)			
C_1-C_4	36.21	25.84	46.17
C_5-C_{11}	27.15	28.78	32.66
C_{12}-C_{18}	11.42	14.71	18.08
C_{19+}	24.40	30.67	3.08
α-1	0.79	0.81	0.85
α-2	0.84	0.86	-

[a]Conversion = (*N*in – *N*out / *N*in) x 100

[b]Usage = r_{H2}/r_{CO}

[c]CH_4 (mol %) = CH_4/ all hydrocarbons

[d]CO_2 (mol %) = CO_2 formed/ CO converted

[e]Olefin fraction = olefin/ (olefin + paraffin)

molecular weight products than the silica supported catalyst. Thus, the 15%Fe/2%K/MCM-48 catalyst produced only light weight hydrocarbons.

The H_2/CO usage ratio for the 15%Fe/2%K/MC and the 15%Fe/2%K/MCM-48 was almost the same as the one fed in the reactor, whereas the H_2/CO usage ratio for the 15%Fe/2%K/AC catalyst was lower. The productivity of the 15%Fe/2%/MCM-48 was more than the other two catalysts.

Figure 9.5 shows the ASF plot of the hydrocarbon product distribution for the three catalysts. The 15%Fe/2%/MCM-48 catalysts produced a slightly higher percentage of gaseous and liquid organic products when compared to the other two catalysts (see Table 9.1). Larger molecular weight products were dominant in the catalyst supported on mesoporous carbon and activated carbon. The alpha values for the activated carbon and mesoporous catalysts are similar. These results show that the K promoter enhanced FTS selectivity to heavier products. The basic sites on the Fe/K/C catalysts provide conditions for facilitating CO dissociation, leading to a relatively high coverage of carbon species on the surface [10]. On the contrary, short chain distribution is speculated to be due to insufficient hydrogen which is present for chain termination rates for the Fe/K/MCM-48.

Supported by quantum chemical calculations Koerts *et al.* [11] suggested a relation between carbon atoms more strongly adsorbed to the metal surface and the formation of higher hydrocarbons. The metal-carbon bond can be affected by the properties of the catalyst, *viz.* a promoter, the presence of more open metal surfaces, or an interaction of the metal phase with the support.

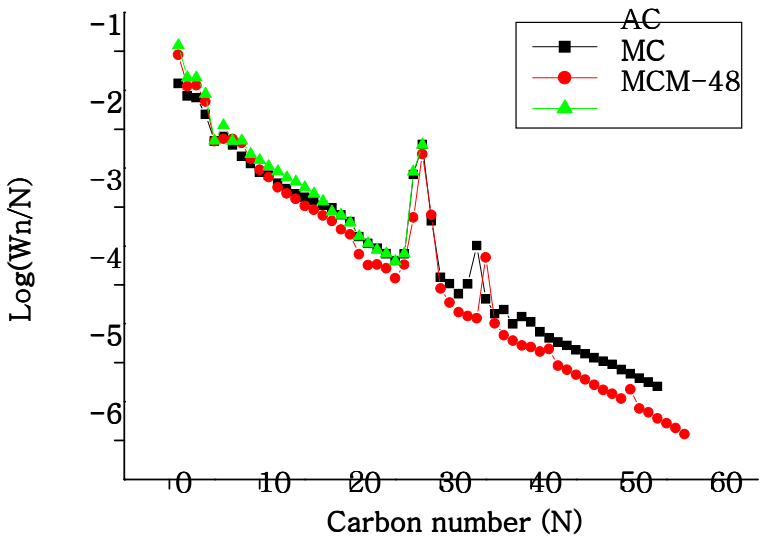

Figure 9.5: ASF distribution of precipitated and promoted Fe catalysts on different supports.

9.6 Conclusion

The CO and syngas conversions showed a similar trend with the different supported catalysts. The MCM-48 support initially appeared to be more stable in terms of CO conversion than the mesoporous carbon and activated carbon supports, however, in the last portion of the run the mesoporous carbon supported catalyst was more stable than the other two catalysts. It appears that the type of the support had a marked effect on the product selectivities and product distributions. The methane selectivity of the three catalysts was shown to be similar and low (between 4 and 6 mol %). The carbon dioxide selectivity was shown to have been suppressed/decreased more with 15%Fe/2%K/MCM-48. The 15%Fe/2%/MCM-48 catalysts produced a slightly higher percentage of gaseous and liquid organic products when compared to the other two catalysts. Larger molecular products were dominant in the catalyst supported on mesoporous carbon and activated carbon.

9.7 References

[1] H.-J. Jung, P. L. Walker Jr. and M. A. Vannice, *J. Catal*., **75**, 416 (1982).

[2] H.-J. Jung, M. A. Vannice, L. N. Mulay, R. M. Stanfield and W. N. Delgass, *J. Catal*., **76** (1982) 208.

[3] A. A. Chen, M. A. Vannice and J. Phillips, *J. Phys. Chem*., **91**, 6257 (1987).

[4] V. K. Jones, L. R. Neubauer and C. H. Bartholomew, *J. Phys. Chem*., **90**, 4832 (1986).

[5] A. P. B. Sommen, F. Stoop and K. Van der Wiele, *Appl. Catal*. *A*, **14**, 227 (1985).

[6] W.-P. Ma,Y.-J. Ding, L.-W. Lin. *Ind. Eng. Chem. Res*., **43**, 2391 (2004).

[7] E. van Steen and F. F. Prinsloo. *Catal. Today*, **71**, 327 (2002).

[8] M. C. Bahome, L. L. Jewell, D. Hilderbrandt, D. Glasser and N. J. Coville, *Appl. Catal. A*., **287**, 60 (2005).

[9] Y.-H. Chin, J. Hu, C. Cao, Y. Gao and Y. Wang, *Catal. Today*, **110**, 47 (2005).

[10] C.-H. Zhang, Y. Yang, B.-T. Teng, T.-Z. Li, H.-Y. Zheng, H.-W. Xiang and Y.-W. Li, *J. Catal*., **237**, 405 (2006).

[11] T. Koerts and R. A. Van Santen, *Catal.Lett*, **6**, 49 (1990).

Chapter Ten

Conclusions

The sol-gel method has become a very simple yet a powerful process for the synthesis of structural materials. The main advantage of the sol-gel process is that it allows careful control of the size and morphology of clusters/particles in the sol or gel during the early process stage, so that high quality end products (in the form of powders, films or coatings) can be developed to fulfil specific demands. The template directed sol-gel method makes the sol-gel method even more versatile because a wide range of materials with various external shapes and internal structures can be synthesized. These materials constitute a challenging domain in materials chemistry, which is experiencing explosive growth. The potential of these new structures has been recognized in the domain of optical devices, catalysis, separation techniques, controlled delivery, adsorption, and sensors.

Optimization of the properties of these materials requires a sound knowledge of the structure-property relationships, as well as a deeper understanding of the formation mechanisms of the materials. In the past five years, the increasing

number of successful synthesis methods to prepare mesostructured and mesoporous silica, metal oxides, etc. is the proof of the deeper knowledge and better design techniques that have become available.

The overview presented in this thesis on the synthesis and preparation of carbon materials demonstrates the flexibility in tailoring their chemical and physical properties of carbons to specific needs, thus illustrating their remarkable wide range of potential applications. However, the future growth of the use of carbon materials in catalysis will depend on the better understanding and subsequent control of the chemistry of the carbon surface, which can then be exploited in the design of truly unique catalysts.

It has been shown that by *in situ* carbonization of organic compounds, carbon nanocomposites and carbons with a well developed pore structure and high surface areas can be obtained. In addition, highly ordered mesoporous carbon materials are now available with a rich variety of structures, by templated synthesis, using mesoporous silica as templates. The templated synthesis of the ordered mesoporous carbons is a remarkable achievement in the field of porous materials because the synthesis is easy, inexpensive and suitable for large-scale production. The resulting high-surface-area materials with uniform pores promise to be suitable as adsorbents, catalyst supports, and materials for advanced

electronics applications. It has been shown that these highly structured mesoporous carbonaceous materials can play an important role in gaining a more fundamental insight of the processes and interactions occurring at carbon surfaces.

A well defined synthesis route to mesoporous graphitic carbon is reported in this work. The use of a template is essential in the synthesis of the mesoporous carbon framework, as carbons synthesised under otherwise identical conditions without a template were found to have low surface areas, and no pore structure. The catalytic carbonisation procedure used has an advantage as uniform infiltration of the carbon precursor can be easily accomplished inside the silica mesopores so that the resultant carbon materials retain the mesostructural order of the silica templates. The experimental observations using the SEM and TEM techniques, revealed that both mesoporous MCM-48 and mesoporous carbon show similar morphologies.

Furthermore, it has been shown that by varying the concentration of polystyrene solution, mesoporous carbons with different pore sizes and surface areas can be obtained, with the pores formed within the parent MCM-48 channels dependent on the amount of polystyrene used. The Raman, XRD and TEM techniques

confirmed the partially graphitic nature of the resultant synthesised carbonaceous materials.

The information given in this thesis has indicated that the Fischer-Tropsch industry is slowly moving from a position of total dependence on crude oil refining to one which co-exists with natural gas refining, built around GLT technology facilities. It has also been shown that catalysts play a pivotal role in FTS. Catalysts in FTS are at the heart of a commercial plant because it is only on the catalyst performance, that the technology providers try to distinguish themselves in the global market. Furthermore, the chain growth probability is a fundamental property of any F-T catalyst, and together with the process operating conditions determines the product distribution.

In this study precipitated iron catalysts supported on activated carbon, mesoporous carbon and MCM-48 were prepared and characterized by XRF, BET, TPR, XRD, SEM and TEM. It was found that the elemental composition of the Fe/K catalysts were comparable to the calculated values. The BET surface area of the mesoporous carbon support was remarkably reduced after impregnation with Fe metal catalyst. The decrease was further observed when potassium was introduced to the porous structure of the supported catalyst. Although potassium

seemed to decrease the surface area of all the supports in this study, it also had a positive effect in that it increased the pore diameters of the catalysts precursors.

Reduction of iron oxide was monitored by TPR analysis and the data revealed that the supported and precipitated catalysts reduce in two steps as reported for the Fe material in the literature. Enhanced reduction in the case of mesoporous carbon based materials could be assumed and it could be due not only to the reductive properties of the carbon but also to the weaker iron oxide−support interaction. Different iron oxide phases were observed and identified from the XRD data provided. Characterization with electron microscopy revealed that the iron was on the surface of the supports and in most cases the Fe nano-particles aggregated with neighbouring particles to form Fe nano-clusters.

The effect of potassium promotion on precipitated iron catalysts supported on activated carbon was investigated. It was observed that the three promoted and precipitated Fe/AC gave initially high rates of conversion that decreased with time on stream. The deactivation was similar for all the catalysts and was speculated to have been due to a contribution of sulfur poisoning, phase changes and also that the deactivation is probably due to complete filling or blockage of catalyst pores and not necessarily to gradual coverage of the iron surface by (inactive) carbon. The catalysts eventually reached stable CO conversions (25, 30

and 31 with the 2, 5 and 10% K loaded catalysts, respectively). The results suggested that a further increase in K loading will not enhance the activity of the FTS catalysts.

The methane selectivity was low (below 6%) and stable, and the overall olefin fraction was found to be good for all three Fe/K/AC catalysts. On average, a CO_2 yield of ~40% was obtained for all the three catalysts, indicating similar water gas shift reaction behaviour. From the study it was shown that middle alpha (α-1 and α-2 both between 0.79 and 0.90) catalysts were prepared and that the potassium promoter increased the hydrocarbon chain growth during the FT synthesis up to C_{55} with the lowest amount of promoter effect (2%). Increasing the amount of promoter from 5 to 10 % K did not show any significant effect in the studied catalysts.

To the best of our knowledge, this is the first reported FTS data that have been presented for an Fe/MC catalyst. Extensive research still needs to be conducted in order to optimize the catalytic behaviour of Fe/MC by varying FTS process variables.

The activity of the catalysts, measured in terms of CO conversion as a function of time on stream, was found to be similar for the 2 and 5% K loaded catalysts.

Whereas, the 10% loaded K catalysts showed slightly lower CO conversion when compared to the other two catalysts. The methane selectivity of all three catalysts was low compared to other reported Fe/C catalysts. The 2% K loaded catalyst exhibited a low methane selectivity of 5 mol % and it was interesting to note that the selectivity to methane was further decreased with an increase in potassium loading. The use of differently loaded K catalysts had a remarkable effect on the CO_2 selectivity. The CO_2 selectivity for all three catalysts was found to be low with the 10 % K loaded catalyst exhibiting a significant decrease (~5 mol %) compared to the 2 % K loaded catalyst (~20 mol%) and the 5% K loaded catalyst (~10 mol%).

It was interesting to see the positive effect potassium had on Fe/MC catalysts. Potassium is thus an effective promoter to restrain the formation of methane and gaseous products and to shift selectivity to higher molecular weight hydrocarbons with Fe/mesosoporous carbons. The catalysts under study were able to suppress the methane selectivity and also produced a high fraction of light olefins.

The CO and syngas conversions showed a similar trend for the different supported catalysts. The MCM-48 support initially appeared to be more stable in terms of CO conversion than the mesoporous carbon and activated carbon supports. However, in the last portion of the run the mesoporous carbon supported catalyst

was more stable than the other two catalysts. It appears that the type of the support had a marked effect on the product selectivities and product distributions. The methane selectivity of the three catalysts was shown to be similar and low (between 4 and 6 mol%). The carbon dioxide selectivity was shown to have decreased more with 15%Fe/2%K/MCM-48. The 15%Fe/2%/MCM-48 catalysts produced a slightly higher percentage of gaseous and liquid organic products when compared to the other two catalysts. Larger molecular products were dominant in the catalyst supported on mesoporous carbon and activated carbon.

The results presented in this thesis are interesting and have demonstrated the promising prospects of the mesoporous carbons for Fischer-Tropsch synthesis.

In future, It would be interesting to conduct studies on reduced Fe catalysts. The data should be evaluated to obtain insight in the obtained crystallite size distribution (TEM, XRD), the dispersion of the crystallites over the support material (TEM), and the degree of reduction of the catalyst, the reducibility of the catalyst precursor, the amount of hydrogen adsorbed (H_2-chemisorption, H_2-spillover!), and the strength of CO-chemisorption (IR). Other characterization techniques such as Mossbauer spectroscopy and XPS can be used to support/validate the data above as well to determine the Fe phases present in the reduced catalyst.

In this study only the effect of potassium loading on the FTS performance of supported Fe catalysts was investigated. It would also be interest to investigate other process conditions like space velocity, temperature, pressure and extended time on stream to determine the life span of the catalyst.